CR-184008

FINAL REPORT

on

SECOND ORDER TENSOR FINITE ELEMENT

CONTRACT #NAS8-37283

MARSHALL SPACE FLIGHT CENTER,

ALABAMA

TR-90-03

JUNE, 1990

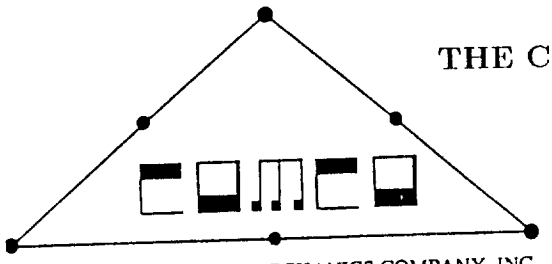

THE COMPUTATIONAL MECHANICS COMPANY, INC.

THE COMPUTATIONAL MECHANIC CO., INC.
LAMAR CREST TOWERS
7701 LAMAR, SUITE 200
AUSTIN, TEXAS 78752
(512)467-0618

FINAL REPORT

on

SECOND ORDER TENSOR FINITE ELEMENT

CONTRACT #NAS8-37283

MARSHALL SPACE FLIGHT CENTER,
ALABAMA

TR-90-03
JUNE, 1990

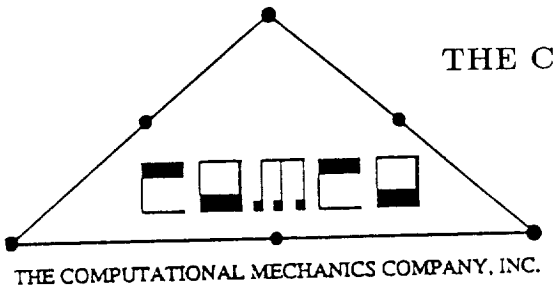

THE COMPUTATIONAL MECHANIC CO., INC.
LAMAR CREST TOWERS
7701 LAMAR, SUITE 200
AUSTIN, TEXAS 78752
(512)467–0618

NASA National Aeronautics and Space Administration

Report Documentation Page

1. Report No.	2. Government Accession No.	3. Recipient's Catalog No.
018-TR-90-03		

4. Title and Subtitle	5. Report Date
Final Report	June 22, 1990
	6. Performing Organization Code

7. Author(s)	8. Performing Organization Report No.
J. T. Oden, J. Fly, C. Berry, W. Tworzydlo, S. Vadaketh, J. Bass	10. Work Unit No.

9. Performing Organization Name and Address	11. Contract or Grant No.
Computational Mechanics Co., Inc. 7701 N. Lamar, Suite 200 Austin, Texas 78752	NAS8-37283
	13. Type of Report and Period Covered Final Report June, 1990
12. Sponsoring Agency Name and Address NASA/MSFC NASA Marshall Space Flight Center, Alabama	14. Sponsoring Agency Code

15. Supplementary Notes

None

16. Abstract

This report presents the results of a research and software development effort for the finite element modeling of the static and dynamic behavior of anisotropic materials, with emphasis on single crystal alloys. Various versions of two–dimensional and three–dimensional hybrid finite elements were implemented and compared with displacement–based elements. Both static and dynamic cases are considered. The hybrid elements developed in the project were incorporated into the SPAR finite element code.

In an extension of the first phase of the project, optimization of experimental tests for anisotropic materials was addressed. In particular, the problem of calculating material properties from tensile tests and of calculating stresses from strain measurements were considered. For both cases, numerical procedures and software for the optimization of strain gauge and material axes orientation were developed.

17. key Words (Suggested by Author(s))	18. Distribution Statement
anisotropic materials, hybrid elements, single crystal alloys, optimization, strain gauges, material constants, turbine blades	Unclassified-Unlimited

19. Security Classif. (of this report)	20. Security Classif. (of this page)	21. No. of pages	22. Price
None	None	104	N/A

Contents

1 Introduction

This final report presents the results of an almost four year effort on finite element modeling of the static and dynamic behavior of anisotropic materials with particular emphasis on single crystal alloys used in the manufacturing of high-performance turbine blades. This effort was motivated by a lack of finite element software capable of representing stress and strain as second order tensors.

During the course of the project, various formulations for two- and three-dimensional hybrid finite elements were developed and implemented into the SPAR finite element code. These formulations were tested and compared with displacement-based approaches for both static and dynamic problems.

In an extension of the original statement of work, a sensitivity analysis of experimental results for anisotropic materials subject to misalignments and other errors was conducted. As a results of this study, a formulation, numerical procedure, and computer software were developed for the calculation of material constants for anisotropic materials and, moreover, for the optimization of strain gauge and material axis orientations of tensile test specimens for highly anisotropic materials. Moreover, as an additional task, a similar procedure and software were developed for the evaluation of stresses by means of strain measurements and for the optimization of the orientation of strain gauges in this case.

This report presents a summary of the technical effort over the course of this project. The report is divided into several sections: In Section 2, general hybrid finite element formulations are studied. Then, in Section 3, two-dimensional finite elements based on hybrid formulations are developed and tested numerically. In the next section, a dynamic analysis, using hybrid finite elements is discussed. This analysis is followed by the formulation of three-dimensional hybrid finite elements (Section 5). In Section 6, alternate hybrid stress elements are studied and verified numerically. As a conclusion of the theoretical developments presented, several numerical examples cases for the SSME turbine blades are presented in Section 7. This section is followed by the formulation of numerical procedures for the optimization of the orientation of material axes and strain gauges in experimental tests for anisotropic materials (Section 8). Several numerical examples are presented to illustrate the performance of the procedure.

In the appendices, updates to the SPAR code manual are presented. In four separate volumes, theory and user's manuals for the two experiment optimization codes—OPTAM-C and OPTAM-S—are included.

2 General Hybrid Element Formulation

2.1 Introduction

This project began with the study of a variety of methods for modeling vibrations of anisotropic elastic blades with particular emphasis given to hybrid finite element formulations and the feasibility of using helical shell elements. Apparently, some authors have attempted to model isotropic curvilinear turbine blades using shell elements of variable thickness based on a shell theory for surfaces generated along a helix. One advantage in this approach is that models with relatively few degrees of freedom can yield quite acceptable results. A disadvantage, of course, is the limited flexibility inherent in shell models for capturing the effects of boundary conditions, three–dimensional stress states, etc.

Several alternative hybrid element formulations were investigated. Purely qualitative studies were made, the objective being to assess *a priori* properties of various elements with regard to

1. accuracy in computing stresses
2. ease in handling anisotropic properties
3. numerical stability in the presence of strong anisotropy
4. compatibility with the SPAR code structure

The basic formulation which generated interest is that which yields a hybrid element from assumed displacement fields. Starting with the principle of minimum potential energy with displacement continuity conditions as constraints, the boundary tractions then appear as Lagrange multipliers. The resulting functional is of the form

$$\pi = \sum_e \left\{ \int_{V_e} \left(\frac{1}{2} C_{ijkl} \varepsilon_{ij}(u) \varepsilon_{kl}(u) - F_i v_i \right) dV - \int_{\partial V_{1e}} T_i u_i ds + \int_{\partial V_{2e}} T_i u_i ds \right\} \qquad (2.1)$$

Here standard notation is used: V_e is a typical element, C_{ijkl} are the elastic constants, ε_{ij} the strains, F_i the body forces, T_i the prescribed tractions on ∂V_{1e} and u_i the prescribed displacements on ∂V_{2e}, where the T_i in this integral are the Lagrange multipliers.

Approximations take the form

$$u = A\beta, \; T = \phi q \qquad (2.2)$$

where β and q are vectors of undetermined parameters. The strains are then

$$\varepsilon = B\beta \qquad (2.3)$$

Denoting

$$H_1 = \int_{V_e} B^T C B dV \quad H_2 = \int_{V_e} A^T F dV$$
$$H_3 = \int_{\partial V_{1e}} A^T \phi dV \quad H_4 = \int_{\partial V_{2e}} u^T \phi dV \tag{2.4}$$

a minimization of π yields

$$\beta = H_1^{-1}(H_{3q} + H_2) \tag{2.5}$$

Hence,

$$\pi = \frac{1}{2}\sum_e (q^T F_e q - 2U_e^T q) \tag{2.6}$$

where

$$F_e = H_3^T (H_1^{-1})^T H_3$$
$$U_e = H_2^T H_1^{-T} H_3 + H_4 \tag{2.7}$$

Equilibrium and continuity of interelement displacements is achieved in the discrete model whenever

$$F_e q = U_e \tag{2.8}$$

The hybrid element stiffness matrix is then

$$K = F_e^{-1} \tag{2.9}$$

Hybrid element formulation

Six stress and displacement type elements were chosen for studies of stress accuracy and utility in vibrational analysis. Two separate finite element formulations were chosen.

1. *Hellinger-Reissner Formulation*

The functional which assumes a stationary value is given by:

$$\pi_r = \int_V \left[-\frac{1}{2}\sigma^T S \sigma + \sigma^T (Du)\right] dV - \int_{\partial V} T^T (u - u) ds \tag{2.10}$$

Here σ is the vector of stress components, D is the differential operator defining the strain-displacement relations ($\varepsilon = Du$), with u the displacement vector, and T the boundary traction.

The displacements u are not assumed to be compatible and the equilibrium equations are not satisfied identically but are brought in as constraints, so that the elements are more "flexible" and the number of stress terms required to suppress zero-energy modes is reduced. The elements also becomes less sensitive to changes in the reference coordinates [12].

The strain–displacement relation is given by

$$\varepsilon = Du \tag{2.11}$$

where the displacement u consists of a compatible part u_c and an incompatible part u_a, which could be a bubble function vanishing on the boundary.

Now,

$$\int_V \sigma^T (Du_a) dV = -\int_V (D^T \sigma)^T u_a dV + \int_{\partial V} (N\sigma)^T u_a ds \tag{2.12}$$

where $N\sigma$ is the trace of σ on the boundary, N being a matrix of direction cosines of the unit exterior normal to ∂V. Thus, if we set $u_a = u - u$ and $N\sigma = T$, we have,

$$\pi_r = \int_V \left[-\frac{1}{2} \sigma^T S \sigma + \sigma^T (Du_c) - (D^T \sigma)^T u_a \right] dV \tag{2.13}$$

We see that the equilibrium equations

$$D^T \sigma = 0 \tag{2.14}$$

appear as a constraint with the u_a being the Lagrange multiplier.

In the finite element implementation, we assume

$$\sigma = P\beta \tag{2.15}$$

where

$$P = \begin{bmatrix} C_1 \\ C_2 \\ \cdot \\ \cdot \end{bmatrix} \tag{2.16}$$

and C_i's are row vectors.

Also, let

$$u_c = Nq \tag{2.17}$$

and

$$u_a = L\lambda \tag{2.18}$$

from which

$$Du_c = Bq \qquad (B = DN) \tag{2.19}$$

and

$$D^T \sigma = E\beta \qquad (E = D^T P) \tag{2.20}$$

so that

$$\pi_r = -\frac{1}{2} \beta^T H \beta + \beta^T G q - \beta^T R_1 \lambda \tag{2.21}$$

where

$$H = \int_V P^T S P dV$$
$$G = \int_V P^T B dV \tag{2.22}$$

and

$$R_1 = \int_V E^T L dV \tag{2.23}$$

Finding the first variation of π_r with respect to β and λ, we get

$$\beta = H^{-1}(Gq - R_1\lambda) \tag{2.24}$$

and

$$R_1^T \beta = 0 \tag{2.25}$$

Now, the strain energy as expressed in terms of a stiffness matrix K and the generalized coordinates q is given by

$$U = \tfrac{1}{2} q^T K q$$
$$U = \int_V \frac{1}{2} \sigma^T \epsilon dV = \frac{1}{2} \int_V \sigma^T S \sigma dV \tag{2.26}$$

Eliminating λ from equations (2.24) and (2.25), substituting β into the expression in equation (2.26) which becomes

$$U = \frac{1}{2} \beta^T H \beta \tag{2.27}$$

gives

$$K = G^T M G - G^T M R_1 (R_1^T M R_1)^{-1} R_1^T M G \tag{2.28}$$

where

$$M = H^{-T} \tag{2.29}$$

The inversion of H becomes easier if the same C_i's are used for all of the normal stress components. For example, in the case of a three–dimensional isotropic solid, when the stress

terms are not coupled,

$$H = 1/E \begin{bmatrix} \phi_1 & -\nu\phi_1 & -\nu\phi_1 & & & \\ -\nu\phi_1 & \phi_1 & -\nu\phi_1 & & 0 & \\ -\nu\phi_1 & -\nu\phi_1 & \phi_1 & & & \\ & & & 2(1+\nu)\phi_4 & & \\ & 0 & & & 2(1+\nu)\phi_5 & \\ & & & & & 2(1+\nu)\phi_6 \end{bmatrix} \tag{2.30}$$

where

$$\phi_i = \int_V P_i^T P_i dV \tag{2.31}$$

H can be easily inverted.

2. *Hu-Washizu Formulation*

Another approach to the development of mixed elements is to use the extended variational principle of Hu and Washizu. The Hu-Washizu variational functional is given by:

$$\pi_{HW} = \int_V \left[\frac{1}{2}\varepsilon^T C\varepsilon - \sigma^T\varepsilon + \sigma^T(Du)\right] dV - \int_{\partial V} T^T(u-u)dS \tag{2.32}$$

where

$$C = S^{-1} \tag{2.33}$$

and the independent variables are the stresses σ, the strains ε, element displacements u, and boundary displacements u.

In the finite element formulation, both σ and ε are approximated by the same shape function:

$$\sigma = P\beta \tag{2.34}$$

and

$$\varepsilon = P\alpha \tag{2.35}$$

The strain energy is then

$$U = \int_\nu \frac{1}{2}\sigma^T \epsilon dV = \frac{1}{2}\beta^T A\alpha \tag{2.36}$$

where

$$A = \begin{bmatrix} B_1 \\ B_2 \\ \cdot \\ \cdot \end{bmatrix} \tag{2.37}$$

and

$$B_i = \int_V P_i^T P_i dV \tag{2.38}$$

The best choice for the reference coordinates should be such that the B_i's are diagonal matrices and the inversion of H becomes easy.

Using the same approximation for u as in equations (2.17) and (2.18) and following a similar line of logic results in the following:

$$\pi_{HW} = \frac{1}{2}\alpha^T J\alpha - \beta^T A\alpha + \beta^T Gq - \beta^T R_1\lambda \tag{2.39}$$

where

$$J = \int_V P^T C P dV \tag{2.40}$$

Setting the first variation of π_{HW} with respect to β and α to zero gives

$$A\alpha = Gq - R_1\lambda \tag{2.41}$$

and

$$J\alpha = \beta^T A \tag{2.42}$$

Substituting the expression for α from equation (2.41) and (2.42) into the strain energy solution (2.36),

$$K = G^T MG - G^T MR_1(R_1^T MR_1)^{-1}R_1^T MG \tag{2.43}$$

where

$$M = A^{-1}JA^{-1} \tag{2.44}$$

Although the finite element formulation using the Hu-Washizu functional exists, all applications are derived with regards to shell/plate theory rather than analysis of continua.

Pian [15] has worked out solutions for three–dimensional brick elements using the modified Reissner principle. He has analyzed the 8 node hexahedral solid and the 20 node hexahedral solid.

Hybrid Element Shortcomings

Stress–hybrid elements possess some shortcomings which must be overcome in order for them to be useful. The first major shortcoming of hybrid stress elements is that they can possess zero energy modes which can have debilitating effects on eigenvalue problems. Babŭska, Oden, and Lee (CMAME, 1978) have shown that such methods are stable and convergent only if a global LBB–condition is statisfied, i.e., conditions of the type

$$\alpha|||\lambda||| \leq \sup_u \frac{|\oint_{\partial V} \lambda u ds|}{||u||_1} \tag{2.45}$$

where λ is a multiplier on the constraint of continuity of displacements u across (interelement) boundaries and $|||\cdot|||, ||\cdot||_1$ are appropriate norms (for details, see [12]). If the constant α is equal to zero, the method is rank deficient and spurious modes exist. If α is a function of mesh size h, the solution may be numerically unstable and its quality may deteriorate with mesh refinement.

To overcome this problem, the method must possess an LBB–parameter

$$0 < \alpha = \text{ constant independent of } h \tag{2.46}$$

A quick check for a necessary condition for stability is to calculate the rank of the matrix associated with the constraint term (e.g., $\oint \lambda u ds$). For the Hellinger-Reissner formulation zero energy modes may normally be suppressed when the number of stress terms is equal to or larger than the total degrees of freedom minus the number of rigid body degrees of freedom. However, these stress terms must be chosen carefully because they do not all contribute to the suppression of zero energy modes.

For the Hu-Washizu formulation, in the eight node solid, the minimum number of stress terms required to eliminate zero–energy modes is $(8 \times 3 - 6 = 18)$. Using these terms, i.e.,

$$\begin{aligned}
\sigma_x &= \beta_1 + \beta_2 y + \beta_3 z + \beta_4 yz \\
\sigma_y &= \ldots \\
\sigma_z &= \ldots \\
T_{xy} &= \beta_{13} + \beta_{14} z \\
T_{yz} &+ \beta_{15} + \beta_{16} x \\
T_{xz} &= \beta_{17} + \beta_{18} y
\end{aligned} \tag{2.47}$$

the bending of a beam was analyzed, and the results were not good.

If, however, the stresses were to be decoupled as suggested, additional terms would be required to eliminate the zero–energy modes, in fact, 21 β's would be necessary.

By using three internal displacement parameters (λ's), the number of β's may be reduced to 18. Results obtained with this formulation were quite good.

For two–dimensional problems, especially plane stress, Spilker [24] has shown the merits of an eight noded quadrilateral with complete stress terms. His paper also considers 4–noded quadrilaterals, using 5 β's for the stress terms and a bilinear displacement approximation. Although the results were good, the element was sensitive to changes in the reference coordinates.

The second major shortcoming for hybrid stress elements is that these elements may yield stiffness matrices that are not invariant under a change in local coordinate systems. Indeed,

the original Pian-hybrid-stress element (now in SPAR) can yield severely different stresses when simple changes in the local coordinate system occur.

Invariance of the stiffness matrices may be guaranteed by introducing appropriate "bubble functions" which serve as multipliers on the equilibrium constraint,

$$D^T\sigma = 0 \tag{2.48}$$

Completeness in all modes of the polynomial expansion is also important, to ensure invariance with respect to the chosen reference coordinates. Another method of achieving invariance is to use local coordinates.

In the modified Hellinger-Reissner formulation, the equilibrium equations are introduced as a constraint and do not have to be satisfied pointwise. The degree of satisfaction depends on the number of internal displacement parameters λ that are used.

The third and one of the most serious shortcomings of stress–hybrid elements is that, in their present form, they are incapable of yielding a consistent approximation of the kinetic energy in an element. This is a deficiency often "swept under the rug" in discussions of applications of hybrid elements to problems of structural vibrations. Traditionally, mass matrices are calculated using displacement or velocity approximations which are completely independent of those used for (or resulting from) calculations of the element stiffness matrices. To overcome this deficiency, it has been observed that the kinetic energy in a body Ω can be written

$$\hat{U} = \int_V \frac{1}{2}\rho v^2 dV = \int_V \frac{1}{2\rho}p^2 dV \tag{2.49}$$

where ρ is the mass density and p is the momentum. The momentum is related to the stress by

$$p = D^T\sigma \tag{2.50}$$

Hence, it may be possible to define a "consistent approximation" of the kinetic energy which should produce more accurate approximations of mode shapes and frequencies.

3 Two–Dimensional Element Definition

3.1 Definition of Element Matrices

Using the Hellinger Reissner formulation and introducing the equilibrium conditions as a constraint into the complementary energy functional and modifying produces the following functional:

$$\pi_{mc} = \sum_n \left\{ \frac{1}{2} \int_{Vn} \sigma^T S \sigma dV - \int_{Vn} \sigma^T (Du) dV + \int_{\partial Vn} u^T T ds \right\} \tag{3.1}$$

where σ, u are the stress and displacement vectors, S is the compliance matrix, D is the differential operator, V_n is the volume of the nth element, and T is the prescribed stress on the boundary S_{σ_n}.

The stresses are interpolated in terms of the stress parameters β and the polynomial shape functions P, i.e.,

$$\sigma = P\beta \tag{3.2}$$

so that equilibrium is satisfied, i.e.,

$$D^T \sigma = 0 \tag{3.3}$$

For isoparametric elements,

$$\begin{aligned} x &= \sum_i N_i(\xi, \eta, \varsigma) x_i \\ y &= \sum_i N_i(\xi, \eta, \varsigma) y_i \\ z &= \sum_i N_i(\xi, \eta, \varsigma) z_i \end{aligned} \tag{3.4}$$

where (ξ, η, ς) form the parent plane and $N_i(\xi, \eta, \varsigma)$ are the appropriate shape functions.

The displacements are interpolated in terms of the shape functions as

$$u = N(\xi, \eta, \varsigma) q \tag{3.5}$$

where q are the element nodal displacements.

Then the strain is given by

$$\varepsilon = Du = B(\xi, \eta, \varsigma) q = \frac{1}{|J|} B^*(\xi, \eta, \varsigma) q \tag{3.6}$$

where $B = DN(x, y, z)$ and $|J|$ is the Jacobian of the transformation.

Substituting equations (3.2), (3.5), and (3.6) into (3.1) and defining

$$\begin{aligned} H &= \int_{-1}^{1}\int_{-1}^{1}\int_{-1}^{1} P^T S P |J| d\xi d\eta d\varsigma \\ G &= \int_{-1}^{1}\int_{-1}^{1}\int_{-1}^{1} P^T B^* d\xi d\eta d\varsigma \\ Q &= \int_{-1}^{1}\int_{-1}^{1} N^T T ds \end{aligned} \tag{3.7}$$

and noting that

$$dV = |J| d\xi d\eta d\varsigma \tag{3.8}$$

gives

$$\pi_{mc} = \sum_n \left\{ \frac{1}{2}\beta^T H \beta - \beta^T G q + Q q^T \right\} \tag{3.9}$$

Equating the first variation of π_{mc} to zero in each element results in

$$\beta = H^{-1} G L q^* = H^{-1} G q \tag{3.10}$$

where $q*$ are the global displacements which are related to the element displacements by the Boolean matrix L_a.

By substituting (3.10) into the expression for $\delta\pi_{mc}$, a new expression for $\delta\pi_{mc}$ may be written as

$$\delta\pi_{mc} = \delta q^{*T} \left\{ \sum_n L^T K L q^* - \sum_n L^T Q \right\} = 0 \tag{3.11}$$

where Q is the element load vector and K is the element stiffness matrix

$$K = G^T H^{-1} G \tag{3.12}$$

The equation (3.7) can be numerically integrated, but care should be taken to ensure that the proper order of integration is used.

It has been proved in the paper by Spilker that if the assumed stresses are complete polynomials, the element stiffness will be invariant to general rotation and translation. To reduce the numbers of β's, the equations of equilibrium are applied to the assumed stress terms. However, lack of invariance does *not* imply poor element performance. In isoparametric elements, however, as the choice of the local orthogonal system is not unique, the element must be inherently invariant for good results.

As expected in plane elements, the optimal sampling points are the Gaussian points of integration for the stresses. However, the results are still better than those in the assumed displacement method, as the stresses in the hybrid method satisfy equilibrium conditions which relate the stress gradients.

3.2 Examination of Different Element Models

The four–node linear displacement model (see Fig. 3.1).

The shape functions $N_i(\xi, \eta)$ for the intra–element displacement field correspond to those for four–node bilinear functions.

Using complete polynomials for the stress approximation we have for a linear field

$$\begin{aligned} \sigma_x &= \beta_1 + \beta_2 y + \beta_6 x \\ \sigma_y &= \beta_3 + \beta_4 x + \beta_7 y \\ \sigma_{xy} &= \beta_5 - \beta_7 x - \beta_6 y \end{aligned} \tag{3.13}$$

which is variant.

The minimum number of β's required, η_β, as a necessary condition for correct stiffness rank is

$$\eta_\beta \geq \eta_{\text{d.o.f}} - \eta_{\text{r.d.o.f}} \tag{3.14}$$

where

$$\begin{aligned} \eta_{\text{d.o.f}} &= \text{number of element d.o.f.} \\ \eta_{\text{r.d.o.f}} &= \text{number of rigid body d.o.f.} \end{aligned} \tag{3.15}$$

Spilker, et al. compares the performance of two elements, one with 7β's (PH7L) and one with five β's (the minimum required by equation (3.14) - PH5L).

The optimal sampling point for both these elements is the centroid of the element. The dimensions of the element are a and b. The stiffness matrix for the element PH7L corresponding to a set of generalized displacement parameters α, (for plane stress) is

$$K^\alpha = 4Eab \begin{bmatrix} \frac{1}{(1-\nu^2)} & 0 & \frac{\nu}{(1-\nu^2)} & 0 & 0 \\ 0 & \frac{1}{3}b^2(1+f_1) & 0 & 0 & 0 \\ \frac{\nu}{(1-\nu^2)} & 0 & \frac{1}{(1-\nu^2)} & 0 & 0 \\ 0 & 0 & 0 & \frac{1}{3}a^2(1+f_2) & 0 \\ 0 & 0 & 0 & 0 & \frac{1}{2}\frac{1}{(1+\nu)} \end{bmatrix} \tag{3.16}$$

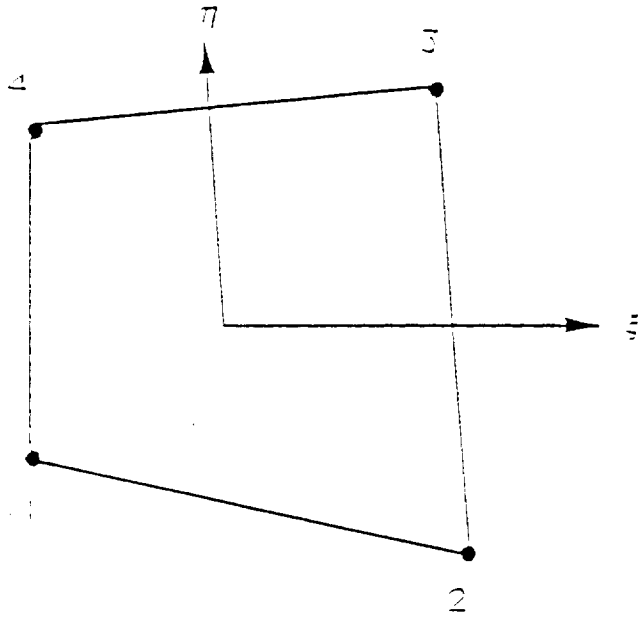

Figure 3.1: The four node linear displacement model.

i.e., the displacements are interpolated as simple bilinear polynomials of x, y in terms of the eight displacement parameters. When the strain displacement relations (3.6) are used, to relate ε to α, only five α's remain as the constant terms fall out. These five α's correspond to stretching and bending along the two axes and pure shear:

$$\begin{aligned}
\alpha_1 &= \tfrac{1}{4}a(-\overline{u}_1 + \overline{u}_2 + \overline{u}_3 - \overline{u}_4) \\
\alpha_2 &= \tfrac{1}{4}ab(\overline{u}_1 - \overline{u}_2 + \overline{u}_3 - \overline{u}_4) \\
\alpha_3 &= \tfrac{1}{4}b(-\overline{v}_1 - \overline{v}_2 + \overline{v}_3 + \overline{v}_4) \\
\alpha_4 &= \tfrac{1}{4}ab(\overline{v}_1 - \overline{v}_2 + \overline{v}_3 - \overline{v}_4) \\
\alpha_5 &= \tfrac{1}{4}ab\ [b(-\overline{u}_1 - \overline{u}_2 + \overline{u}_3 + \overline{u}_4) + a(-\overline{v}_1 + \overline{v}_2 + \overline{v}_3 - \overline{v}_4)]
\end{aligned} \tag{3.17}$$

where all of the displacements correspond to the local coordinate system used.

The terms f_1 and f_2 are

$$\begin{aligned}
f_1 &= \frac{[(a/b)^2 - v]^2}{[1 - \nu^2 + (a/b)^2 2(1+\nu)]} \\
f_2 &= \frac{[(b/a)^2 - \nu]^2}{[1 - \nu^2 + (b/a)^2 2(1+\nu)]}
\end{aligned} \tag{3.18}$$

K^α is definite and hence, PH7L has no spurious zero energy modes.

In PH5L, f_1 and f_2 are different and, therefore, cause a difference in the analysis of the bending problem. Element $PH5L$ shows no spurious zero energy modes at $\theta = 0$. But since K depends on θ the stiffness rank should be explored.

Computing the G matrix at an arbitrary angle θ, in terms of the general displacement parameters

$$G^\alpha = \begin{bmatrix}
4ab & 0 & 0 & 0 & 0 \\
0 & \frac{4}{3}(ab^3 - a^3bc_2) & 0 & -\frac{4}{3}ab^3c_1 & 0 \\
0 & 0 & 4ab & 0 & 0 \\
0 & \frac{4}{3}a^3bc_1 & 0 & \frac{4}{3}(a^3b - ab^3c_2) & 0 \\
0 & 0 & 0 & 0 & 4ab
\end{bmatrix} \tag{3.19}$$

where

$$c_1 = \frac{sc(c^2 - s^2)}{s^6 + c^6}; \quad c_2 = \frac{s^2c^2}{c^6 + s^6} \tag{3.20}$$

with $s = \sin\theta$ and $c = \cos\theta$.

It is found that the matrix G becomes singular for $\theta = 45°$ leading to two zero–energy modes, so that PH5L is not completely invariant. Thus, this element should be used with great care.

A pure bending problem was solved using each of these two elements; the results are summarized in Fig. 3.2. PH7L leads to a "stiff" solution that converges only when more than ten elements are used. However, it is invariant, unlike PH5L, and gives good results at all θ's.

The eight node quadratic displacement model (see Fig. 3.3) .

The shape functions here correspond to those for eight node isoparametric serendipity elements (for the displacement approximation).

For this 16 degree of freedom element, a minimum of 13 β's is required. The smallest stress field that satisfies this requirement in equilibrium and invariance, is a cubic.

After equilibrium conditions are satisfied, an 18 β field is derived

$$\begin{aligned}
\sigma_x &= \beta_1 + \beta_6 x + \beta_2 y + \beta_8 y^2 + 2\beta_9 xy + \beta_{10} x^2 + \beta_{13} x^3 \\
&\quad + 3\beta_{14} x^2 y + 3\beta_{15} x y^2 + \beta_{17} y^3 \\
\sigma_y &= \beta_3 + \beta_4 x + \beta_7 y + 2\beta_{11} xy + \beta_{12} x^2 + \beta_{10} y^2 + 3\beta_{13} x y^2 \\
&\quad + \beta_{14} y^3 + 3\beta_{16} x^2 y + \beta_{18} x^3 \\
\sigma_{xy} &= \beta_5 - \beta_7 x - \beta_6 y - \beta_{11} x^2 - \beta_9 y^2 - 2\beta_{10} xy - 3\beta_{13} x^2 y \\
&\quad - 3\beta_{14} x y^2 - \beta_{15} y^3 - \beta_{16} x^3
\end{aligned} \tag{3.21}$$

which is invariant and has no spurious zero–energy modes.

To reduce the number of β's, the Beltrami-Mitchell compatibility conditions (for plane strain) are employed, where

$$\nabla^2(\sigma_x + \sigma_y) = 0 \tag{3.22}$$

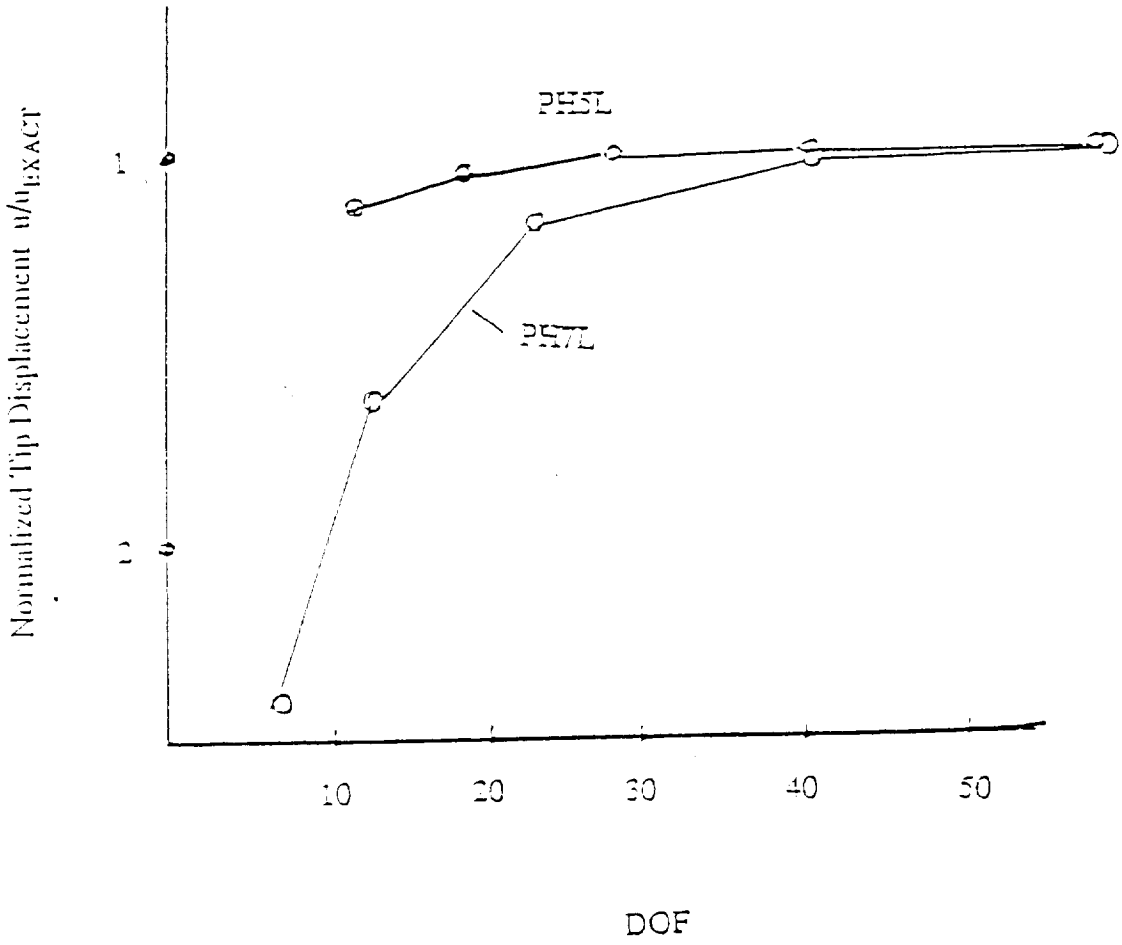

Figure 3.2: Comparison of pure bending results for a four node quad with 7 β's vs. 5 β's.

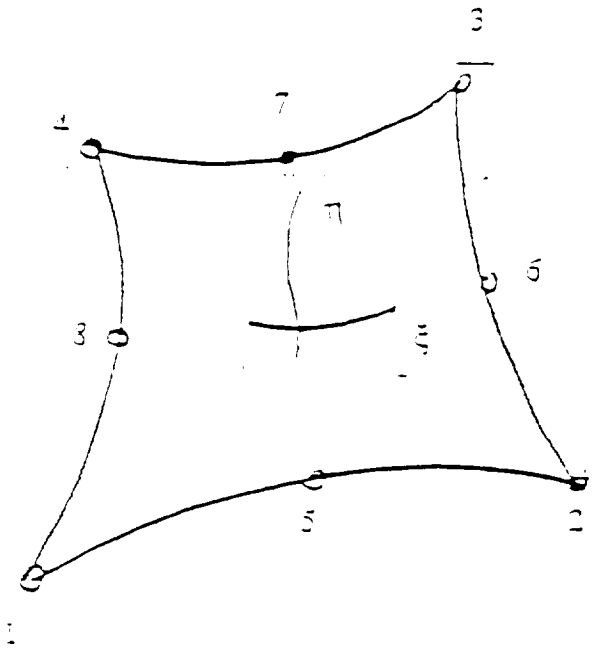

Figure 3.3: The eight node quadratic displacement model.

Then, after re-numbering,

$$\begin{aligned}
\sigma_x &= \beta_1 + \beta_6 x + \beta_2 y + \beta_8 y^2 + 2\beta_9 xy + \beta_{10} x^2 + \beta_{12} x^3 \\
&\quad + \beta_{13}(3x^2 y - 2y^3) + 3\beta_{14} xy^2 - \beta_{15} y^3 \\
\sigma_y &= \beta_3 + \beta_4 x + \beta_7 y + 2\beta_{11} xy - \beta_8 x^2 + \beta_{10}(y^2 - 2x^2) \\
&\quad + \beta_{12}(3xy^2 - 2x^3) + \beta_{13} y^3 + 3\beta_{15} x^2 y - \beta_{14} x^3 \\
\sigma_{xy} &= \beta_5 - \beta_7 x - \beta_6 y - \beta_{11} x^2 - \beta_9 y^2 - 2\beta_{10} xy - 3\beta_{12} x^2 y \\
&\quad - 3\beta_{13} xy^2 - \beta_{14} y^3 - \beta_{15} x^3
\end{aligned} \tag{3.23}$$

This element (PH15Q) is still a complete cubic with only 15 β's and is invariant and has no spurious energy modes. The optimal sampling points for both the PH15Q and PH18Q elements are the 2×2 Gaussian points.

Another reportedly good element is the 14 β element developed and tested by Hershell. However, it is not invariant.

Some example problems were solved and the results, as well as the conclusions, are summarized in Fig. 3.4.

The previous graph gives the results for a plane stress problem. The performance of the PH14Q element is excellent, even when the order of integration is reduced to 3×3. However, the PH18Q element stiffness becomes singular when the integration order is reduced.

3.3 Numerical Experiments

Some numerical experiments were conducted to compare hybrid stress elements with traditional displacement method elements. Results show remarkable deficiencies in traditional displacement methods for anisotropic materials. The analysis of a cantilever beam under the effect on an end shear load was selected as the test problem, as shown in Fig. 3.5. The data for the problem include the following:

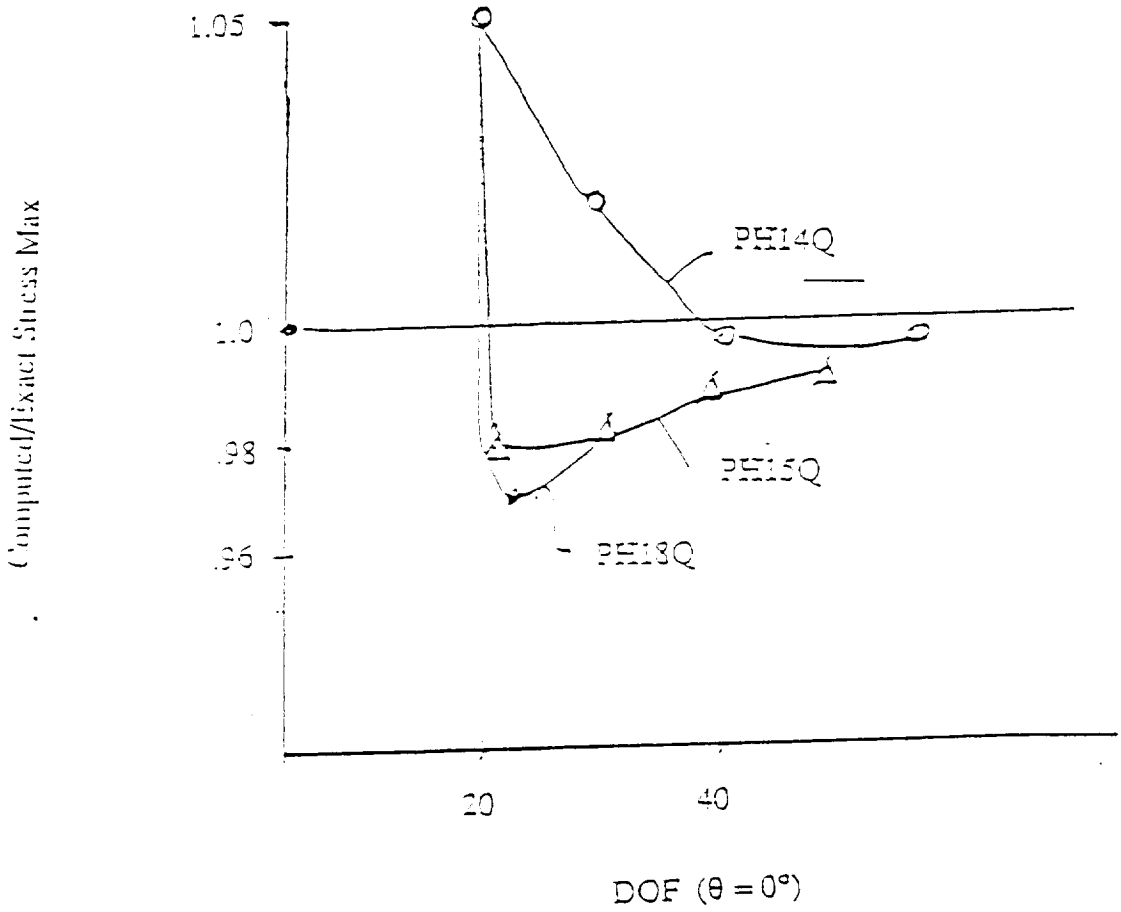

Figure 3.4: Comparison of a plane stress problem for an eight node quad with 14, 15, and 18 β's.

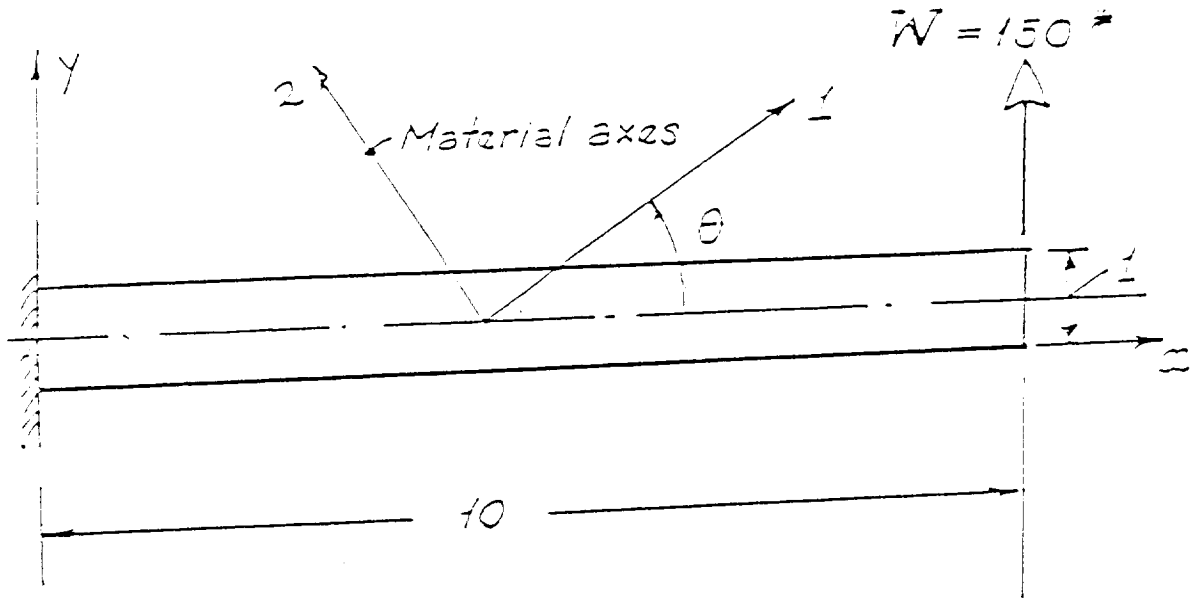

Figure 3.5: Anisotropic cantilever beam with an end load.

E_1 = Young's modulus in direction 1

E_2 = Young's modulus in direction 2

ν_2 = Poisson's ratio

G_{12} = Shear modulus (independent)

θ = angle between material and global axes

For the isotropic case, classical beam theory gives the following expression for the tip deflection:

$$u_{\text{tip}} = \frac{Wl^3}{3EI}. \tag{3.24}$$

We shall use

$$W = 150\text{lb.},\ l = 10",\ E = 3.10^7\text{lb/in}^2,\ I = h^3/12 = \frac{1}{2} \tag{3.25}$$

Then

$$u_{\text{tip}} = .02" \tag{3.26}$$

The assumption of plane stress was made.

(a) Isotropic case

1. Linear quadrilateral elements (4 nodes, 7β, meshes shown in Fig. 3.6)

No. of nodes (elements) (mesh)	u_{tip} (hybrid)/$u_{\text{anal.}}$	u_{tip} (disp.)/$u_{\text{anal.}}$	$\frac{(\sigma_x)_{\max}\text{ (hybrid)}}{(\sigma_x)_{\max}\text{ (anal.)}}$	$\frac{(\sigma_x)_{\max}\text{(disp.)}}{(\sigma_x)_{\max}\text{ (anal.)}}$
22 (10) (A)	0.8815	0.6789	0.7837	0.7036
33 (20) (B)	0.8297	0.7110	0.7442	0.7152
44 (30) (C)	0.8128	1.1578	0.7418	1.2239
63 (40) (D)	0.9690	0.8950	0.9064	0.9176

2. Quadratic quadrilateral elements (8 nodes, 15 β)

No. of nodes (elements)	u_{tip} (hybrid)/$u_{\text{anal.}}$	u_{tip} (disp.)/$u_{\text{anal.}}$	$\frac{(\sigma_x)_{\max}\text{ (hybrid)}}{(\sigma_x)_{\max}\text{ (anal.)}}$	$\frac{(\sigma_x)_{\max}\text{(disp.)}}{(\sigma_x)_{\max}\text{ (anal.)}}$
28 (5)	1.0070	0.9885	0.9841	0.9693

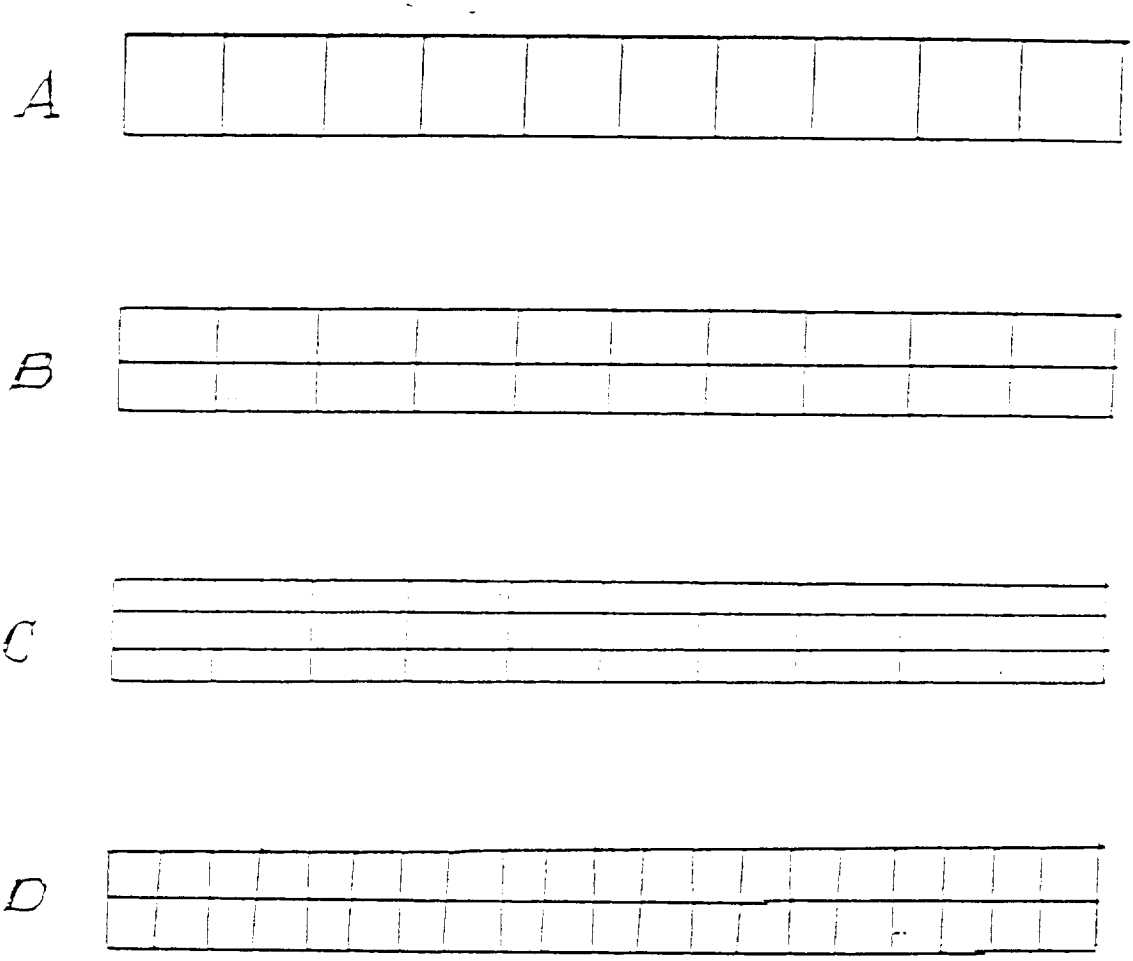

Figure 3.6: Finite element meshes used for testing the two–dimensional hybrid stress models.

A. 10 elements B. 20 elements

C. 30 elements D. 40 elements

(b) Anistropic case

1(a) Linear quadrilateral elements

$$E_1 = 3 \times 10^7 \text{psi}, \qquad \text{E}_2 = 3 \times 50^5 \text{psi}, \text{v}_{12} = 0.3$$

$$G_{12} = 1.1538 \times 10^7 \text{psi}, \quad \theta = 30°$$

No. of nodes (elements)	u_{tip} (hybrid)	u_{tip} (displ.)	$(\sigma_x)_m$ (hybrid)	$(\sigma_x)_m$ (displ.)
63 (40)	0.1136"	0.6271"	6994.3 psi	2353.4 psi

1(b) Quadratic quadrilateral elements

$$\text{No. of nodes } = 28, \theta = 30°, \qquad E_1/E_2 = 100$$

u_{tip} (hybrid)	u_{tip} (displ.)	$(\sigma_x)_m$ (hybrid)	$(\sigma_x)_m$ (displ.)	τ_{xy} (hybrid)	τ_{xy} (displ.)
0.1411"	0.8799	6827.0 psi	6452.8 psi	697.8 psi	419.2 psi

Similarly, for the same values of $E_1, E_2, G_{12}, \nu_{12}$, but for $\theta = 45°$ and $\theta = 0°$, the above cases were run. The results obtained were:

2(a) Linear quadrilateral elements $\theta = 45°$

u_{tip} (hybrid)	u_{tip} (displ.)	$(\sigma_x)_m$ (hybrid)	$(\sigma_x)_m$ (displ.)	τ_{xy} (hybrid)	τ_{xy} (displ.)
0.4049"	0.4131"	6867.2 psi	10174 psi	1362.8 psi	733.3 psi

2(b)Quadratic quadrilateral elements $\theta = 45°$

u_{tip} (hybrid)	u_{tip} (displ.)	$(\sigma_x)_m$ (hybrid)	$(\sigma_x)_m$ (displ.)	τ_{xy} (hybrid)	τ_{xy} (displ.)
0.4964"	0.8831"	6682.0 psi	7844.6 psi	876.3 psi	953.2 psi

3(a)Linear elements $\theta = 0°$

u_{tip} (hybrid)	u_{tip} (displ.)	$(\sigma_x)_m$ (hybrid)	$(\sigma_x)_m$ (displ.)	τ_{xy} (hybrid)	τ_{xy} (displ.)
0.02009"	.018359"	6859.3.0 psi	6314.5 psi	214.6 psi	1019.4 psi

3(b) Quadratic elements $\theta = 0°$

u_{tip} (hybrid)	u_{tip} (displ.)	$(\sigma_x)_m$ (hybrid)	$(\sigma_x)_m$ (displ.)	τ_{xy} (hybrid)	τ_{xy} (displ.)
0.02022"	0.02007"	6804.1 psi	6687 psi	215.2 psi	248.2 psi

The analytic solution for the case with $\theta = 0°$ is

$$\sigma_x = 6971.4 \text{ psi}$$

$$\tau_{xy} = 225 \text{ psi}$$

So, the errors in the hybrid element model are:

$$\sigma_x: 2.4\% \ ; \ \tau_{xy}: 4.4\%$$

and in the displacement model, the errors are

$$\sigma_x: 4.2\% \text{(at best)} \ ; \ \tau_{xy}: 11.1\% \text{ (at best)} .$$

Next, the case of a tapered cantilever beam was considered (see Fig. 3.7). Only the elements that gave reasonably accurate results were used (the quadratic quadrilateral hybrid stress elements), which were compared with the regular displacement type elements. The tip displacement, as determined by elementary beam theory for a uniform load W/length is $u = 4.08 \times 10^{-3}$ inches. Beam theory gives for the bending stress at any point is $\sigma_x = \frac{WLy}{I}$ at that section, and is maximum at the supported end.

(a) Isotropic case – using quadratic quadrilateral elements (8 nodes, 15 β),

No. of nodes (elements)	$\frac{u_{tip}(\text{hybrid})}{u_{tip(\text{anal.})}}$	$\frac{u_{tip}(\text{disp.})}{u_{tip(\text{anal.})}}$	$\frac{\sigma_x \text{hybrid}}{\sigma_x \text{ anal.}}$	$\frac{\sigma_x \text{disp.}}{\sigma_x \text{ anal.}}$
45 (10)	1.0298	1.0164	1.0180	1.0323

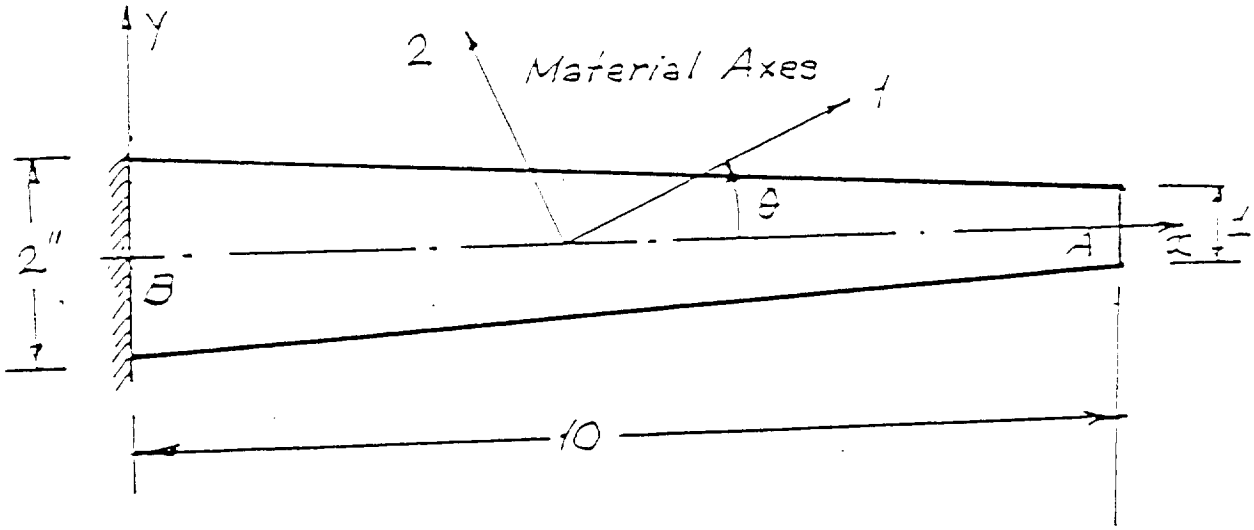

Figure 3.7: Anistropic tapered cantilever subjected to a uniform load.

(b) Anisotropic case – 8 nodes, 15 β elements

$$E_1 = 3 \times 10^7 \text{psi} \;\; ; \;\; E_2/E_1 = 1/100$$

No. of Nodes (elements)	u_{tip} (hybrid)	u_{tip} (displ.)	σ_x hybrid	σ_x displ.
$\theta = 45°$				
45 (10)	0.1060"	0.2012"	2068.0 psi	2636.8 psi
$\theta = 30°$				
45 (10)	0.0315"	0.03876"	1968.5 psi	2076.0 psi
$\theta = 0°$				
45 (10)	0.00423"	0.00419"	2027.3 psi	1999.0 psi

Discussion of Numerical Experiments

For isotropic materials, when the analysis was conducted using four-node quadrilateral elements, neither the hybrid nor the displacement models captured the cubic variation of the displacement until the mesh was sufficiently refined. However, the stresses from the hybrid model were better, though only marginally, since only a linear variation in the stress was used. When quadratic elements were used, the hybrid element model gave excellent results, both for stresses and displacements, as the stress shape function was a complete cubic and was thus able to approximate the bending moment and shear stress very accurately.

For anisotropic materials, although the results obtained using linear and quadratic hybrid models were close, the displacement models gave significantly different results, in both displacements and stresses. This behavior is especially significant when the material axes are inclined to the global axes. While the hybrid element model continues to give excellent stresses, the displacement model gives very poor results.

For a tapered cantilever beam, again, the hybrid model gave better displacements than the displacement model, especially for anisotropic materials with material axes that do not coincide with the global axes.

4 Vibrational Analysis

4.1 A Variational Principle for Dynamic Analysis

The equations for dynamic equilibrium are given by:

$$\sigma_{ij,j} + F_i = r_i \qquad \text{in } V \text{ at all } t \tag{4.1}$$

where r_i = inertia impulse vector.

Equation (4.1) may be written as

$$\delta\left[\int_0^t (\sigma_{ij,j} + F_i - r_i)dt\right] = 0 \tag{4.2}$$

Hence, another way of writing this equation would be

$$\tau_{ij,j} + f_i = r_i \tag{4.3}$$

where $\tau_{ij} = \sigma_{ij}$ and $f_i = F_i$. The tensor τ_{ij} is referred to as the impulse tensor field.

The boundary conditions are prescribed velocities and surface impulses, specified on mutually exclusive regions, i.e.,

$$u_i = u_i \qquad \text{on } s_u \tag{4.4}$$

and

$$\tau_{ij} n_j = b_i \text{ on } s_\tau \tag{4.5}$$

where n_j is the component of the unit normal vector on s_τ.

The strain–displacement relation is

$$\varepsilon_{ij} = \frac{1}{2}(u_{i,j} + u_{j,i}) \tag{4.6}$$

and the kinetic energy function is

$$\hat{U} = \int_V \hat{u}_1(r_i)dV \tag{4.7}$$

while the complementary strain energy is

$$U^* = \int_V u_1^*(\tau_{ij})dV \tag{4.8}$$

where

$$\partial u_1^*/\partial \tau_{ij} = \varepsilon_{ij} \tag{4.9}$$

In linear elasticity,

$$u_1^* = \frac{1}{2} S_{ijkl}\tau_{ij}\tau_{kl} \tag{4.10}$$

Corresponding to Hamilton's principle, we can define a functional as

$$\pi_c = \int_{t_1}^{t_2} \left[\hat{U}(r_i) - U^*(\sigma_{ij,j}) - \int_{s_u} t_i u_i ds \right] dt \tag{4.11}$$

where the assumed stresses must satisfy the equations of motion and the traction (impulse) boundary conditions of s_τ.

In the finite element formulation, equilibrium must be satisfied in each element and on inter-element boundaries so that

$$\pi = \int_{t_1}^{t_2} \sum_p \left[\hat{U}_p - U_p^*(\sigma_{ij,j}) - \int_{s_{uP}} t_i u_i ds - \int_{s_{NP}} u_i t_i ds \right] dt \tag{4.12}$$

where s_{uP} denotes the part of the surface of V_P on which velocities are prescribed and s_{NP} denotes the interelement boundary of V_P, the particular element

$$s_P = s_{uP} + s_{\tau P} + s_{NP} \tag{4.13}$$

so that

$$\pi = \int_{t_1}^{t_2} \sum \left[\hat{U}_p - U_p^* - \int_{S_P} t_i u_i ds - \int_{S_{\tau P}} u_i t_i ds \right] dt \tag{4.14}$$

The admissible surface velocities and the impulses must satisfy the following conditions:

1. Prescribed at arbitrary times t_1 and t_2.
2. Continuous first derivatives for τ_{ij}, continuous m.
3. Equilibrium conditions (dynamic/boundary conditions).

4.2 Formulation of Element Matrices for Dynamic Analysis

For dynamic analysis using the hybrid/displacement models, a consistent mass matrix was generated with a kinetic energy term that was introduced into the energy functional, so that

$$\pi_{\text{dyn}} = \frac{1}{2} \int_V \sigma^T \boldsymbol{S} sig dV - \int_V sig^T \boldsymbol{D} u dV + \int_{s_\sigma} u^T T ds - \int_V \rho \dot{u}^T \dot{u} dV \tag{4.15}$$

When discretized, this becomes

$$\pi_{\text{dyn}} = \sum_n \left[\int_{V_n} \sigma^T S \sigma dV - \int_{V_n} \sigma^T D u dv + \int_{s_\sigma} u^T T ds - \int_{V_n} \rho \dot{u}^T \dot{u} dV \right] \tag{4.16}$$

If $u = Nq$, the kinetic energy term becomes

$$\int_V \rho \dot{q}^T N^T N \dot{q} dV = \dot{q}^T M \dot{q} \tag{4.17}$$

where

$$M = \int_V N^T \rho N |J| d\xi d_\eta \tag{4.18}$$

is the mass matrix for each element.

After the element mass matrices are assembled to form the global mass matrix, the generalized eigenvalue problem

$$Kx = \lambda Mx \tag{4.19}$$

is solved for the first few eigenpairs.

4.3 Numerical Experiments for Hybrid Stress Element Vibrational Analysis

Problem Definition

A cantilever beam is analyzed for its first few natural frequencies (eigenvalues) and mode shapes using both the assumed–displacement and the hybrid–stress method.

A consistent mass is generated and the generalized eigenvalue problem

$$M\ddot{q} + Kq = 0 \tag{4.20}$$

is solved for its eigenpairs, which are the natural frequencies and mode shapes of the physical system. Since the size of the matrices is not very large, a solver from IMSL that determines the eigenvalues and eigenvectors is used instead of the sub–space iteration scheme suggested by Bathe [2].

For Bernoulli-Euler beams composed of isotropic materials (neglecting the effect of shear deformation and rotatory inertia since only the first two modes will be considered where the correction introduced as a result of these effects is small), the equation of motion of transverse vibration is

$$\frac{d^2}{dx^2}\left(EI\frac{d^2u}{dx^2}\right) + \rho A\frac{d^2u}{dt^2} = 0 \tag{4.21}$$

where

u = $u(x,t)$ is the transverse displacement

A = area of cross section of the beam

x = axial distance from the point of support

ρ = mass density of the material

I = centroidal moment of inertia of the cross section

The boundary conditions for the cantilever are:

At the fixed end:

$$u = 0 \quad \text{and} \quad \frac{du}{dx} = 0 \tag{4.22}$$

At the free end:

$$\frac{d^2u}{dx^2} = 0 \quad \text{and} \quad \frac{d^3u}{dx^3} = 0 \tag{4.23}$$

Substituting the boundary conditions into the general solution, we get three homogeneous linear algebraic equations which would give a non-trivial solution only if the determinant of the coefficients vanishes, are derived

$$1 + \cos\ \lambda L\ \cosh \lambda L + 1 = 0 \tag{4.24}$$

which is the characteristic equation whose roots are the eigenvalues λr times length L. A numerical solution alone exists for the above equations, determined by Craig and Bampton. The first few values are

$$\begin{aligned} \lambda_1 L &= 1.8751 \\ \lambda_2 L &= 4.6941 \end{aligned} \tag{4.25}$$

and the natural frequencies for the cantilever are given by

$$\omega_r = \frac{(\lambda_r L)^2}{L^2} \left(\frac{EI}{\rho A}\right)^{\frac{1}{2}} \tag{4.26}$$

so that

$$\omega_1 = \frac{3.516}{L^2} \left(\frac{EI}{\rho A}\right)^{\frac{1}{2}} \tag{4.27}$$

and

$$\omega_2 = \frac{22.03}{L^2} \left(\frac{EI}{\rho A}\right)^{\frac{1}{2}} \tag{4.28}$$

Substituting the numerical values for the given problem results in the following:

$$\omega_1 = 17.58\text{Hz}\ ,\ \omega_2 = 110.15\text{Hz} \tag{4.29}$$

The mode shapes are given by

$$V_r(x) = \cosh(\lambda_4 x) - \cos(\lambda_r x) - k_r[\sinh(\lambda_r x) - \sin(\lambda_r x)] \tag{4.30}$$

where

$$k_r = \frac{\cosh(\lambda_r L) + \cos(\lambda_r L)}{\sinh(\lambda_r L) + \sin(\lambda_r L)} \tag{4.31}$$

as in Craig.

The first two mode shapes for a cantilever in free vibration are shown in Fig. 4.1.

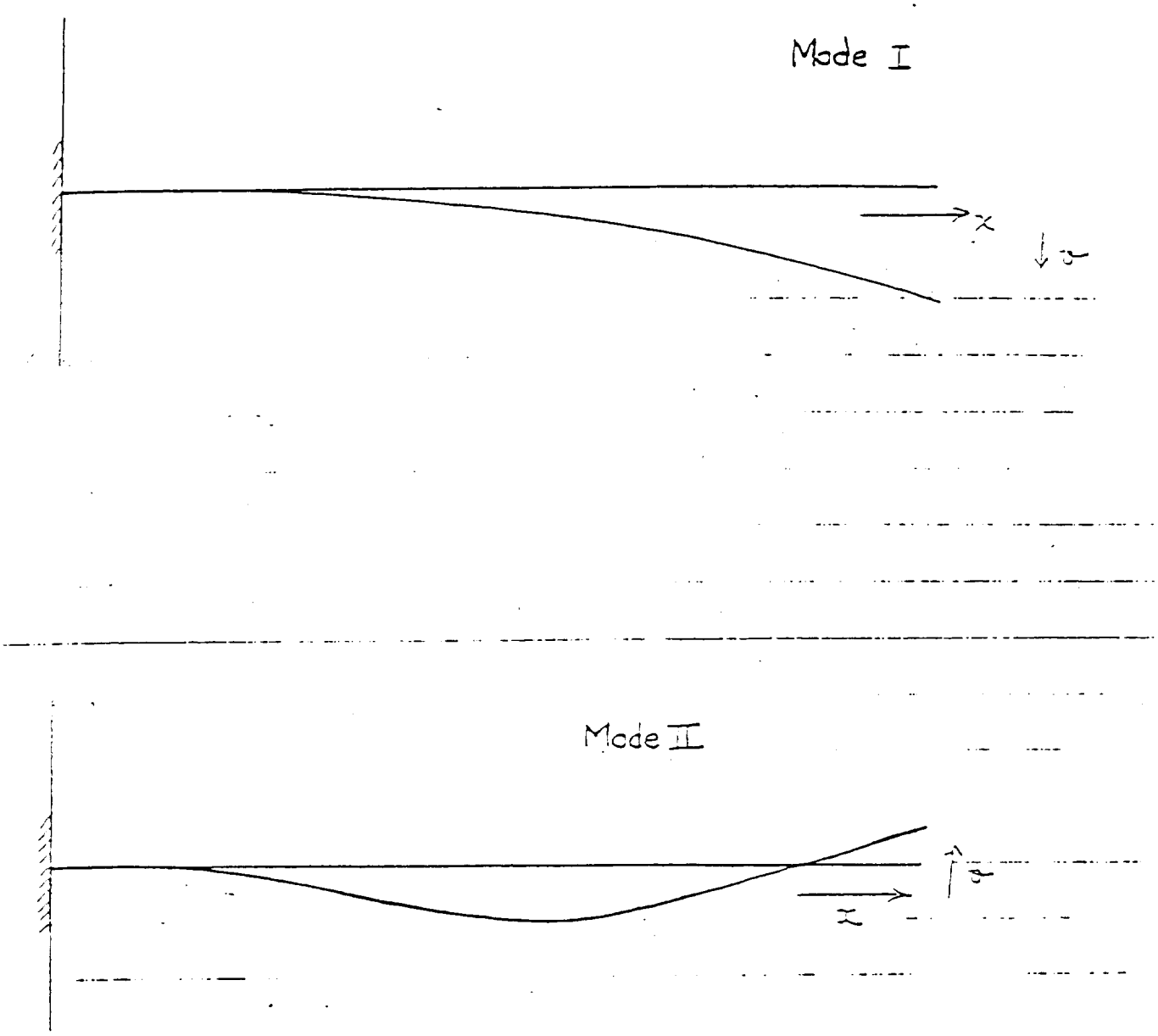

Figure 4.1: Mode shapes of a freely vibrating cantilever beam.

Linear Element Results

The meshes that were used for the static problem are used here, with the number of elements varying from 10 to 80.

The normalized natural frequencies (ω_1 anal./ω_1 f.e. and ω_2 anal./ω_2 f.e.) are plotted against the number of elements, and are shown in Figs. 4.2 and 4.3.

For the isotropic case, the hybrid model converges to the analytical solution faster than the assumed displacement model. The mode shapes however do not seem to vary much, as seen in Fig. 4.4 (for the mesh with 80 elements).

The material model chosen for the anisotropic case is that of cubic syngony with the same properties as in the static case, and the 40 element mesh. The first two natural frequencies, for various angles of rotation of the material axes, using both finite element approximations are tabulated in Table 4.1

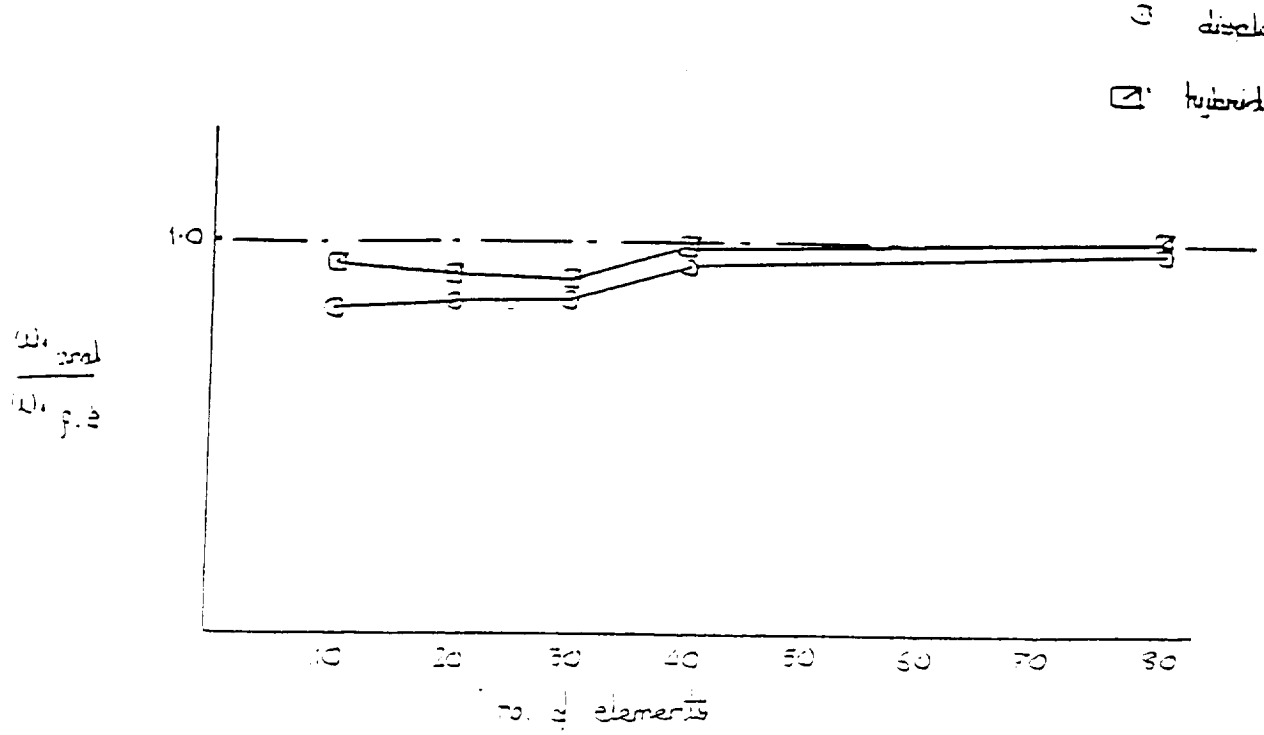

Figure 4.2: Normalized natural frequencies (mode 1 analytical solution vs. mode 1 finite element solution) for various linear element mesh sizes.

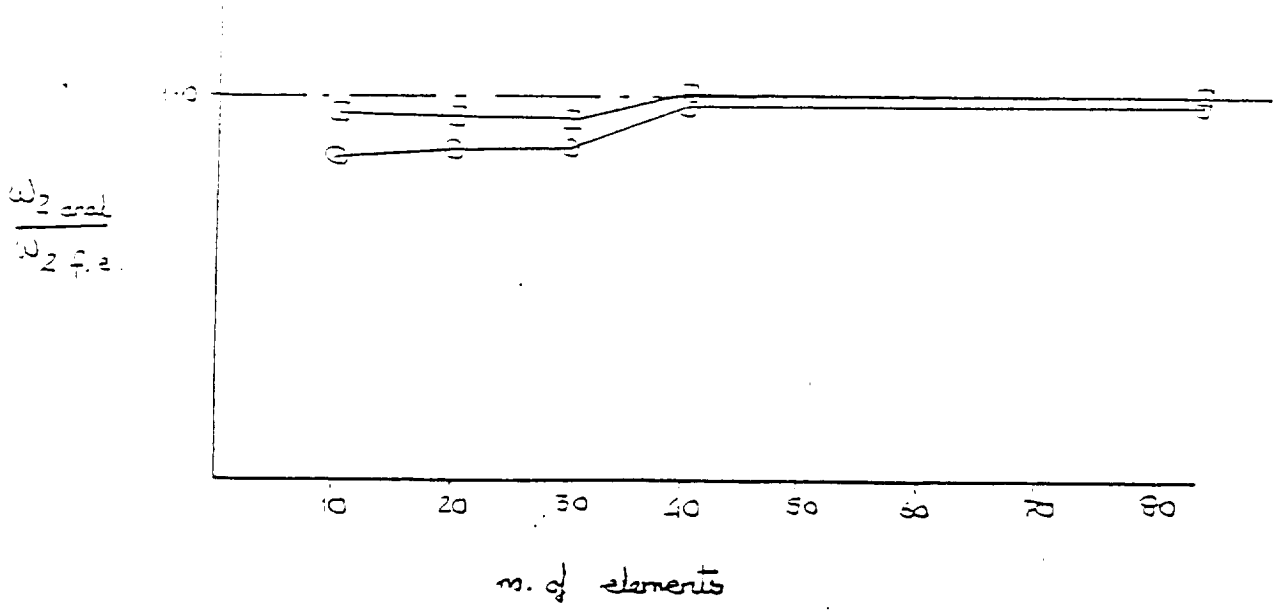

Figure 4.3: Normalized natural frequencies (mode 2 analytical solution vs. mode 2 finite element solution) for various linear element mesh sizes.

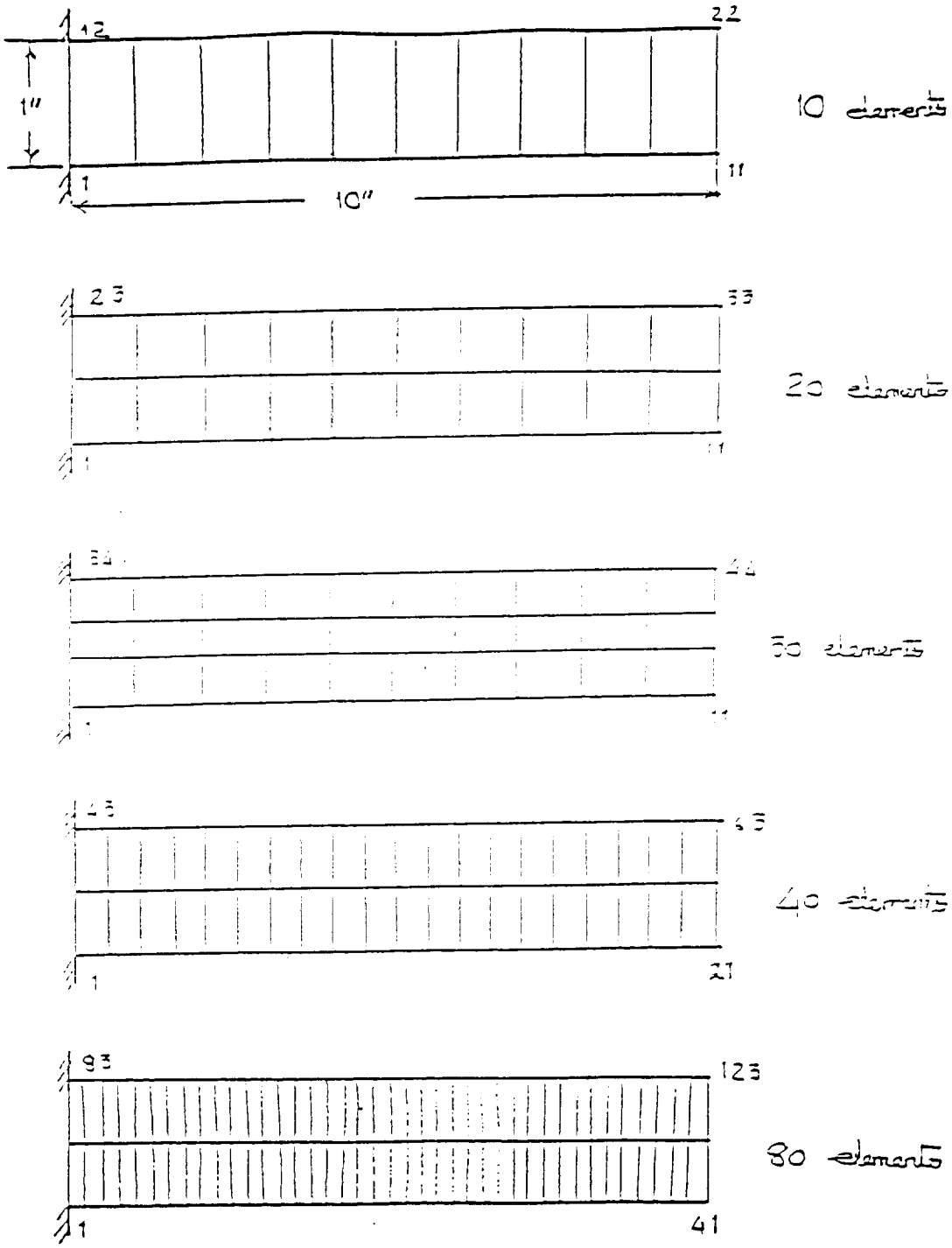

Figure 4.4: Linear quadrilateral finite element meshes used for the numerical experiments with hybrid stress elements and vibration analysis.

TABLE 4.1

Natural frequencies for an anisotropic cantilever beam
using 40 linear elements for different material axes' orientations

Orientation of Axes	ω_1 (hybrid)	ω_1 (displ.)	ω_2 (hybrid)	ω_2 (displ.)
0°	14.351 Hz	14.785 Hz	85.950 Hz	88.341 Hz
30°	13.307 Hz	14.726 Hz	80.673 Hz	88.0945 Hz
45°	12.873 Hz	14.058 Hz	78.379 Hz	85.011 Hz
60°	13.307 Hz	14.547 Hz	80.673 Hz	87.318 Hz
90°	14.351 Hz	14.247 Hz	85.950 Hz	85.934 Hz

From the above table it is observed that the hybrid model gives identical results for a rotation of 90° and no rotation of the material axes, and for 30° and 60° rotations of the axes. The displacement method however gives results that vary, even though the moduli E_1 and E_2 are equal.

Quadratic Element Results

The natural frequencies and mode shapes of the isotropic and anisotropic cantilever beams are now calculated using an eight noded finite element mesh with the number of elements varying from 3 to 20. The meshes used are the same as those for the static case.

The normalized natural frequencies (ω_1 anal./ω_1 f.e. and ω_2 anal./ω_2 f.e.) are plotted against the number of elements, and are shown in Figs. 4.5 and 4.6. Again, it is observed that the hybrid model converges to the analytical solution faster than the assumed-displacement method. The mode shapes however are very similar in both models, except for the maximum "amplitude" (when 20 quadratic elements are used) as shown in Fig. 4.7.

The first two natural frequencies for various angles of rotation of the material axes, in an anisotropic cantilever beam, using both the displacement and hybrid approximations are tabulated in Table 4.2. The material properties and the material model assumed are the same as for the static anisotropic case, i.e., 3 independent constants in a crystal with cubic syngony, where

$$\begin{aligned} E_1 &= E_2 = 1.9716 \times 10^7 \text{lb/in}^2 \\ \nu_{12} &= 0.2875 \\ G_{12} &= 5.4758 \times 10^6 \text{lb/in}^2 \end{aligned} \tag{4.32}$$

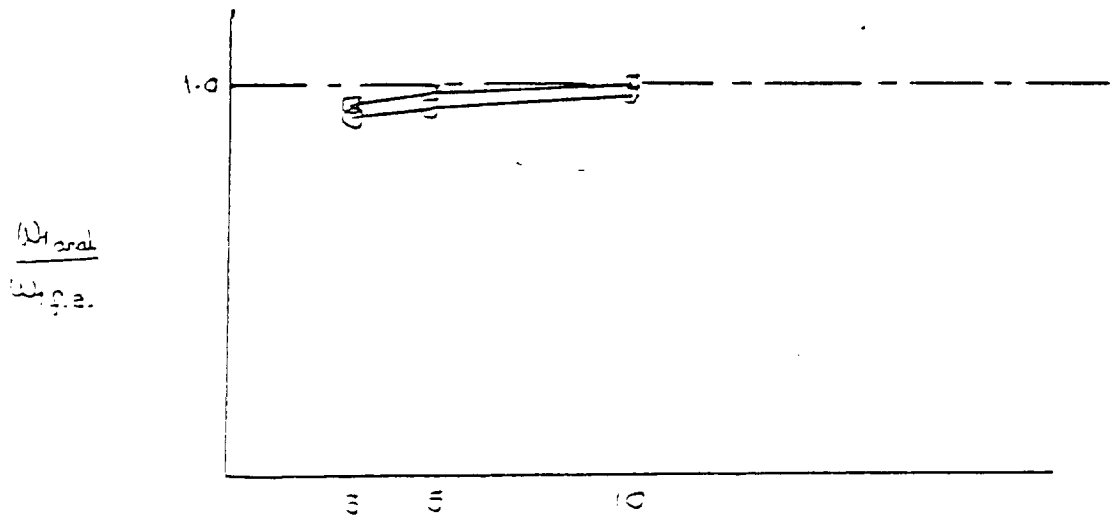

Figure 4.5: Normalized natural frequencies (mode 1 analytical solution vs. mode 1 finite element solution) for various quadratic finite element mesh sizes.

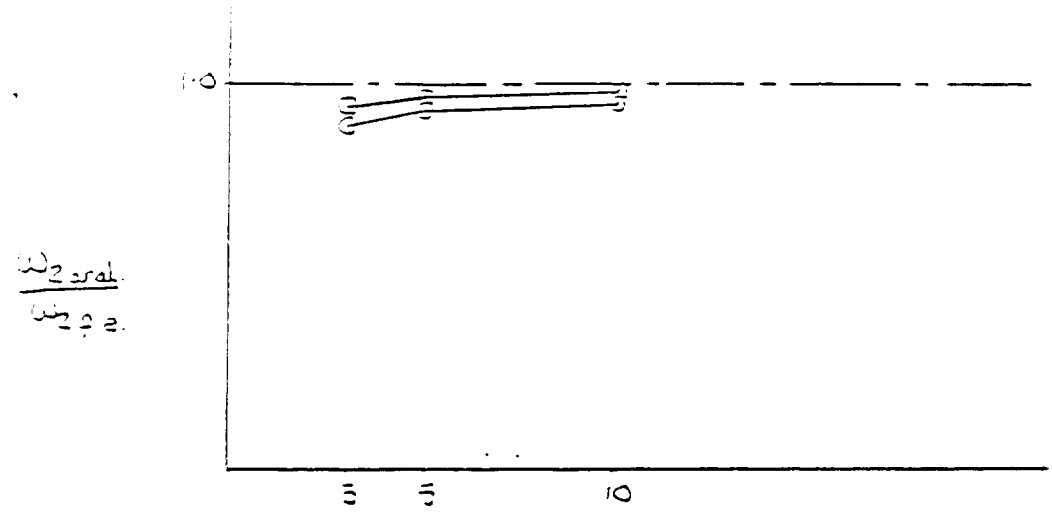

Figure 4.6: Normalized natural frequencies (mode 2 analytical solution vs. mode 2 finite element solution) for various quadratic finite element mesh sizes.

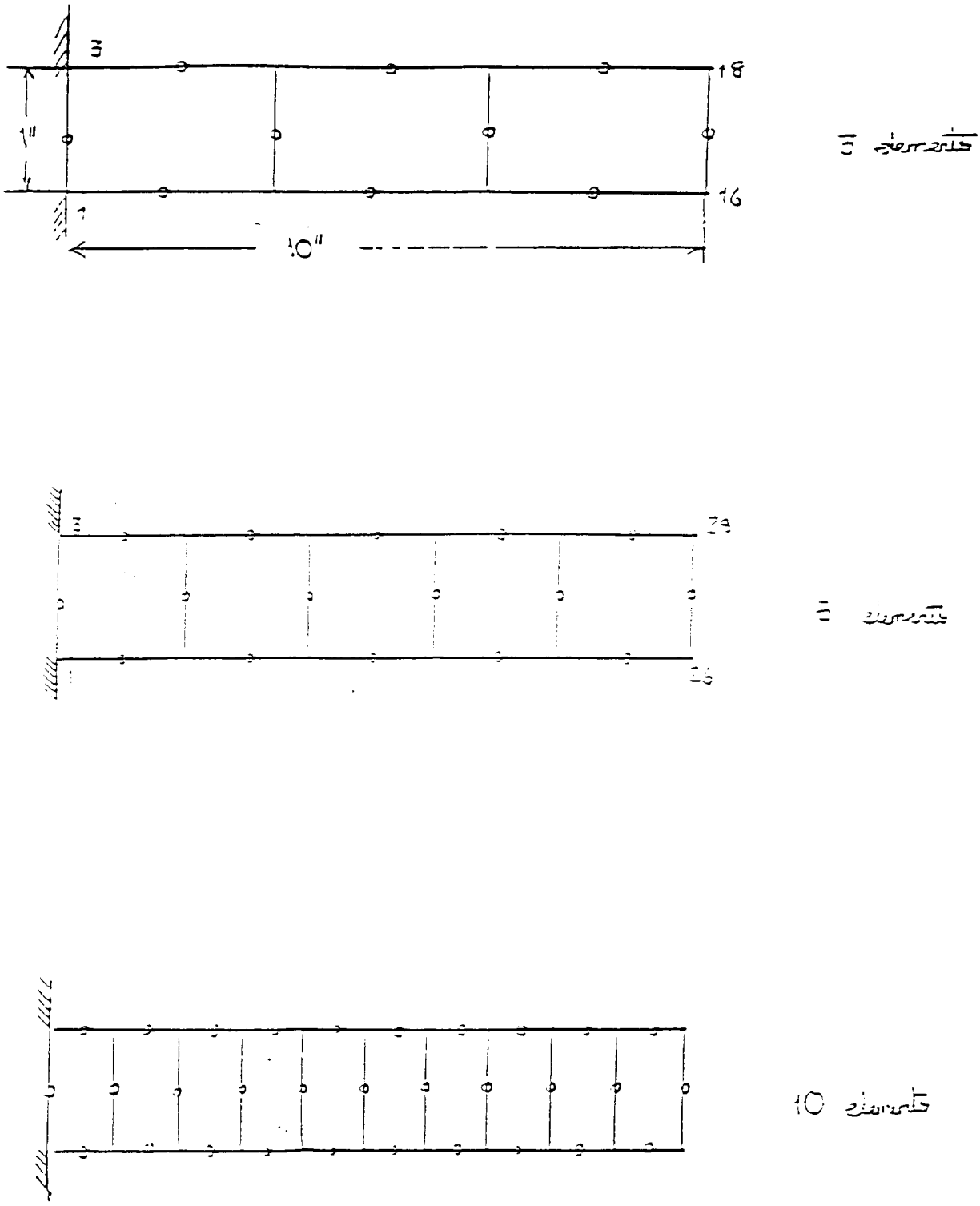

Figure 4.7: Quadratic quadralateral finite element meshes used to study the behavior of hybrid stress elements in vibration analysis.

TABLE 4.2
Natural frequencies for an anisotropic cantilever beam
using 10 quadratic elements for different material axes orientations.

Orientation of the Axes	ω_1 (hybrid)	ω_1 (displ.)	ω_2 (hybrid)	ω_2 (displ.)
0°	14.130 Hz	14.197 Hz	83.675 Hz	84.682 Hz
30°	13.020 Hz	14.061 Hz	78.264 Hz	83.995 Hz
45°	12.679 Hz	13.058 Hz	76.499 Hz	78.911 Hz
60°	13.020 Hz	13.707 Hz	78.264 Hz	82.211 Hz
90°	14.130 Hz	13.276 Hz	83.675 Hz	80.023 Hz

The results of the hybrid model are as expected, with frequencies falling as the angle of rotation is increased, reaching a minimum at a rotation of 45°, and then increasing symmetrically (since $E_1 = E_2$) up to a rotation of 90°.

The results of the displacement model do not show symmetry about $\theta = 45°$, and are not as invariant under a rotation of the axes.

A Specific Numerical Example

A tapered cantilever beam consisting of three crystals of the same material but with different orientations of the material axes is considered next and analyzed for its displacements, stresses, natural frequencies, and mode shapes. The beam is shown in Fig. 4.8. Since the nickel alloy for which experimental data was provided exhibits cubic syngony in its crystals, the same material properties are considered as used in the previous. Also, since of all the elements tested, the 8 noded hybrid–stress element gave the best results, this element is used in the mesh shown in Fig. 4.9.

The following are specifications for the beam:

$\ell = 5$ in; depth at fixed end $= -5$ in; depth at free end $= 1$ in;

static load $= 150$ lb; crystal orientation $= 0°$, $30°$ and $45°$ (see Fig. 4.7).

The results are tabulated below:

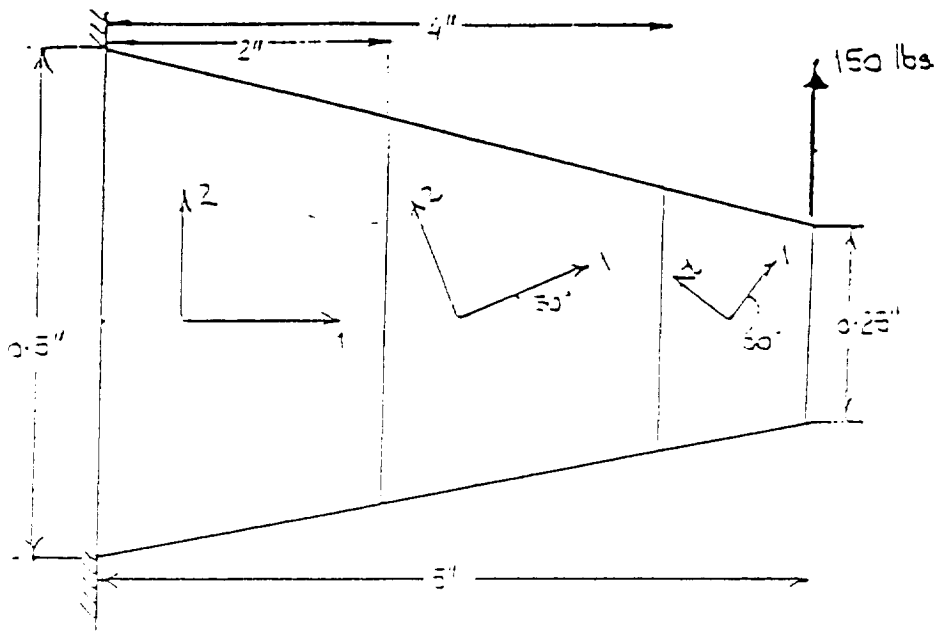

Figure [illegible] A tapered cantilever beam consisting of 3 crystals subjected to a static load.

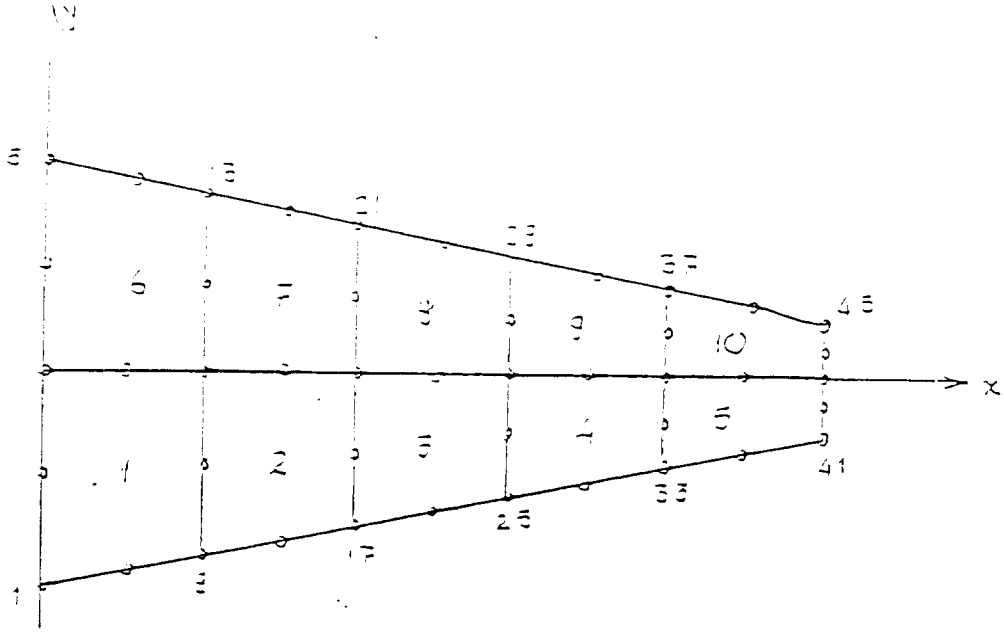

Figure 4.9: Eight noded quadrilateral finite element mesh for the tapered cantilever beam shown in Fig. 4.8.

TABLE 4.3

Comparison of hybrid displacement mode results for a tapered, 3–crystal anisotropic cantilever beam

Parameter	Hybrid Method	Displacement Method
u_{tip}	0.0539 in	0.0502 in
$\sigma_{bending(max)}$	1.632×10^5 psi	1.519×10^4 psi
τ_{max}	1.643×10^5 psi	1.511×10^4 psi
ω_1	30.198 Hz	30.869 Hz
ω_2	131.482 Hz	143.976 Hz

The displacements and stresses differ, at most, by about 6.5%, and the natural frequencies by even less. However, if the 30° rotation is changed to a 60° rotation, all errors increase rapidly to a maximum of almost 12%.

The location of the points of maximum bending and shear stress are predicted accurately by both models, although the predicted magnitudes differ. The maximum bending stress is observed in elements 1,6 while the maximum shear stress is observed in elements 5,10 as the material axes in these two elements are rotated by 45° relative to the global frame.

5 Three–Dimensional Element Definition

The formulation of the three–dimensional hybrid stress elements is identical to the formulation of the two–dimensional elements. The static complementary energy functional, subject to equilibrium conditions, is given by:

$$\pi_{mc} = \sum_n \left\{ \frac{1}{2} \int_{V_n} \sigma^T S \sigma dV - \int_{V_n} \sigma^T (Du) dV + \int_{s_{\sigma n}} u^T T ds \right\} \tag{5.1}$$

The stresses are interpolated using the stress parameters β and the polynomial stress shape function P,

$$\sigma = P\beta \tag{5.2}$$

such that the homogeneous equilibrium conditions are satisfied:

$$D^T \sigma = 0 \tag{5.3}$$

A primary difference between three–dimensional and two–dimensional hybrid stress element calculations is in the calculation of the P matrix in the above equation. As shown by Spilker, et al, in order for an element to be invariant under rotation, the stress interpolation functions must be formed from a complete set of basis functions and the number of independent stress parameters must be equal to or greater than the number of rigid body modes:

$$n_\beta \leq n_F - n_R \tag{5.4}$$

For a quadratic twenty node brick, $n_F = 60$ and $n_R = 6$, so that the minimum number of stress parameters is $60 - 6 = 54$. Not only must there be at least this minimum number of stress parameters, but also the stress interpolation functions must be formed from a complete set of basis functions, in this case, complete polynomials. Complete quadratics would yield a total of 60 stress parameters, but if the stresses are to satisfy equilibrium, the number of stress parameters is reduced to 48, six short of the number required for invariance. Thus, full cubics must be used to calculate the stress interpolation functions. Initially, the P matrix would be:

$$P = \begin{bmatrix} 1 \ldots z^3 & 0 & 0 & 0 & 0 & 0 \\ 0 & 1 \ldots z^3 & 0 & 0 & 0 & 0 \\ 0 & 0 & 1 \ldots z^3 & 0 & 0 & 0 \\ 0 & 0 & 0 & 1 \ldots z^3 & 0 & 0 \\ 0 & 0 & 0 & 0 & 1 \ldots z^3 & 0 \\ 0 & 0 & 0 & 0 & 0 & 1 \ldots z^3 \end{bmatrix} \tag{5.5}$$

where $1 \ldots z^3$ represents a complete cubic polynomial of 20 elements and each zero represents 20 zeros. The P matrix is then a 6×120 matrix and there would be 120 stress parameters.

The number of stress parameters can be reduced by applying the homogeneous equilibrium equations:

$$\begin{aligned} \frac{\partial \sigma_x}{\partial x} + \frac{\partial \tau_{xy}}{\partial y} + \frac{\partial \tau_{xz}}{\partial z} &= 0 \\ \frac{\partial \tau_{xy}}{\partial x} + \frac{\partial \sigma_y}{\partial y} + \frac{\partial \tau_{yz}}{\partial z} &= 0 \\ \frac{\partial \tau_{xz}}{\partial x} + \frac{\partial \tau_{yz}}{\partial y} + \frac{\partial \sigma_z}{\partial z} &= 0 \end{aligned} \tag{5.6}$$

Each of these equations yields a reduced order polynomial with 10 terms. For the equations to be satisfied for arbitrary values of x, y, and z, the coefficients for each term must equal zero. Thus, 30 equations are generated relating the stress parameters to each other and the P matrix is reduced to a 6×90 matrix.

For an isotropic case, the number of stress parameters can be further reduced by applying the Beltrami-Michel stress compatibility equations. These equations are essentially a reformation of the compatibility conditions in terms of the stresses. For the anisotropic case, one must again start with the strain compatibility conditions and reformulate the stress compatibility equations using an anisotropic stress–strain law. The strain compatibility equations are:

$$\begin{aligned} \frac{\partial^2 \varepsilon_x}{\partial y^2} + \frac{\partial^2 \varepsilon_y}{\partial x^2} &= \frac{\partial^2 \gamma_{xy}}{\partial x \partial y} & 2\frac{\partial^2 \varepsilon_x}{\partial y \partial z} &= \frac{\partial}{\partial x}\left(-\frac{\partial \gamma_{yz}}{\partial x} + \frac{\partial \gamma_{xz}}{\partial y} + \frac{\partial \gamma_{xy}}{\partial z} \right) \\ \frac{\partial^2 \varepsilon_y}{\partial z^2} + \frac{\partial^2 \varepsilon_z}{\partial y^2} &= \frac{\partial^2 \gamma_{yz}}{\partial y \partial z} & 2\frac{\partial^2 \varepsilon_y}{\partial x \partial z} &= \frac{\partial}{\partial y}\left(\frac{\partial \gamma_{yz}}{\partial x} - \frac{\partial \gamma_{xz}}{\partial y} + \frac{\partial \gamma_{xy}}{\partial z} \right) \\ \frac{\partial^2 \varepsilon_z}{\partial x^2} + \frac{\partial^2 \varepsilon_x}{\partial z^2} &= \frac{\partial^2 \gamma_{xz}}{\partial x \partial z} & 2\frac{\partial^2 \varepsilon_z}{\partial x \partial y} &= \frac{\partial}{\partial z}\left(\frac{\partial \gamma_{yz}}{\partial x} + \frac{\partial \gamma_{xz}}{\partial y} - \frac{\partial \gamma_{xy}}{\partial z} \right) \end{aligned} \tag{5.7}$$

The stress–strain law for a fully anisotropic material is given by:

$$\varepsilon_i = S_{ij}\sigma_j \tag{5.8}$$

where the compliance matrix S is

$$S = \begin{matrix} a_{11} & a_{12} & a_{13} & a_{14} & a_{15} & a_{16} \\ a_{12} & a_{22} & a_{23} & a_{24} & a_{25} & a_{26} \\ a_{13} & a_{23} & a_{33} & a_{34} & a_{35} & a_{36} \\ a_{14} & a_{24} & a_{34} & a_{44} & a_{45} & a_{46} \\ a_{15} & a_{25} & a_{35} & a_{45} & a_{55} & a_{56} \\ a_{16} & a_{26} & a_{36} & a_{46} & a_{56} & a_{66} \end{matrix} \qquad \text{since } a_{ij} = a_{ji} \tag{5.9}$$

$$\varepsilon_i = S_{ij} P_{jk} \beta_k$$

The stress compatibility equations become

$$\frac{\partial^2 S P_{1k} \beta_k}{\partial y^2} + \frac{\partial^2 S P_{2k} \beta_k}{\partial x^2} = \frac{\partial^2 S P_{4k} \beta_k}{\partial x \partial y} \tag{5.10}$$

$$\vdots$$

Since S is constant, the compliance matrix can be pulled out of the differential, giving

$$S_{i1} \frac{\partial^2 P_{1k} \beta_k}{\partial y^2} + S_{i2} \frac{\partial^2 P_{2k} \beta_k}{\partial x^2} = S_{i4} \frac{\partial^2 P_{4k} \beta_k}{\partial x \partial y} \tag{5.11}$$

$$\vdots$$

This procedure yields six equations, each with four terms. Again, since these equations must be satisfied at all points in the element, each coefficient must be zero and 24 equations are generated to eliminate stress parameters, leaving a total of 66 stress parameters.

The solution for the P matrix can be obtained in closed form for both the constraints due to equilibrium and due to stress compatibility, however, the algebra is quite tedious. This procedure can be accomplished by a series of matrix manipulations on the original P matrix and on the various derivatives of the P matrix. Both the first and second order derivatives must be defined beforehand, and since the position of a particular term (i.e., the xy^2 term) will vary with which derivative is being taken, a careful account of the variables associated with each term in the derivatives is necessary so that the constraint equations can be properly formulated. The P matrix is statically condensed using first the equilibrium constraints and then the stress compatibility constraints resulting in a 6×66 matrix.

Because the number of stress parameters is above the minimum number of 54, the solution may be overly stiff, but this can be determined by a comparison of this fomulation with the 54 stress parameter element of Rubenstein, Arluri, and Punch [20] while using an isotropic material model.

For an eight node brick, $n_F = 24$ while $n_R = 6$, so that the minimum number of stress

parameters n_β is 18. If trilinear stress interpolation functions are used, σ is given by

$$\begin{aligned}
\sigma_x &= \beta_1 + \beta_2 x + \beta_3 y + \beta_4 z \\
\sigma_y &= \beta_5 + \beta_6 x + \beta_7 y + \beta_8 z \\
\sigma_z &= \beta_9 + \beta_{10} x + \beta_{11} y + \beta_{12} z \\
\tau_{xy} &= \beta_{13} + \beta_{14} x + \beta_{15} y + \beta_{16} z \\
\tau_{xz} &= \beta_{17} + \beta_{18} x + \beta_{19} y + \beta_{20} z \\
\tau_{yz} &= \beta_{21} + \beta_{22} x + \beta_{23} y + \beta_{24} z
\end{aligned} \tag{5.12}$$

Introducing σ into the equilibrium equations gives

$$\begin{aligned}
\beta_{20} &= -\beta_2 - \beta_{15} \\
\beta_{24} &= -\beta_{14} - \beta_7 \\
\beta_{23} &= -\beta_{12} - \beta_{18}
\end{aligned} \tag{5.13}$$

Substituting and renumbering yields

$$\begin{aligned}
\sigma_x &= \beta_1 + \beta_2 x + \beta_3 y + \beta_4 z \\
\sigma_y &= \beta_5 + \beta_6 x + \beta_7 y + \beta_8 z \\
\sigma_z &= \beta_9 + \beta_{10} x + \beta_{11} y + \beta_{12} z \\
\tau_{xy} &= \beta_{13} + \beta_{14} x + \beta_{15} y + \beta_{16} z \\
\tau_{xz} &= \beta_{17} + \beta_{18} x + \beta_{19} y - (\beta_2 + \beta_{15}) z \\
\tau_{yz} &= \beta_{20} + \beta_{21} x - (\beta_{12} + \beta_{18}) y - (\beta_7 + \beta_{14}) z
\end{aligned} \tag{5.14}$$

Twenty-one stress parameters remain and thus the element should be free from spurious zero-energy modes.

A minimum stress parameter element from an eight noded brick has been proposed by Punch and Atluri [18]. Here certain symmetries of the elements are assumed and methods of group theory are used to eliminate some of the stress parameters without affecting the rotational invariance of the element. This method is clearly adequate for isotropic materials and may be adequate for materials which, while not isotropic, have high degrees of symmetry, but they are not applicable to fully anisotropic materials.

The stress approximation for this 18β element is given by:

$$\begin{aligned}
\sigma_x &= (\beta_1 + \beta_3) + 2\beta_7 x + \beta_{18} yz \\
\sigma_y &= (\beta_1 + \beta_4 - \beta_3) + 2\beta_8 y + \beta_{17} xz \\
\sigma_z &= (\beta_1 - \beta_4) + 2\beta_9 z + \beta_{16} xy \\
\tau_{xy} &= \beta_{10} + (\beta_{14} - \beta_8)x + (\beta_{13} - \beta_7)y + (\beta_{13} + \beta_7)z \\
\tau_{xz} &= \beta_{11} + (\beta_{15} - \beta_9)x + (\beta_2 + \beta_6)y - (\beta_{13} + \beta_7)z \\
\tau_{yz} &= \beta_{12} + (\beta_2 - \beta_5 - \beta_6)x - (\beta_8 + \beta_9)y - (\beta_9 + \beta_{15})z
\end{aligned} \tag{5.15}$$

The stiffness matrix is calculated as before

$$K = G^T H^{-1} G \tag{5.16}$$

where

$$H = \int_0^1 \int_0^1 \int_0^1 P^T S P |J| d\xi d\eta d\varsigma \tag{5.17}$$

and

$$G = \int_0^1 \int_0^1 \int_0^1 P^T B^* d\xi d\eta d\varsigma \tag{5.18}$$

The calculation of the compliance matrix is made in the material axes and a rotated compliance matrix S is calculated with respect to the global axes. The new terms are given by:

$$a'_{ij} = \sum_m \sum_n a_{mn} q_{im} q_{jn} \tag{5.19}$$

where a_{mn} are the components of the compliance matrix in the material axis and the q_{im} and q_{jn} are functions of the direction cosines relating to the material and global axes.

6 Alternate Hybrid Stress Element Formulations

6.1 The Eight–Node Punch and Alturi Brick Element

An alternative approach to the assumed stress field was proposed by Punch and Alturi. The basic hybrid stress model is developed in the same manner as previously outlined regardless of the form of stress interpolation. The Punch and Alturi approach is based upon symmetry group theory. The method defines a set of 'natural' irreducible strain subspaces which are invariant to element translation and to the 24 symmetric rotations of a cube. For each such strain space, at least one stress space must be defined which is also invariant. For an eight node brick, there are eighteen natural strain subspaces along with six rigid body modes. A minimum of 18 independent stress subspaces are required. If complete quadratic functions are used to generate the equilibrated stress subspaces, a total of 48 stress subspaces are created. Using all 48 subspaces would be equivalent to using complete polynomials and eliminating 12 of the resulting 60 stress parameters by applying equilibrium constraints.

The difference with this formulation and those given earlier is that here each stress parameter is related to an invariant subspace rather than to an individual term in an equilibrated complete polynomial. Thus, any stress parameter can be removed without affecting the invariance of the resulting element. After the parameter is deleted, the rank of the resulting stress function matrix, G, must be at least 18. Certain linear terms must be included, but most of the quadratic terms can be eliminated without affecting the rank of G. However, once subspaces are removed, the resulting G matrix is composed of incomplete polynomials, and may no longer contain all of the cardinal stress states of pure bending. Therefore, the resulting element must be evaluated to be sure that the bending stiffness is adequate.

For a least order formulation, these stress subspaces are presented below as second order tensors in 3–space:

$$
\begin{aligned}
\sigma_1 &= \begin{bmatrix} 1 & 0 & 0 \\ 0 & 1 & 0 \\ 0 & 0 & 1 \end{bmatrix} \beta_1 \\
\sigma_2^{(1)} &= \begin{bmatrix} 0 & z & y \\ z & 0 & x \\ y & x & 0 \end{bmatrix} \beta_2 \\
\sigma_3^{(1)} &= \begin{bmatrix} 1 & 0 & 0 \\ 0 & -1 & 0 \\ 0 & 0 & 0 \end{bmatrix} \beta_3 + \begin{bmatrix} 0 & 0 & 0 \\ 0 & 1 & 0 \\ 0 & 0 & -1 \end{bmatrix} \beta_4 \\
\sigma_3^{(2)} &= \begin{bmatrix} 0 & z & 0 \\ z & 0 & -x \\ 0 & -x & 0 \end{bmatrix} \beta_5 + \begin{bmatrix} 0 & 0 & y \\ 0 & 0 & -x \\ y & -x & 0 \end{bmatrix} \beta_6 \\
\sigma_4^{(2)} &= \begin{bmatrix} 2x & -y & -z \\ -y & 0 & 0 \\ -z & 0 & 0 \end{bmatrix} \beta_7 + \begin{bmatrix} 0 & -x & 0 \\ -x & 2y & -z \\ 0 & -z & 0 \end{bmatrix} \beta_8 + \begin{bmatrix} 0 & 0 & -x \\ 0 & 0 & -y \\ -x & -y & 2z \end{bmatrix} \beta_9 \\
\sigma_5^{(1)} &= \begin{bmatrix} 0 & 1 & 0 \\ 1 & 0 & 0 \\ 0 & 0 & 0 \end{bmatrix} \beta_{10} + \begin{bmatrix} 0 & 0 & 1 \\ 0 & 0 & 0 \\ 1 & 0 & 0 \end{bmatrix} \beta_{11} + \begin{bmatrix} 0 & 0 & 0 \\ 0 & 0 & 1 \\ 0 & 1 & 0 \end{bmatrix} \beta_{12} \\
\sigma_5^{(3)} &+ \begin{bmatrix} y & 0 & 0 \\ 0 & 0 & 0 \\ 0 & 0 & -y \end{bmatrix} \beta_{13} + \begin{bmatrix} 0 & 0 & 0 \\ 0 & x & 0 \\ 0 & 0 & -x \end{bmatrix} \beta_{14} + \begin{bmatrix} z & 0 & 0 \\ 0 & -z & 0 \\ 0 & 0 & 0 \end{bmatrix} \beta_{15} \\
\sigma_5^{(4)} &= \begin{bmatrix} 0 & 0 & 0 \\ 0 & 0 & 0 \\ 0 & 0 & xy \end{bmatrix} \beta_{16} + \begin{bmatrix} 0 & 0 & 0 \\ 0 & xz & 0 \\ 0 & 0 & 0 \end{bmatrix} \beta_{17} + \begin{bmatrix} yz & 0 & 0 \\ 0 & 0 & 0 \\ 0 & 0 & 1 \end{bmatrix} \beta_{18}
\end{aligned}
\tag{6.1}
$$

The corresponding stress space function matrix is given below:

$$
\begin{bmatrix} \sigma_x \\ \sigma_y \\ \sigma_z \\ \tau_{xy} \\ \tau_{xz} \\ \tau_{yz} \end{bmatrix}
\begin{bmatrix}
1 & 0 & 1 & 0 & 0 & 0 & 2x & 0 & 0 & 0 & 0 & 0 & y & 0 & z & 0 & 0 & yz \\
1 & 0 & -1 & 1 & 0 & 0 & 0 & 2y & 0 & 0 & 0 & 0 & 0 & x & -z & 0 & xz & 0 \\
1 & 0 & 0 & -1 & 0 & 0 & 0 & 0 & 2z & 0 & 0 & 0 & -y & -x & 0 & xy & 0 & 0 \\
0 & z & 0 & 0 & z & 0 & -y & -x & 0 & 1 & 0 & 0 & 0 & 0 & 0 & 0 & 0 & 0 \\
0 & y & 0 & 0 & 0 & y & -z & 0 & -x & 0 & 1 & 0 & 0 & 0 & 0 & 0 & 0 & 0 \\
0 & x & 0 & 0 & -x & -x & 0 & -z & -y & 0 & 0 & 1 & 0 & 0 & 0 & 0 & 0 & 0
\end{bmatrix}
\begin{bmatrix} \beta_1 \\ \beta_2 \\ \cdot \\ \cdot \\ \cdot \\ \beta_{18} \end{bmatrix}
\tag{6.2}
$$

This element performs well in tension, pure shear, and pure bending with isotropic material properties. It also performs well in both tension and pure shear with fully anisotropic material properties as long as the loads are applied separately and along the axis of a cubic

element. When the loads are combined, the performance begins to degrade. However, exact solutions of the stresses and strains in these combined loading situations must be completed before the full extent of the degradation can be determined.

One additional problem exists with this element. The formulation of the stress and strain subspaces was based upon the symmetric transformations of a cube. As the geometry of the element is distorted, the performance of the element is degraded. A similar degradation may occur if the anisotropy of the material is increased, especially when non–symmetric loads are applied. It should be noted, though, that in most cases these elements give better results than eight noded displacement elements, although the computational effort is significantly greater.

6.2 The Twenty Node Punch and Alturi Brick Element

A twenty node hybrid element has been developed based upon the work of Punch and Atluri. This element uses the same lines and quadratic terms that are used for the eight node element described above, but adds six linear terms, eighteen quadratic terms, and twelve cubic terms for a total of 54 stress parameters. The following stress subspaces make up the twenty node elements:

Linear Terms

$$
\begin{aligned}
\Gamma_1 : \sigma_1^{(1)} &= \begin{bmatrix} 1 & 0 & 0 \\ 0 & 1 & 0 \\ 0 & 0 & 1 \end{bmatrix} \beta_1 \\
\Gamma_2 : \sigma_2^{(1)} &= \begin{bmatrix} 0 & z & y \\ z & 0 & x \\ y & x & 0 \end{bmatrix} \beta_2 \\
\Gamma_3 : \sigma_3^{(1)} &= \begin{bmatrix} 1 & 0 & 0 \\ 0 & -1 & 0 \\ 0 & 0 & 0 \end{bmatrix} \beta_3 + \begin{bmatrix} 0 & 0 & 0 \\ 0 & 1 & 0 \\ 0 & 0 & -1 \end{bmatrix} \beta_4 \\
\sigma_3^{(2)} &= \begin{bmatrix} 0 & z & 0 \\ z & 0 & -x \\ 0 & -x & 0 \end{bmatrix} \beta_5 + \begin{bmatrix} 0 & 0 & y \\ 0 & 0 & -x \\ y & -x & 0 \end{bmatrix} \beta_6 \\
\Gamma_4 : \sigma_4^{(1)} &= \begin{bmatrix} y & 0 & 0 \\ 0 & 0 & 0 \\ 0 & 0 & y \end{bmatrix} \beta_7 + \begin{bmatrix} 0 & 0 & 0 \\ 0 & x & 0 \\ 0 & 0 & x \end{bmatrix} \beta_8 + \begin{bmatrix} z & 0 & 0 \\ 0 & z & 0 \\ 0 & 0 & 0 \end{bmatrix} \beta_9 \\
\sigma_4^{(2)} &= \begin{bmatrix} 2x & -y & -z \\ -y & 0 & 0 \\ -z & 0 & 0 \end{bmatrix} \beta_{19} + \begin{bmatrix} 0 & -x & 0 \\ -x & 2y & -z \\ 0 & -z & 0 \end{bmatrix} \beta_{20} + \begin{bmatrix} 0 & 0 & -x \\ 0 & 0 & -y \\ -x & -y & 2z \end{bmatrix} \beta_{21} \\
\Gamma_5 : \sigma_5^{(1)} &= \begin{bmatrix} 0 & 1 & 0 \\ 1 & 0 & 0 \\ 0 & 0 & 0 \end{bmatrix} \beta_{10} + \begin{bmatrix} 0 & 0 & 1 \\ 0 & 0 & 0 \\ 1 & 0 & 0 \end{bmatrix} \beta_{11} + \begin{bmatrix} 0 & 0 & 0 \\ 0 & 0 & 1 \\ 0 & 1 & 0 \end{bmatrix} \beta_{12} \\
\sigma_5^{(2)} &= \begin{bmatrix} y & 0 & 0 \\ 0 & 0 & 0 \\ 0 & 0 & -y \end{bmatrix} \beta_{13} + \begin{bmatrix} 0 & 0 & 0 \\ 0 & x & 0 \\ 0 & 0 & -x \end{bmatrix} \beta_{14} + \begin{bmatrix} z & 0 & 0 \\ 0 & -z & 0 \\ 0 & 0 & 0 \end{bmatrix} \beta_{15} \\
\sigma_5^{(3)} &= \begin{bmatrix} 0 & y & z \\ y & 0 & 0 \\ -z & 0 & 0 \end{bmatrix} \beta_{22} + \begin{bmatrix} 0 & x & 0 \\ x & 0 & -z \\ 0 & -z & 0 \end{bmatrix} \beta_{23} + \begin{bmatrix} 0 & 0 & x \\ 0 & 0 & -y \\ x & -y & 0 \end{bmatrix} \beta_{24}
\end{aligned}
\tag{6.3}
$$

Quadratic Terms

$$
\begin{aligned}
\Gamma_1 : \sigma_1^{(2)} &= \begin{bmatrix} x^2 & -xy & -xz \\ -xy & y^2 & -yz \\ -xz & -yx & z^2 \end{bmatrix} \beta_{25} \\
\Gamma_2 : \sigma_2^{(2)} &= \begin{bmatrix} -y^2+z^2 & 0 & 0 \\ 0 & x^2-z^2 & 0 \\ 0 & 0 & -x^2+y^2 \end{bmatrix} \beta_{26} \\
\Gamma_3 : \sigma_3^{(4)} &= \begin{bmatrix} 2(y^2-z^2) & 0 & 0 \\ 0 & -(z^2-x^2) & 0 \\ 0 & 0 & -(x^2-y^2) \end{bmatrix} \beta_{27} + \begin{bmatrix} -(y^2-z^2) & 0 & 0 \\ 0 & 2(z^2-x^2) & 0 \\ 0 & 0 & -(x^2-y^2) \end{bmatrix} \beta_{28} \\
\sigma_3^{(5)} &= \begin{bmatrix} 0 & -2xy & 2xz \\ -2xy & y^2 & 0 \\ 2xz & 0 & -z^2 \end{bmatrix} \beta_{29} + \begin{bmatrix} x^2 & 0 & -2xz \\ 0 & -y^2 & 2yz \\ -2xz & 2yz & 0 \end{bmatrix} \beta_{30} \\
\Gamma_4 \sigma_4^{(3)} &= \begin{bmatrix} 2xy & (x^2-y^2) & 0 \\ (x^2-y^2) & -2xy & 0 \\ 0 & 0 & 0 \end{bmatrix} \beta_{31} + \begin{bmatrix} 2xz & 0 & (x^2-z^2) \\ 0 & 0 & 0 \\ (x^2-z^2) & 0 & -2xz \end{bmatrix} \beta_{32} \\
&\quad + \begin{bmatrix} 0 & 0 & 0 \\ 0 & 2yz & (y^2-z^2) \\ 0 & (y^2-z^2) & -2yz \end{bmatrix} \beta_{33} \\
\sigma_4^{(4)} &= \begin{bmatrix} 0 & 2xz & -2xy \\ 2xz & 0 & (y^2-z^2) \\ -2xy & (y^2-z^2) & 0 \end{bmatrix} \beta_{34} + \begin{bmatrix} 0 & -2yz & (z^2-x^2) \\ -2yz & 0 & 2xy \\ (z^2-x^2) & 2xy & 0 \end{bmatrix} \beta_{35} \\
&\quad + \begin{bmatrix} 0 & (x^2-y^2) & 2yz \\ (x^2-y^2) & 0 & -2xz \\ 2yz & -2xz & 0 \end{bmatrix} \beta_{36} \\
\Gamma_5 : \sigma_5^{(5)} &= \begin{bmatrix} 0 & 0 & 0 \\ 0 & 0 & x^2 \\ 0 & x^2 & 0 \end{bmatrix} \beta_{37} + \begin{bmatrix} 0 & 0 & y^2 \\ 0 & 0 & 0 \\ y^2 & 0 & 0 \end{bmatrix} \beta_{38} \\
&\quad + \begin{bmatrix} 0 & z^2 & 0 \\ z^2 & 0 & 0 \\ 0 & 0 & 0 \end{bmatrix} \beta_{39}
\end{aligned}
\tag{6.4}
$$

$$\sigma_5^{(6)} = \begin{bmatrix} 0 & 0 & 0 \\ 0 & 0 & 0 \\ 0 & 0 & xy \end{bmatrix} \beta_{16} + \begin{bmatrix} 0 & 0 & 0 \\ 0 & xz & 0 \\ 0 & 0 & 0 \end{bmatrix} \beta_{17} + \begin{bmatrix} yz & 0 & 0 \\ 0 & 0 & 0 \\ 0 & 0 & 0 \end{bmatrix} \beta_{18}$$

$$\sigma_5^{(7)} = \begin{bmatrix} 2xy & -(x^2+y^2) & 0 \\ -(x^2+y^2) & 2xy & 0 \\ 0 & 0 & 0 \end{bmatrix} \beta_{40} + \begin{bmatrix} 2xz & 0 & -(x^2+z^2) \\ 0 & 0 & 0 \\ -(x^2+z^2) & 0 & 2xz \end{bmatrix} \beta_{41} + \begin{bmatrix} 0 & 0 & 0 \\ 0 & 2yz & -(y^2+z^2) \\ 0 & -(y^2+z^2) & 2yz \end{bmatrix} \beta_{42}$$

Cubic Terms

$$
\begin{aligned}
\Gamma_2 : \sigma_2^{(4)} &= \begin{bmatrix} -4xyz & z(x^2+y^2) & y(x^2+z^2) \\ z(x^2+y^2) & -4xyz & x(y^2+z^2) \\ y(x^2+z^2) & x(y^2+z^2) & -4xyz \end{bmatrix} \beta_{43} \\
\Gamma_3 : \sigma_3^{(8)} &= \begin{bmatrix} 0 & -z(2x^2+y^2) & y(2x^2+z^2) \\ -z(2x^2+y^2) & 6xyz & x(y^2-z^2) \\ y(2x^2+z^2) & x(y^2-z^2) & -6xyz \end{bmatrix} \beta_{44} + \begin{bmatrix} -6xyz & z(y^2-x^2) & y(x^2+2z^2) \\ z(y^2-x^2) & 6xyz & -x(y^2+2z^2) \\ y(x^2+2z^2) & -x(y^2+2z^2) & 0 \end{bmatrix} \beta_{45} \\
\Gamma_4 : \sigma_4^{(6)} &= \begin{bmatrix} yz^2 & 0 & 0 \\ 0 & 0 & 0 \\ 0 & 0 & x^2y \end{bmatrix} \beta_{46} + \begin{bmatrix} 0 & 0 & 0 \\ 0 & xz^2 & 0 \\ 0 & 0 & xy^2 \end{bmatrix} \beta_{47} \\
&\quad + \begin{bmatrix} zy^2 & 0 & 0 \\ 0 & zx^2 & 0 \\ 0 & 0 & 0 \end{bmatrix} \beta_{48} \\
\sigma_4^{(7)} &= \begin{bmatrix} 2x^3 & -3x^2y & -3x^2z \\ -3x^2y & 0 & 6xyz \\ -3x^2z & 6xyz & 0 \end{bmatrix} \beta_{49} + \begin{bmatrix} 0 & -3xy^2 & 6xyz \\ -3xy^2 & 2y^3 & -3y^2z \\ 6xyz & -3y^2z & 0 \end{bmatrix} \beta_{50} \\
&\quad + \begin{bmatrix} 0 & 6xyz & -3xz^2 \\ 6xyz & 0 & -3yz^2 \\ -3xz^2 & -3yz^2 & 2z^3 \end{bmatrix} \beta_{51} \\
\Gamma^5 : \sigma_5^{(12)} &= \begin{bmatrix} -yz^2 & 0 & 0 \\ 0 & 0 & 0 \\ 0 & 0 & yx^2 \end{bmatrix} \beta_{52} + \begin{bmatrix} 0 & 0 & 0 \\ 0 & -xz^2 & 0 \\ 0 & 0 & xy^2 \end{bmatrix} \beta_{53} \\
&\quad + \begin{bmatrix} -zy^2 & 0 & 0 \\ 0 & zx^2 & 0 \\ 0 & 0 & 0 \end{bmatrix} \beta_{54}
\end{aligned}
\tag{6.5}
$$

The twenty node hybrid element has an H matrix of rank 54 which must be invertible. The H matrix is given by

$$H = \sum_{i=1}^{L} P^T S P$$

where L is the number of integration points. The matrix S is of rank six so that a minimum of nine integration points is required for H to be of full rank and thus invertible. Without *a priori* knowledge of the mesh, the integration scheme must be symmetric. Using a Gaussian quadrature, this requires 27 integration points (i.e., $3 \times 3 \times 3$), and consequently the computational effort is 3 times what is actually required. Irons has implemented on a 14 point integration scheme, which is basically a $2 \times 2 \times 2$ scheme with an additional integration point at the center of each face of the hexahedral element. This integration scheme gave identical results to five decimal places to the Gaussian quadrature scheme with essentially

60% of the computational effort. A $2 \times 2 \times 2$ integration scheme was also formulated with an additional integration point at the center of the hexahedral element for a total of nine integration points, the minimum number required. The stress space function matrix for the 54 term model is shown below.

6.3 The 42 Parameter Hybrid Stress Brick Element

An alternative element which does not suffer from these symmetry-related problems was also developed. Complete polynomial stress functions are used and equilibrium constraints are applied, yielding a 48-parameter element. The strain compatibility equations are then satisfied using a fully anisotropic material model. This constraint reduces the number of stress parameters to 42. This is an inordinately large number of stress parameters and may yield an overly stiff element, but it may also yield an element that is far less sensitive to distortion and anisotropy.

While the calculations for the polynomials can be derived in closed form, the algebra is extremely tedious. However, the constraint equations can be formed as a set of matrices showing the initial relationship between the stress parameters as derived from the equilibrium equations and the stress compatibility.

The equilibrium constraint matrix contains only constants while the compatibility constraint matrix contains ratios of the compliance matrix constants. The constraint matrices are first internally reduced eliminating the constrained parameters from the constraint matrices. The P matrix initially contains only the complete basis functions as:

$$\begin{matrix} P & 0 & & 0 \\ 0 & P & & 0 \\ 0 & 0 & & 0 \\ 0 & 0 & \ldots & 0 \\ 0 & 0 & & 0 \\ 0 & 0 & & P \end{matrix} \tag{6.6}$$

where P represents the following 10 terms for the eight node element:

$$1 \quad 2x \quad 2y \quad 2z \quad x^2 \quad 2xy \quad 2xz \quad y^2 \quad 2yz \quad z^2 \tag{6.7}$$

and each 0 represents 10 zeros. For the eight node element, P is initially a 6×60 matrix, while for the twenty node element, full cubic basis functions are required so that the P matrix is 6×120. For the eight node element, there are 12 equilibrium constraint equations and six compatability constraint equations, while for the twenty node element there are 30 equilibrium constraints and 24 compatibility constraints.

The elements of the P matrix are functions of position, therefore, the P matrix must be calculated for each integration point and then the constraint equations are used to eliminate the constrained stress parameters. The P matrix is then statically condensed to yield a 6×42 matrix for the eight node element and a 6×66 matrix for the twenty node element.

6.4 Numerical Experiments

The eight node and twenty node hybrid elements were compared to the standard displacement elements for both single elements and for a six element beam. The single elements were tested in pure tension, pure shear, bending, and torsion using both isotropic and anisotropic properties. As is shown in Table 6.1, all elements gave exact solutions for pure tension and pure shear with isotropic material properties. For pure bending, the eight node displacement element is overly stiff but all of the hybrid elements again gave exact results. None of the elements is able to give exact results for torsion, but the hybrid elements perform as well or better than the corresponding displacement element.

Table 6.1. Displacements Produced by Cardinal Stress States for Isotropic Material Properties

Element	Pure Tension	Pure Shear	Pure Bending	Pure Tortion
DM 8	100	100	67	84
H8-42	100	100	100	84
H8-18	100	100	100	84
DM 20	100	100	100	95
H20-54	100	100	100	102

As the degree of anisotropy is increased, the performance of the displacement elements decreases. Table 6.2 shows information equivalent to Table 6.1 for anisotropic material properties. Here the ratio of E_{11}/E_{33} is 3 and the material axis is rotated with respect to the element axis by the direction cosines given below:

Direction Cosines:

.5774	.574	.5774
.7071	-.7071	.0000
-.4082	-.4082	.8165

Both of the displacement elements show deterioration in bending and torsion as the degree of anisotropy increases although the degradation is less for the twenty node element.

Table 6.2. Displacements Produced by Cardinal Stress States for Anisotropic Material Properties

Element	Pure Tension	Pure Shear	Pure Bending	Pure Torsion
DM 8	100	100	46	76
H8-42	100	100	100	84
H8-18	100	100	100	84
DM 20	100	100	97	92
H20-54	100	100	100	95

These calculations were performed using double precision for all real variable calculations. The result for the twenty node elements were compared for three integration rules: a $4 \times 4 \times 4$, a $3 \times 3 \times 3$, and the 14 point rule proposed by Irons [7]. The differences in results were less than one percent. Spilker [22] stated that the 14 point rule produced some ill conditioning of H but no such ill conditioning was detected in these runs. Consequently the 14 point rule was used for all subsequent calculations except for occasional checks to assure that the results were indeed the same for the 14 point and $3 \times 3 \times 3$ rules.

A six element cantilever beam was analyzed using both eight node and twenty node bricks. These beams are shown in Fig. 6.1. The beams were analyzed both with a pure moment loading and a uniform end shear and for isotropic material properties as well as a series of anisotropic material properties. Figure 6.2 shows the normalized tip displacement for a pure moment load with eight node bricks as a function of the degree of anisotropy where the degree of anisotropy is given by the ratio of the Young's moduli in the primary material axes. Figure 6.3 shows the normalized tip displacement of the cantilever beam for uniform end shear as a function of the degree of anisotropy. The hybrid stress elements are clearly less sensitive to the degree of anisotropy than the displacement. This is true even for the least-order formulations of Punch and Atluri which depend upon element symmetry for their formulation. Figure 6.4 shows a comparison of σ_z in the cantilever beam for a pure moment load on the end of the beam as a function of the degree of anisotropy. The stresses in the beam should not change as the material properties change and all stresses except σ_z should be zero. This is clearly not the case for the displacement elements, even for the twenty node brick. The eight node element actually gives better results than the twenty node brick because the stresses were interpolated at the $2 \times 2 \times 2$ Gauss points which are the optimum points.

The hybrid stress elements clearly give better displacements and stresses for highly anisotropic material properties than their corresponding displacement elements but at some calculational expense. The calculation times are shown in Table 6.3 for calculation of the six element cantilever beam. The hybrid stress elements require up to three times as long for the calculations but the displacement elements require at least twice as many elements to obtain the same degree of accuracy in σ_z. The accuracy in the shear stresses and in σ_x and σ_y, though, are still better in the hybrid stress elements.

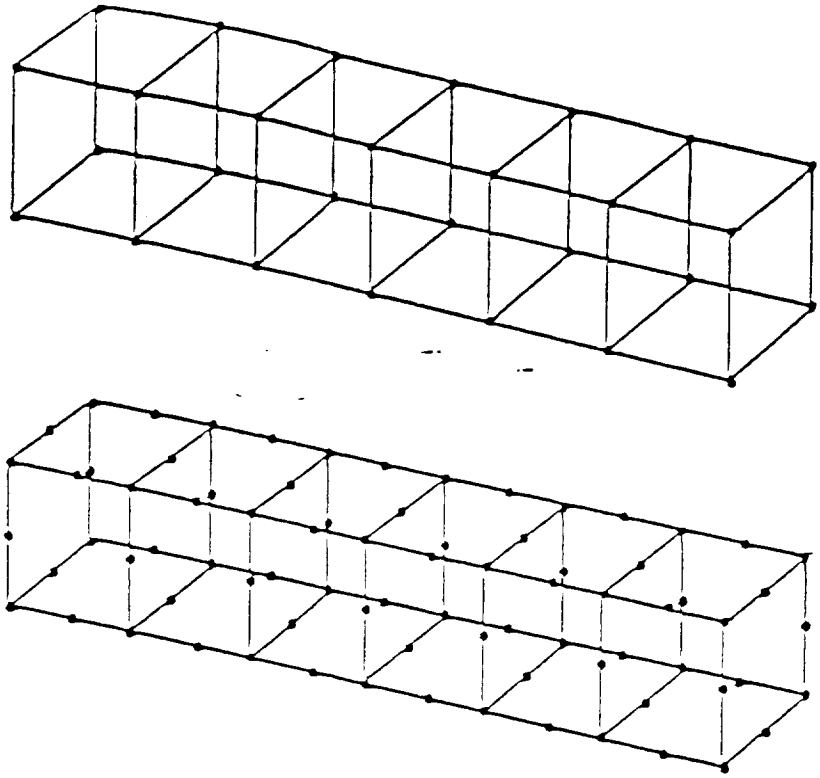

Figure 6.1: Three–dimensional finite element meshes of a cantilever beam.

A. Eight node brick elements

B. Twenty node brick elements

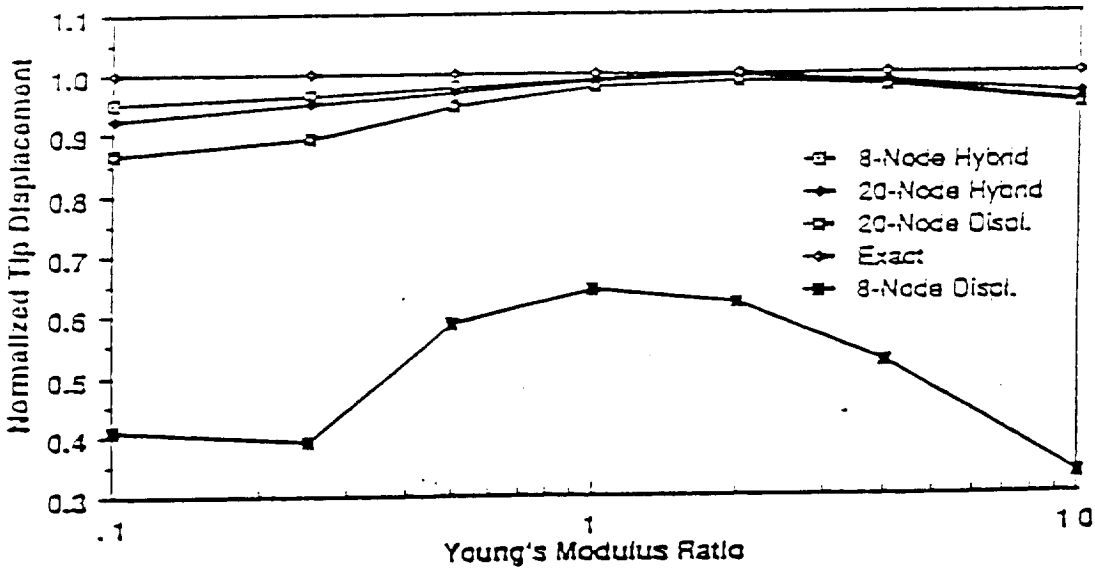

Figure 6.2: Normalized tip displacement for a cantilever beam with pure moment loading for various three–dimensional hybrid stress elements vs. the analytical solution as a function of the degree of anisotropy.

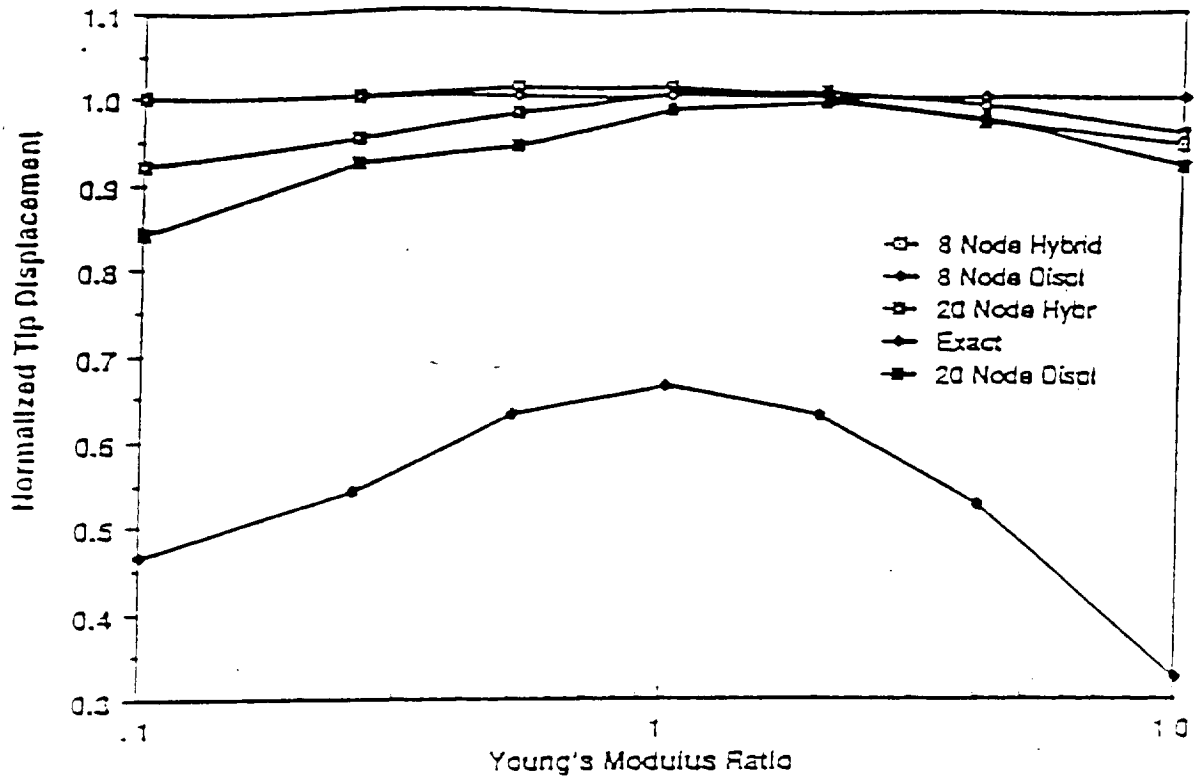

Figure 6.3: Normalized tip displacement for a cantilever beam with uniform end shear for various three–dimensional hybrid stress elements vs. the analytical solution as a function of the degree of anisotropy.

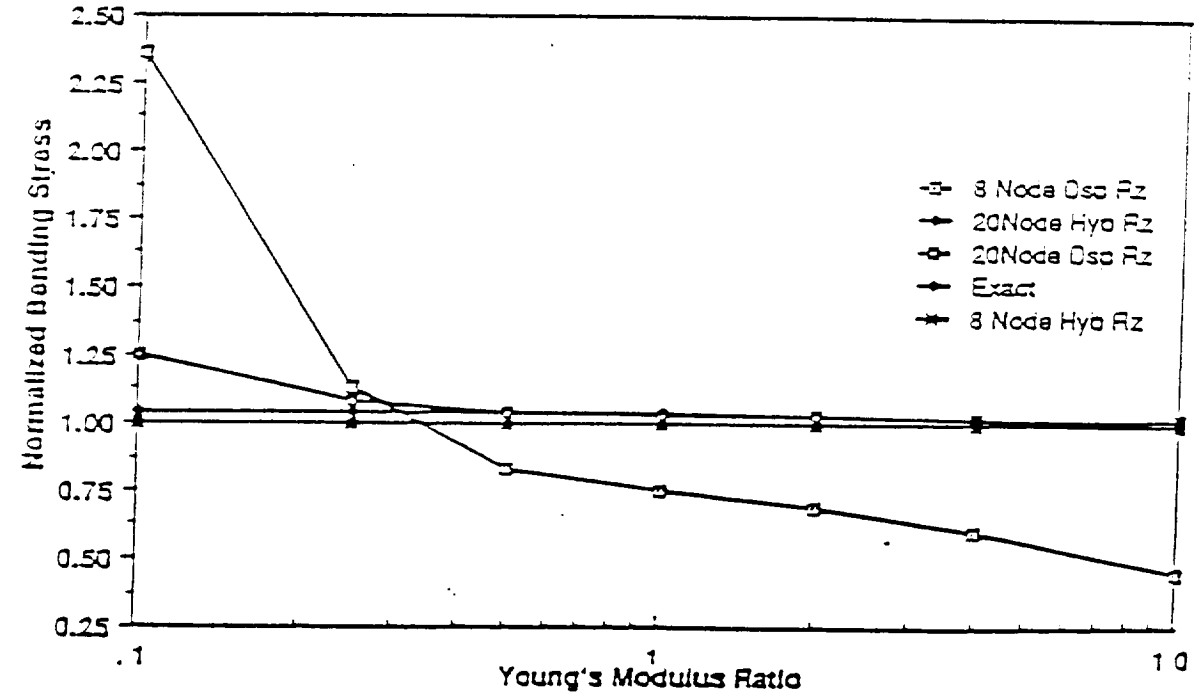

Figure 6.4: Normalized Bending stress for a cantilever beam with pure moment loading for various three–dimensional hybrid stress elements vs. the analytical solution as a function of the degree of anisotropy.

Calculation Time for a Six Element Cantilever Beam

	DM 8	DM 20	H8-18	H8-42	H20-54
Time(sec)	67	552	108	562	1422

6.5 Conclusions

The hybrid stress elements presented here can provide significantly improved accuracy in the calculation of both displacements and stresses for highly anisotropic materials in areas of high stress gradients. The twenty node hybrid stress brick element provides increased accuracy over the twenty node displacement element at a cost of approximately a three to one increase in computational time. The eight node hybrid element H8-18 provides much improved results over the standard eight node displacement element with less than twice the computational time. The most surprising result, however, is that the eight node hybrid element provides almost the same degree of accuracy as the twenty node displacement element at one–fifth of the calculational effort. For high degrees of anisotropy, this element gives results superior to the twenty node displacement element.

7 Numerical Examples

The final objective of this study was to incorporate the finite element methodologies, algorithms, and solution schemes developed for the stress and vibrational analysis of anisotropic elastic bodies into the SPAR finite element code. The COMCO three–dimensional anisotropic hybrid stress elements were incorporated into SPAR on the NASA/MSFC EADS computer system as SPAR solid element types S42 and S82.

A routine for calculating element material (compliance) matrices for non–isotropic materials was implemented as a TAB sub–processor (SMAT). The stress calculation and display functions were incorporated into the SPAR GSF and PSF processors. Documentation of these features is provided in the form of updates to the SPAR Reference Manual (Appendix A).

A number of example cases were executed to test the new code and to study the effects of various crystal configurations on SSME turbine blades. The first example consists of a one inch square by ten inch long cantilever beam modeled with 10 S82 eight–node solid elements as shown in Fig. 7.1. This example is a three–dimensional version of one of the example two–dimensional problems reported in Reference 19. As in the two–dimensional problem, the material chosen was that of cubic syngony to simulate the single crystal turbine blade nickel alloy. The cantilever beam problem was solved statically for an end shear load of 250 lb. for material axis rotations of 0, 30, 45, 60, and 90 degrees. The results are presented in Table 7.1, and compared with the two–dimensional results from Reference 13. As in the two–dimensional example, it is seen that material axis rotation by pairs of angles that are complementary produce nearly identical results. This problem was also solved dynamically for natural frequencies. The results are presented in Table 7.2. As in the static case, the frequencies calculated for 0 and 90 degree rotations, and 30 and 60 degree rotations are almost identical.

The second example consists of the same cantilever beam modeled with 40 S82 eight–node solid elements, as shown in Fig. 7.2. This problem is also a three–dimensional extension of a two–dimensional example problem from Reference 13. This 40–element model was executed with the same loads and material axis rotations as before. The results, compared with the two–dimensional results, are presented in Table 7.3. The results from the 40–element model are also compared with the ten–element model results and presented in Table 7.4.

The third example consists of a three–dimensional model of an SSME turbine blade constructed for use in studying the modal characteristics of various crystal configurations in a typical turbine blade application. This model was developed from a two–dimensional plate model of a blade currently in use at MSFC. A plot of this model is shown in Fig. 7.3. A series of runs was made with this model for a blade material of cubic syngony to simulate the single crystal nickel alloy. The material axes were rotated about each of the principal axes in turn, and frequencies were calculated for each orientation. The results are presented in Table 7.5. The material properties used are also given in the table. Rotations of the material axes about the global y axis produced the greatest effect, with an 8.8% increase in the second mode frequency for a material axis rotation of 45 degrees. The frequencies for the

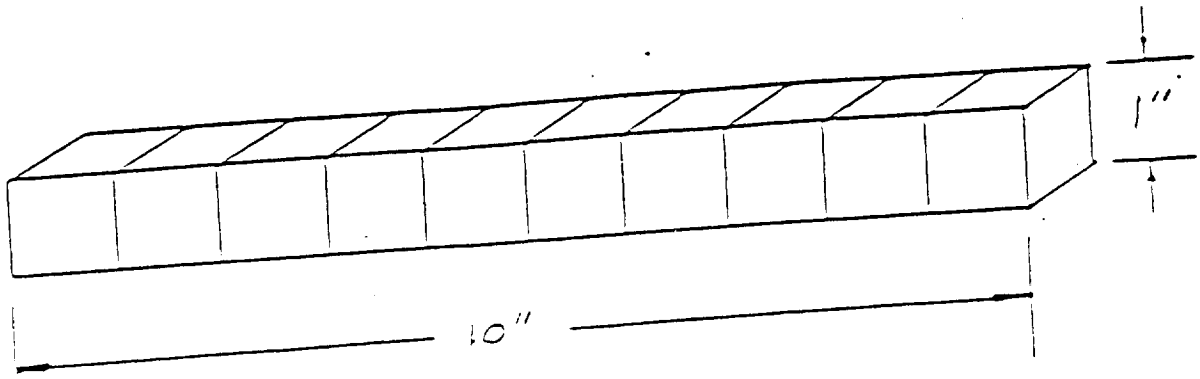

Figure 7.1: Three–dimensional finite element model of a cantilever beam, 10 S82 eight node solid elements.

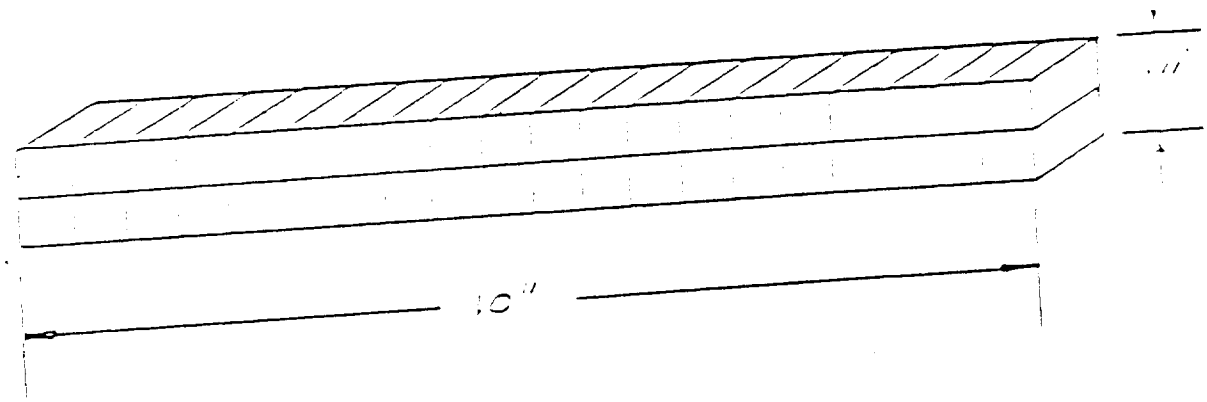

Figure 7.2: Three–dimensional finite element model of a cantilever beam, 40 S82 eight node solid elements.

Material properties for Cubic Syngony

$E1 = E2 = E3 =$	$1.9716E+07$	psi
$G =$	$5.4658E+06$	psi
$v =$	0.2875	

TABLE 7.1

Anisotropic beam modeled with 10 S82 three–dimensional elements compared with two–dimensional solution for ten element model.

	3–D		2–D	
Material Axis Rot. (deg)	u–tip (in)	max S (psi)	u–tip (in)	max S (psi)
0	.0509	14201	.0512	11532
30	.0606	14242	.0605	12272
45	.0639	14256	.0638	12566
60	.0606	14230	.0605	12273
90	.0509	14201	.0512	11532

TABLE 7.2

Anisotropic beam modeled with 40 S82 three–dimensional elements compared with two–dimensional solution for 40 element model.

	3–D		2–D	
Material Axis Rot. (deg)	u–tip (in)	max S (psi)	u–tip (in)	max S (psi)
0	.0508	14618	.0496	11117
30	.0612	14172	.0579	10579
45	.0660	15341	.0619	11023
60	.0613	15546	.0579	10579
90	.0508	14618	.0496	11117

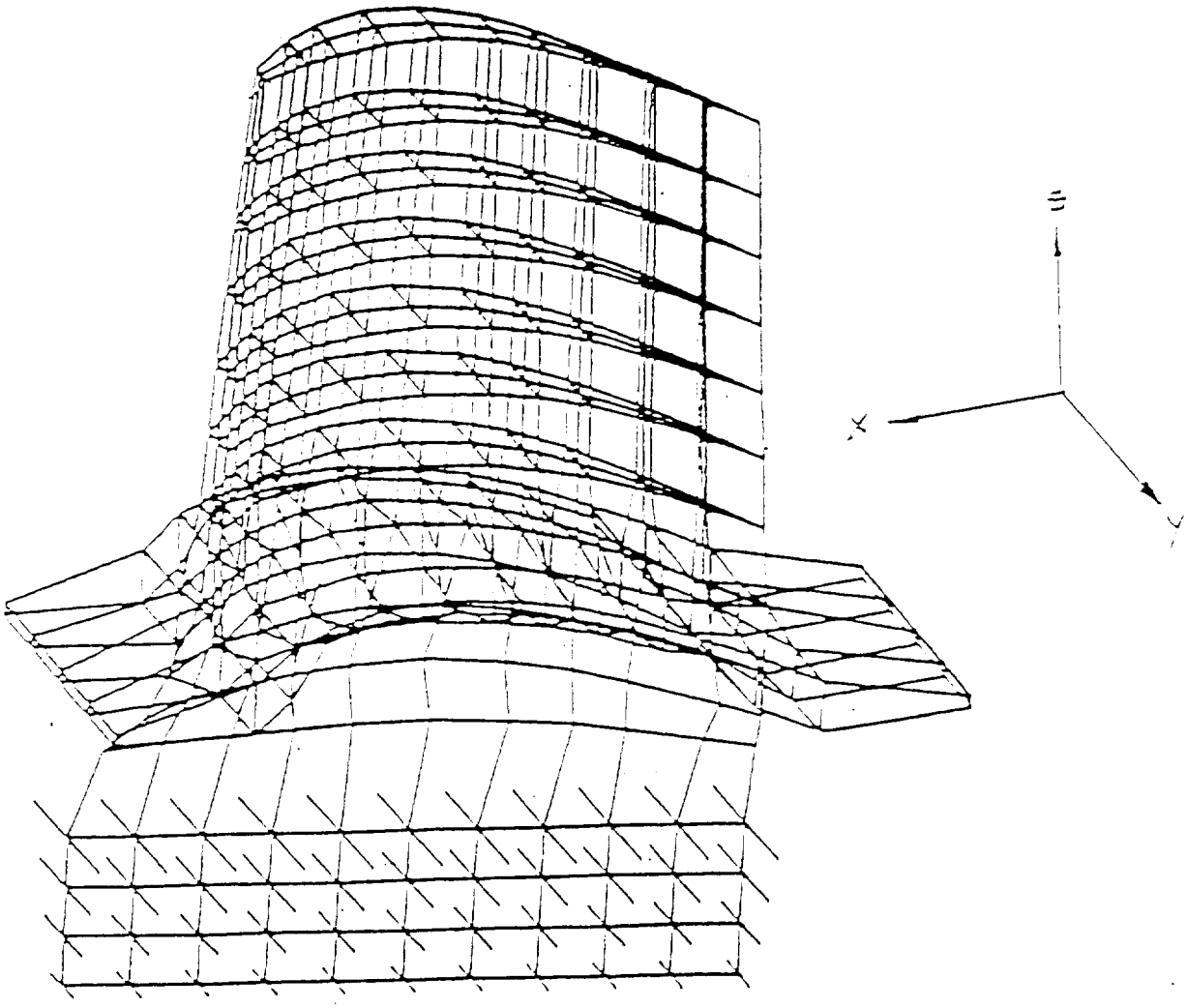

Figure 7.3: Three–dimensional model of a SSME turbine blade.

TABLE 7.3

Anisotropic beam modeled with 40 S82 three–dimensional elements compared with three–dimensional solution for ten element model.

	3–D (40 elem)		3–D (10 elem)	
Material Axis Rot. (deg)	u–tip (in)	max S (psi)	u–tip (in)	max S (psi)
0	.0508	14618	.0509	14201
30	.0612	14172	.0606	14242
45	.0660	15341	.0639	14256
60	.0613	15546	.0606	14230
90	.0508	14618	.0509	14201

TABLE 7.4

Anisotropic beam modeled with 40 S82 three–dimensional elements compared with three–dimensional solution for ten element model.

	3–D (40 elem)	3–D (10 elem)
Material Axis Rot. (deg)	Frequency (Hz)	Frequency (Hz)
0	260.53	260.69
30	238.24	239.19
45	230.42	233.27
60	238.48	239.36
90	260.53	260.69

TABLE 7.5

Effect of orientation of material axes on frequencies for SSME turbine blade with material of cubic syngony to simulate the single crystal nickel alloy.

Rotation about X–axis (deg)	f1 (Hz)	f2 (Hz)	f3 (Hz)
0	4379	9388	11818
30	4348	9375	11718
45	4334	9318	11676
60	4337	9298	11707
90	4376	9388	11816

Rotation about Y–axis (deg)	f1 (Hz)	f2 (Hz)	f3 (Hz)
0	4379	9388	11818
30	4378	9918	11820
45	4361	10216	11826
60	4362	10101	11834
90	4378	9388	11816

Rotation about Z–axis (deg)	f1 (Hz)	f2 (Hz)	f3 (Hz)
0	4379	9388	11818
30	4379	9337	11814
45	4380	9306	11815
60	4382	9347	11813
90	4380	9393	11816

Material properties for Cubic Syngony

$E1 = E2 = E3 =$	$1.9716E+07$	psi
$G =$	$5.4658E+06$	psi
$\upsilon =$	0.2875	

first and third modes changed very little with material orientation. The largest change in the first mode frequency occurred with a material rotation of 45 degrees about the global x axis. This orientation resulted in a first mode frequency reduction of 1.0%. Material axis rotations about the global z axis produced very little change in frequency, the largest change being a 0.9% reduction in the second mode frequency for a material axis rotation of 45 degrees.

The fourth example consists of the previous blade example modified to incorporate the S82 solid elements in the base region of the blade, including the "fir tree" portion. A plot of the modified blade model is shown in Fig. 7.4. The same series of runs made for the previous configuration was made for this model. The material axes were again rotated about each of the principal axes and frequencies calculated for each orientation. Since the S82 elements were used throughout the blade, the material orientations were effective from the tip to the base of the blade. The frequency results are summarized in Table 7.6. Once again, rotations of the material axes about the global y axis produced the greatest effect, with an 8.4% increase in the second mode frequency for a material axis rotation of 45 degrees. However, unlike the previous configuration, rotations about the global x axis also produced a significant effect. A reduction to the first mode frequency of -7.6% occurred for a material axis rotation of 45 degrees about x. Material axis rotations about the global z axis again produced very little change in frequency. The largest change was a 0.8% reduction in the second mode frequency for a material axis rotation of 45 degrees. The largest change in the third mode frequency was a 2.8% reduction which occurred for a 30 degree rotation about the x axis.

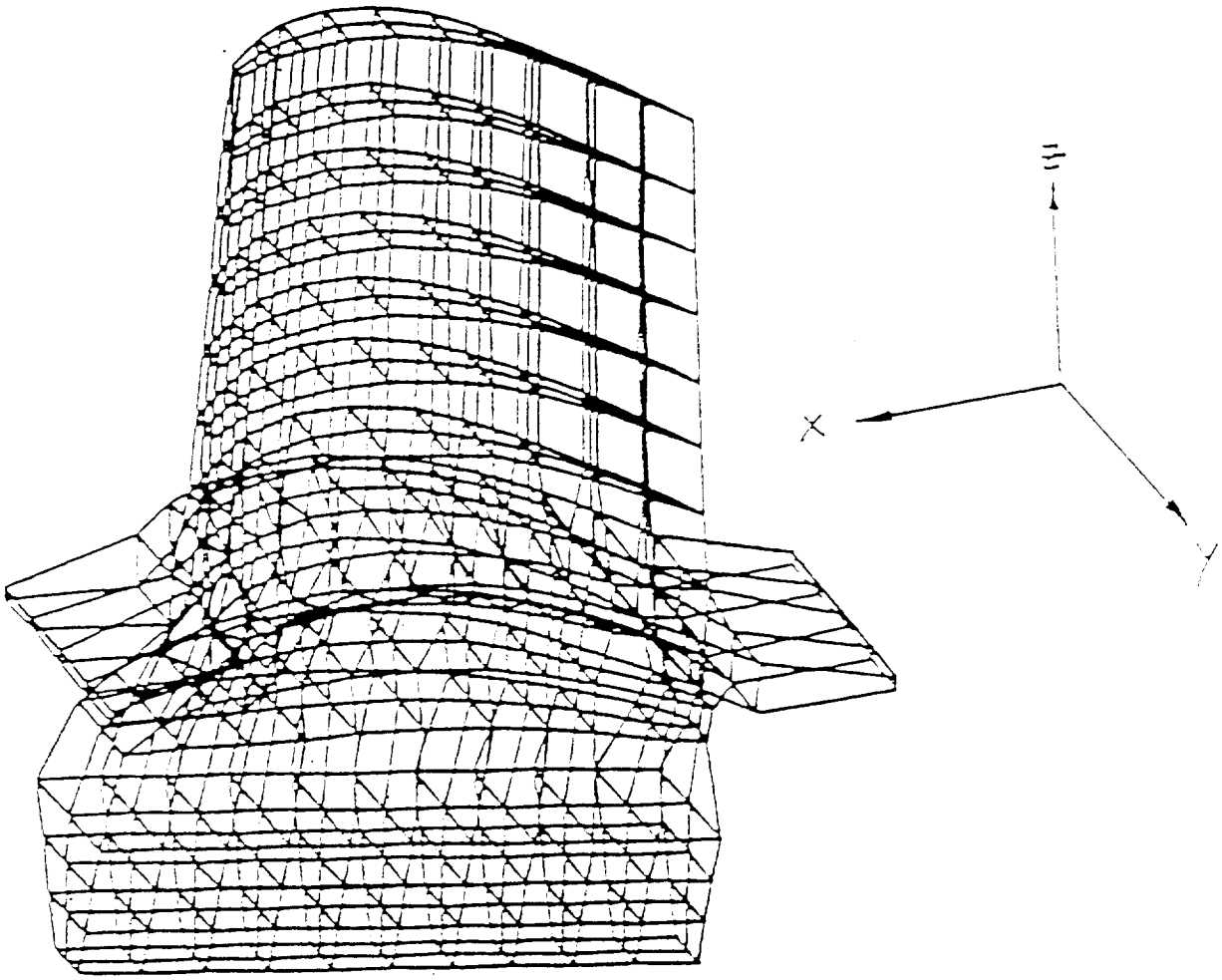

Figure 7.4: Three–dimensional model of a SSME turbine blade modified to incorporate the S82 solid elements in the base region of the blade.

TABLE 7.6

Effect of orientation of material axes on frequencies for SSME turbine blade with material of cubic syngony to simulate the single crystal nickel alloy.

Rotation about X-axis (deg)	f1 (Hz)	f2 (Hz)	f3 (Hz)
0	4969	8764	11849
30	4679	8755	11516
45	4593	8677	11561
60	4678	8644	11754
90	4967	8764	11847

Rotation about Y-axis (deg)	f1 (Hz)	f2 (Hz)	f3 (Hz)
0	4969	8764	11849
30	4828	9218	11980
45	4737	9499	12059
60	4769	9426	12045
90	4969	8764	11847

Rotation about Z-axis (deg)	f1 (Hz)	f2 (Hz)	f3 (Hz)
0	4969	8764	11849
30	4957	8722	11837
45	4957	8694	11837
60	4963	8728	11836
90	4971	8768	11847

Material properties for Cubic Syngony

$E1 = E2 = E3 =$	$1.9716E+07$	psi
$G =$	$5.4758E+06$	psi
$v =$	0.2875	

8 Calculation of Material Constants and Stress Measurements for Anisotropic Materials

8.1 Introduction

Anisotropic materials, in particular single crystal alloys, are widely recognized for their superior mechanical properties as compared with multi-grain materials. In many applications, in particular high-performance turbine blades, anisotropic properties allow for fine "tuning" of the dynamic characteristics by means of a proper orientation of the material axes. As a result, single crystal alloys are finding more and more applications in the aerospace industry.

The anisotropic properties of these alloys introduce additional complications into computational and experimental procedures. Many experimental and computational methods which are very effective for isotropic materials may be inapplicable or perform very poorly in the case of strong anisotropy. It was shown in previous sections that displacement-based finite elements do not perform well in the static and dynamic analysis of anisotropic materials and that a hybrid finite element formulation is better suited for these applications. Similarly, strong anisotropy inherent in single crystal alloys requires special attention in the design and interpretation of experimental results. For example, it can be observed that the calculation of material constants for anisotropic materials depends on the fourth powers of the direction cosines of the the crystallographic axes. It is obvious that the calculated values of the material constants will be strongly dependent on all misalignments of the crystallographic axes or strain gauges (or other measurement devices). Thus, the design of robust methods for the evaluation of anisotropic materials requires special attention.

In the spirit of these remarks, we will take a closer look at some experimental procedures for anisotropic materials and at the sensitivity of their results to errors, misalignments, etc. Moreover, we will try to optimize certain experimental parameters in order to minimize this sensitivity and thus develop robust procedures for the parametric evaluation of anisotropic materials.

The particular experiments considered here include:

- the calculation of elastic material constants from tensile test experiments at an arbitrary orientation of the material axes and of the strain gauges
- the calculation of stresses from strain measurements at an arbitrary orientation of the material axes and of the strain gauges

For both types of experiments, a general procedure is formulated, taking into account arbitrary types of crystals and arbitrary orientation of the material axes and strain gauges. Furthermore, a study of the sensitivity of the experimental results to various parameters is presented. The conclusions of this sensitivity study are the basis for optimization of the configuration of the material axes and strain gauges.

Several numerical examples illustrate the basic ideas and effectiveness of the procedures developed.

8.2 Stress, Strain and Compliance for Anisotropic Materials

8.2.1 Definitions

In the general theory of elasticity the stress and strain measures are defined as second order tensors: $\boldsymbol{\sigma}$ and $\boldsymbol{\epsilon}$, respectively. The general representation of these tensors in any Cartesian coordinate system $\{x_i\}$, $i = 1, 2, 3$ with base vectors $\boldsymbol{e}_i$ is of the form (see reference [6]):

$$\boldsymbol{\sigma} = \sigma_{ij}\, \boldsymbol{e}_i \otimes \boldsymbol{e}_j \tag{8.1}$$

$$\boldsymbol{\epsilon} = \varepsilon_{ij}\, \boldsymbol{e}_i \otimes \boldsymbol{e}_j \tag{8.2}$$

The fourth order compliance tensor $\boldsymbol{S}$ is defined by:

$$\boldsymbol{S} = \frac{\partial \boldsymbol{\epsilon}}{\partial \boldsymbol{\sigma}} \tag{8.3}$$

and has a representation

$$\boldsymbol{S} = S_{ijkl}\,(\boldsymbol{e}_i \otimes \boldsymbol{e}_j) \circledcirc (\boldsymbol{e}_k \otimes \boldsymbol{e}_l) \tag{8.4}$$

8.2.2 Transformation Under Rotation of a Coordinate System

Consider two different coordinate systems: $\{\hat{x}_i\}$ with base $\hat{\boldsymbol{e}}_i$ and $\{x_i\}$ with base $\boldsymbol{e}_i$. Then the stress tensor $\boldsymbol{\sigma}$ has two different representations in each of these systems, related by the transformation law:

$$\sigma_{ij} = r_{ik} r_{jl} \hat{\sigma}_{kl} \tag{8.5}$$

where the elements of the rotation matrix r_{ij} are defined by

$$r_{ij} = \boldsymbol{e}_i \cdot \hat{\boldsymbol{e}}_j \tag{8.6}$$

Using matrix notation, the above can be expressed as

$$[\sigma] = [R][\hat{\sigma}][R]^T \tag{8.7}$$

where the rotation matrix $[R]$ has the property

$$[R]^{-1} = [R]^T \tag{8.8}$$

The components of the strain tensor are transformed according to a similar formula

$$[\varepsilon] = [R][\hat{\varepsilon}][R^T] \tag{8.9}$$

Note that matrix notation is used here to emphasize the fact that tensors $\boldsymbol{\sigma}$ and $\boldsymbol{\epsilon}$ (defined as linear operators) remain unchanged and that only their representations change.

8.2.3 Stress, Strain and Compliance – Technical Notation

In practical applications a slightly different notation is usually introduced to represent stress, strain and compliance. Instead of the two–dimensional matrices, stress and strain vectors are introduced:

$$\boldsymbol{\sigma} = \{\sigma_i\} = \{\sigma_{11}, \sigma_{22}, \sigma_{33}, \sigma_{12}, \sigma_{13}, \sigma_{23}\}^T \tag{8.10}$$

$$\boldsymbol{\varepsilon} = \{\varepsilon_i\} = \{\varepsilon_{11}, \varepsilon_{22}, \varepsilon_{33}, \varepsilon_{12}, \varepsilon_{13}, \varepsilon_{23}\}^T \tag{8.11}$$

The compliance matrix is defined by

$$\boldsymbol{S} = \frac{\partial \boldsymbol{\varepsilon}}{\partial \boldsymbol{\sigma}}$$

and has, in the most general case, 21 independent components. For cubic systems, which are of primary interest here, the number of independent constants is equal to 3.

It should be noted that, with the technical notation introduced in the previous section, the stress vector, strain vector and compliance matrix are **not** elements of tensor spaces defined on the three dimensional Euclidean space anymore. Therefore, they do not necessarily obey the rules relating to objects of these spaces (tensor laws), in particular, the rules of transformation under rotation equations (8.7) and (8.9). Thus, in technical notation, boldface symbols represent vectors and matrices, not tensors.

It can be shown, however, that the transformation of the components of the stress and strain vectors under the rotation of a coordinate system are represented by

$$\boldsymbol{\sigma} = \boldsymbol{Q}\hat{\boldsymbol{\sigma}} \tag{8.12}$$

and

$$\boldsymbol{\varepsilon} = \boldsymbol{Q}\hat{\boldsymbol{\varepsilon}} \tag{8.13}$$

where the matrix $\boldsymbol{Q}$ consists of the appropriate combinations of products of elements of the rotation matrix $\boldsymbol{R}$. Note that, since tensor laws are not valid for the technical notation, the inverse matrix $\boldsymbol{Q}^{-1}$ is not equal to $\boldsymbol{Q}^T$ and has to be reconstructed from elements of the matrix $\boldsymbol{R}^T$.

For the compliance matrix, it can be shown that it transforms according to the formula:

$$\boldsymbol{S} = \boldsymbol{Q}\hat{\boldsymbol{S}}\boldsymbol{Q}^{-1} \tag{8.14}$$

Note that the compliance matrices $\boldsymbol{S}$ and $\hat{\boldsymbol{S}}$ are non–symetric. The symmetric compliance matrices are obtained if new measures of strains $\gamma_{ij} = 2\varepsilon_{ij}$ are introduced into vector $\boldsymbol{\varepsilon}$. However, since this new strain vector requires a different transformation matrix than $\boldsymbol{Q}$ in (8.13), it will not be used in the computations. If needed, the symmetric compliance matrix can be easily reconstructed from the matrix $\boldsymbol{S}$ by the use of the formula

$$\begin{aligned} {}^{S}S_{ij} &= S_{ij} \quad i = 1,2,3, \quad j = 1,\ldots,6 \\ {}^{S}S_{ij} &= 2S_{ij} \quad i = 4,5,6 \quad j = 1,\ldots,6 \end{aligned} \tag{8.15}$$

8.2.4 Compliance Matrix in the Local Coordinate System

The compliance matrices have the simplest forms in the local coordinate systems $\{\hat{x}_i\}$ associated with the crystallographic axes of the particular crystal type. In these systems, the compliance matrices may have as many as 21 independent constants (for triclinic systems) or as low as two independent constants (for isotropic materials). For cubic systems, which are of primary interest here, there are three independent constants a_1, a_2, and a_3, located in $\hat{\boldsymbol{S}}$ in the following locations:

$$\hat{\boldsymbol{S}} = \begin{bmatrix} a_1 & a_2 & a_2 & 0 & 0 & 0 \\ a_2 & a_1 & a_2 & 0 & 0 & 0 \\ a_2 & a_2 & a_1 & 0 & 0 & 0 \\ 0 & 0 & 0 & \frac{1}{2}a_3 & 0 & 0 \\ 0 & 0 & 0 & 0 & \frac{1}{2}a_3 & 0 \\ 0 & 0 & 0 & 0 & 0 & \frac{1}{2}a_3 \end{bmatrix} \tag{8.16}$$

In order to clearly represent the number of independent constants and the structure of the compliance matrix for arbitrary crystal systems, one can introduce a locator matrix $\boldsymbol{L}$, so that

$$\hat{\boldsymbol{S}} = \boldsymbol{L}\boldsymbol{a} \tag{8.17}$$

In the above, $\boldsymbol{a}$ is the vector of unknown constants, $\boldsymbol{a} = \{a_1, a_2, \ldots a_n\}^T$ and the locator matrix is a three–dimensional $(6 \times 6 \times n)$ matrix consisting of the appropriate coefficients, with non–zero entries corresponding to actual locations of consecutive elements a_α. It's form can easily be reconstructed from the structure of the matrix $\hat{\boldsymbol{S}}$. Typical forms of this matrix for various crystal classes are shown (in the symmetric version ${}^S\boldsymbol{S}$) in reference [8]. They are also briefly presented in Appendix C of this report.

8.3 Evaluation of Material Constants for Anisotropic Materials

8.3.1 Basic Formulation

In this section, we will derive a general formula for the calculation of the elastic constants for anisotropic materials from tensile tests (or other tests with a prescribed stress state).

A typical test is presented in Fig. 8.1: a sample of anisotropic material, with material axes defined by the coordinate system $\{\hat{x}_i\}$, is subject to a certain stress state $\boldsymbol{\sigma}$ (usually pure tension) defined in the coordinate system $\{x_i\}$. The strains are measured by strain gauges (or other techniques) aligned with the coordinate systems $\{x_i^{(\alpha)}\}$ where α is the number of a gauge (single measurement). In general, systems $\{\hat{x}_i\}$, $\{x_i\}$ and $\{x_i^{(\alpha)}\}$ need not be aligned.

Introducing the transformation matrices:

$$\boldsymbol{Q} - \text{ representing transformation from } \{\hat{x}_i\} \text{ to } \{x_i\} \tag{8.18}$$

and

$$\boldsymbol{Q}^{(\alpha)} - \text{ representing transformation from } \{x_i\} \text{ to } \{x_i^{(\alpha)}\} \tag{8.19}$$

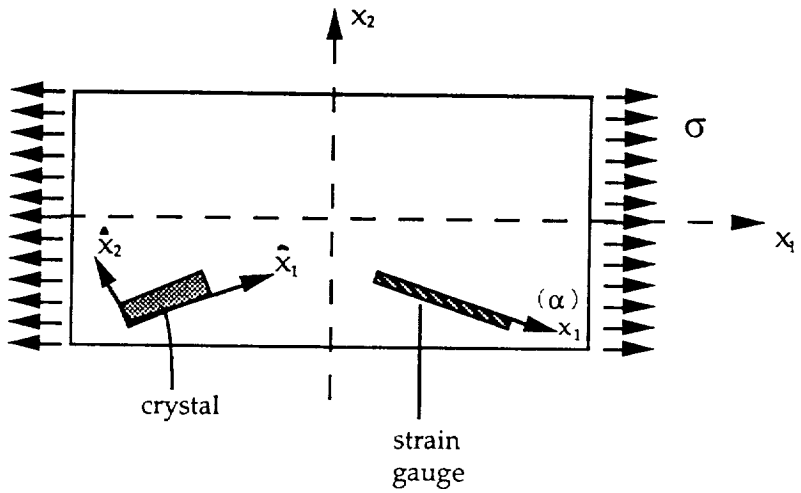

Figure 8.1: A typical test for anisotropic materials.

the formula for measured stress ε_α can be written as:

$$\boldsymbol{Q}_{(1)}^{(\alpha)} \cdot \boldsymbol{Q}\hat{\boldsymbol{S}}\boldsymbol{Q}^{-1}\boldsymbol{\sigma}^{(\alpha)} = \varepsilon_\alpha \tag{8.20}$$

where $\boldsymbol{Q}_{(1)}^{(\alpha)}$ represents the first row of the matrix $\boldsymbol{Q}^{(\alpha)}$. Note that the index (α) in parentheses indicates quantities associated with measurement number α, but not necessarily measured in the direction of x^α. In particular, $\boldsymbol{\sigma}^{(\alpha)}$ is represented in the coordinate system $\{x_i\}$.

Introducing the locator matrix $\boldsymbol{L}$ to represent the specific crystal class, this equation becomes

$$\boldsymbol{Q}_{(1)}^{(\alpha)} \cdot \boldsymbol{QLaQ}^{-1}\boldsymbol{\sigma}^{(\alpha)} = \varepsilon_\alpha \tag{8.21}$$

or in the index notation

$$Q_{1m}^{(\alpha)} Q_{mi} Q_{jn}^{-1} \sigma_n^{(\alpha)} L_{ij\beta} a_\beta = \varepsilon_\alpha \tag{8.22}$$

It can be noted that the unknowns in this equation are material constants a_i. For a tensile test, the stress vector is defined as $\boldsymbol{\sigma} = \{\sigma, 0, 0, 0, 0, 0\}$ and the above equation can be recast in a "normalized" version

$$Q_{1m}^{(\alpha)} Q_{mi} Q_{j1}^{-1} L_{ij\beta} a_\beta = \frac{\varepsilon_\alpha}{\sigma^{(\alpha)}} \tag{8.23}$$

Assuming that a total of m independent measurements are made, the system of equations used to determine the material constants is of the form

$$\boldsymbol{Ka} = \boldsymbol{e} \tag{8.24}$$

or, using index notation:

$$K_{\alpha\beta} a_\beta = \frac{\varepsilon_\alpha}{\sigma^{(\alpha)}} \tag{8.25}$$

where $\beta = 1 \ldots n$ (number of material constants), $\alpha = l \ldots m$ (number of measurements) and

$$K_{\alpha\beta} = Q_{1m}^{(\alpha)} Q_{mi} Q_{j1} L_{ij\beta} \tag{8.26}$$

Note that α is a counter for single measurements (strain readings). If several strain gauges are used on the same sample, then each gauge reading is counted as one measurement providing one piece of information (one equation in (8.24)). If several different samples are used to determine the material constants for the same crystal, then measurements on consecutive samples are added as new equations to the system (8.24), with α being an accumulative counter of single measurements (strain readings). Note that in this case, elements of the matrices $\boldsymbol{Q}$ may change from sample to sample, due to different orientations of the crystal axes.

8.3.2 Calculation of Material Constants From "Too Many" Experiments

The necessary condition for the system (8.24) to have a unique solution is that the number of single measurements is at least equal to the number of unknown coefficients $m \geq n$. In practice, the number of single measurements will usually be larger, so that $m > n$, and the system (8.24) will be overdetermined (provided that the equations are linearly independent). For such systems, the exact solution usually does not exist and can be only found in the approximate sense.

One of the popular methods for the solution of such systems is the least squares method, based on the minimization of the norm of the residual of the system (8.24):

$$r = \|\boldsymbol{K}\boldsymbol{a} - \boldsymbol{e}\|^2 \tag{8.27}$$

A detailed derivation of this method can be found in reference [5]. Here, we will present only a final form of the square system of equations to be solved:

$$(\boldsymbol{K}^T\boldsymbol{K})\boldsymbol{a} = \boldsymbol{K}^T\boldsymbol{e} \tag{8.28}$$

or, in index notation:

$$(K_{\gamma\alpha}K_{\gamma\beta})a_\beta = K_{\gamma\alpha}\frac{\varepsilon_\gamma}{\sigma^{(\alpha)}} \tag{8.29}$$

8.4 Evaluation of Stress Components for Anisotropic Materials

8.4.1 Basic Formulation

Calculation of stresses in machine elements from strain gauge measurements is a very typical operation in structural mechanics. However, for anisotropic materials, this procedure may be very sensitive to various experimental errors, particularly to misalignments of the strain gauges.

A typical setup for obtaining measurements is presented in Figure (8.2). The figure presents a section of an anisotropic body (say, a turbine blade) with the directions of the crystallographic axes defined by the coordinate system $\{\hat{x}_i\}$. At a given point on the surface of the body, a local Cartesian coordinate system $\{x_i\}$ is defined, with axes x_1 and x_2 tangent to the surface and axis x_3 normal to this surface. In order to measure strains, a number

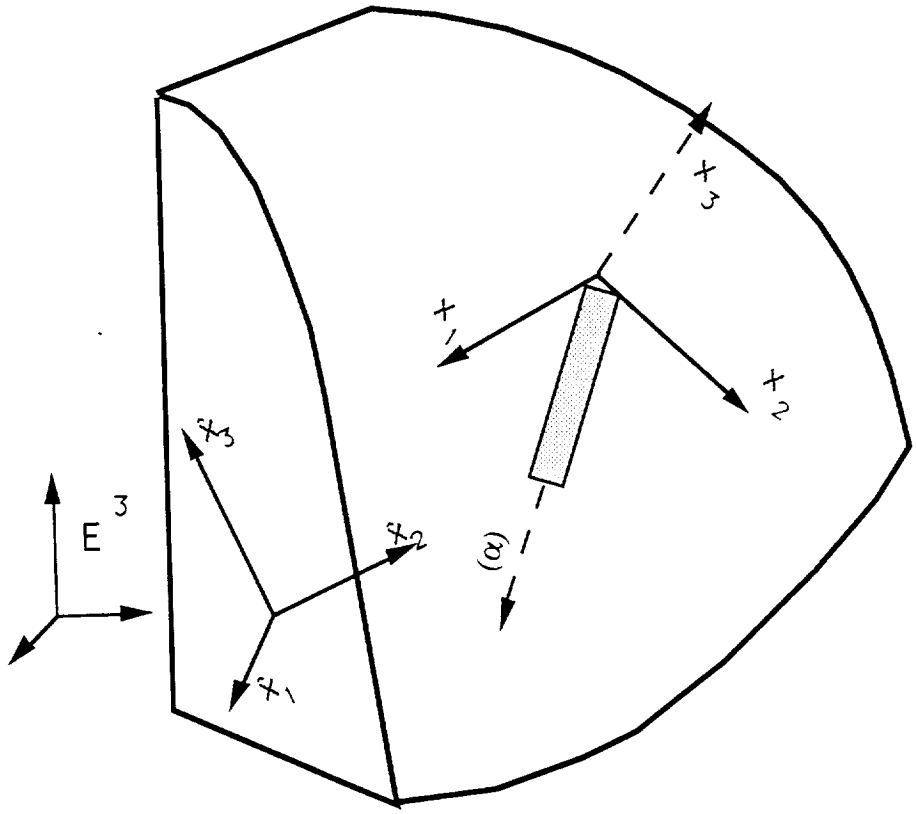

Figure 8.2: A typical setup for evaluation of stresses in anisotropic materials from strain measurements.

of strain gauges is located on the surface of the body (usually strain gauges are assembled into strain rosettes). In Figure (8.2), only one gauge, with the associated coordinate system $\{x_i^{(\alpha)}\}$ is indicated.

The stress–strain relationship in the material coordinate system $\{\hat{x}_i\}$ is of the standard form:

$$\hat{\boldsymbol{S}}\hat{\boldsymbol{\sigma}} = \hat{\boldsymbol{\varepsilon}} \tag{8.30}$$

After transformation to the surface coordinate system $\{x_i\}$ the above equation becomes:

$$\boldsymbol{Q}\hat{\boldsymbol{S}}\boldsymbol{Q}^{-1}\boldsymbol{\sigma} = \boldsymbol{\varepsilon} \tag{8.31}$$

where $\boldsymbol{Q}$ represents transformation from $\{\hat{x}_i\}$ to $\{x_i\}$. Note that, in the absence of surface tractions, the stress components on the surface satisfy $\sigma_{i3} = 0,\ i = 1, 2, 3$ so that the essential non–zero components of stress can be organized into a vector

$$\overline{\boldsymbol{\sigma}} = \{\sigma_{11}, \sigma_{22}, \sigma_{12}\} \tag{8.32}$$

related to the three–dimensional version by a simple permutation

$$\sigma_i = P_{i\beta}\overline{\sigma}_\beta \tag{8.33}$$

As mentioned before, in order to calculate stress, one performs strain measurements in various directions on the surface. Each measurement provides one piece of information (one equation) in the form

$$\boldsymbol{Q}_{(1)}^{(\alpha)} \cdot \boldsymbol{Q}\hat{\boldsymbol{S}}\boldsymbol{Q}^{-1}\boldsymbol{P}\overline{\boldsymbol{\sigma}} = \varepsilon_\alpha \tag{8.34}$$

where ε_α is a strain measurement in the gauge α. If the total of m strain gauges is used, then the stresses can be calculated from the system of equations

$$\boldsymbol{K}\overline{\boldsymbol{\sigma}} = \boldsymbol{e} \tag{8.35}$$

or

$$K_{\alpha\beta}\sigma_\beta = \varepsilon_\alpha \tag{8.36}$$

where

$$K_{\alpha\beta} = Q_{im}^{(\alpha)}Q_{mi}\hat{S}_{ij}Q_{jn}^{-1}P_{n\beta} \tag{8.37}$$

and $\alpha = 1, \ldots, m,\ \beta = 1, 2, 3$. From the structure of a matrix $\boldsymbol{K}$ it can be concluded that the calculated values of the stresses are sensitive to the precise specification of the orientation of material axes and the strain gauges. Thus, there may exist certain configuration of the strain gauges that will minimize this sensitivity and produce the most robust setups. This question will be addressed in the next section.

8.5 Optimization of The Strain Gauge Orientation in Tests for Anisotropic Materials

8.5.1 Problem Statement

Consider the problem of the calculation of the material constants (8.24) or of the calculation of stresses from strain measurements (8.64). It can be noted, that the actual form of the coefficient matrix $\boldsymbol{K}$ depends on the orientation of material axes (matrix $\boldsymbol{Q}$) and strain gauges for consecutive measurements (matrices $\boldsymbol{Q}^{(\alpha)}$). Thus, it makes sense to pose the following problem:

Find a combination of coefficients (in particular, Q_{ij} and $Q^{(\alpha)}_{lm}$) such that:

1. The system is non-singular:
$$r(\boldsymbol{K}) = n \tag{8.38}$$
where $r(\boldsymbol{K})$ is the rank of the coefficient matrix, and n is the number of unknown material constants.

2. The solution of the system is the least sensitive to the variation of the orientation of material axes or strain gauges (in case of the calculation of stresses, only the latter is of interest).

The solution to this problem is suggested by the theory sensitivity of linear systems of equations, presented, for example, in reference [5]. This theory is summarized in the next section.

8.5.2 Background—Sensitivity Analysis

Consider the system of linear equations:

$$\boldsymbol{K}\boldsymbol{a} = \boldsymbol{b} \tag{8.39}$$

and suppose that the coefficient matrix $\boldsymbol{K}$ is perturbed by $\varepsilon\boldsymbol{F}$ where $\boldsymbol{F}$ is an arbitrary matrix such that $\|\boldsymbol{F}\| = 1$ (in the appropriate norm). Then, it can be shown [5] that the sensitivity of the solution $\boldsymbol{a}$ to the perturbation ε satisfies the inequality:

$$\frac{\|\boldsymbol{a}(\varepsilon) - \boldsymbol{a}\|}{\|\boldsymbol{a}\|} \leq \kappa(\boldsymbol{K})\rho(\boldsymbol{K}) + o(\varepsilon^2) \tag{8.40}$$

where $a(\varepsilon)$ denotes the solution of a perturbed system of equations and:

$$\kappa(\boldsymbol{K}) = \|\boldsymbol{K}\|\,\|\boldsymbol{K}^{-1}\| = \text{spectral radius of } \boldsymbol{K}$$

$$\rho_K = \frac{\varepsilon}{\|\boldsymbol{K}\|} = \text{norm of the variation of } \boldsymbol{K}$$

If we decide to use the natural square norm $\|\cdot\|_2$, then we have $\|\boldsymbol{K}\|_2 = \sigma_{\max}(\boldsymbol{K})$ and $\kappa(\boldsymbol{K}) = \sigma_{\max}(\boldsymbol{K})/\sigma_{\min}(\boldsymbol{K})$ and the sensitivity inequality becomes

$$\frac{\|\boldsymbol{a}(\varepsilon) - \boldsymbol{a}\|_2}{\|\boldsymbol{a}\|_2} \leq \frac{1}{\sigma_{\min}(\boldsymbol{K})} + o(\varepsilon^2) \tag{8.41}$$

In the above, $\sigma_{\min}(\boldsymbol{K})$ is the minimum singular value of the matrix $\boldsymbol{K}$.

The calculation of singular values is not a very typical operation and there is no software readily available for this procedure. Then, it is useful to observe that singular values of $\boldsymbol{K}$ are defined as square roots of the eigenvalues of $\boldsymbol{K}^T\boldsymbol{K}$, namely

$$\sigma_i^{(K)} = \sqrt{\lambda_i^{(K^TK)}} \qquad i = 1, \ldots, n \tag{8.42}$$

8.5.3 Optimization of Strain Gauge Orientation and Material Axes

With the background presented in the previous section, it is easy to observe that in order to satisfy criterion (2) presented in Section 8.81, we need to:

> *Find a combination of the orientations of the strain gauges and the material axes, which maximizes the minimum eigenvalue of the matrix K^TK.*

Note, that the results of this analysis are useful for the satisfaction of criterion (1) - existence of the solution. This is because the rank of matrix $\boldsymbol{K}$ is equal to the number of nonzero singular values of $\boldsymbol{K}$, which, in turn, is equal to the number of nonzero eigenvalues of $\boldsymbol{K}^T\boldsymbol{K}$. Therefore, the solution to the system exists if the minimum eigenvalue $\lambda_{\min}^{(K^TK)}$ is greater than zero.

To present the above optimization criterion in a more formal way, we denote all the free optimization parameters by $p_i, i - 1, \ldots K$ (these may be angles of strain gauges, Miller indices, etc.). Then, to satisfy criteria (1) and (2), one needs to:

Find $\{\overline{p}_i\}$ and corresponding $\overline{\lambda}_{\min}^{(K^TK)}$ such that:

$$\overline{\lambda}_{\min}^{(K^TK)} = \max_{\{p_i\}} \left(\lambda_{\min}^{(K^TK)} \right) > 0 \tag{8.43}$$

It should be noted that this general approach can be used both for the optimization of the calculation of material constants and the calculation of stresses from strains.

8.5.4 Numerical Procedure

In order to solve the optimization problem (8.43), a variety of procedures may be applied. In this work, it was assumed that the number of free parameters is small enough and the evaluation of eigenvalue $\lambda_{\min}^{(K^TK)}$ is cheap enough that a simple searching procedure can be effectively applied. This procedure is based on two steps:

1. Scan all the possible values of $\{p_i\}$ with sufficiently small resolution and evaluate, for each combination, the minimum eigenvalue $\lambda_{\min}^{(K^TK)}$ (using, for example, the Jacobi method [1]).

2. Select the combination $\{\overline{p}_i\}$, corresponding to the maximum:

$$\overline{\lambda}_{\min}^{(K^TK)} = \max_{\{p_i\}} \left(\lambda_{\min}^{(K^TK)} \right)$$

This procedure is general enough to be applied to the optimization of the orientation of material axes and of location and orientation of strain gauges.

8.6 Numerical Examples

The formulation and procedures, presented above, were the basis for the development of a computer software package designed to optimize the orientation of strain gauges in tensile tests and in stress measurements on real samples. In this section, a few selected introductory examples of this optimization will be presented. It should be noted that the formulation presented in this section and implemented in the program is very general and can be applied to any type of crystal as well as to isotropic materials (the differences between various material classes are restricted to the locator matrix $\boldsymbol{L}$). For the sake of simplicity and easy intuitive verification, the examples presented here deal with rather simple classes of materials, namely isotropic materials and cubic systems.

8.6.1 Optimization of the Calculation of Material Constants

The first example illustrating the correctness of the procedure is the calculation of material constants for an isotropic material from tensile tests (Fig. 8.3). In this case, there are two independent material constants, so it suffices to consider one sample with two strain gauges. In order to test the optimization procedure, we assume that the orientations of both gauges are unknown, so there are two independent optimization parameters, namely the angles α_1 and α_2. After application of the optimization procedure, the calculated optimal configuration of the strain gauges is: $\alpha_1 = 0, \alpha_2 = 90$ (or any equivalent configuration). At this configuration, the calculation of material constants is the least sensitive to alignment errors, a result that intuitively seems to be correct. This optimal configuration is presented in Fig. 8.3b. The same configuration is obtained if the three gauge rosette presented in Fig. 8.3c is considered. In this case, there is one optimization parameter (angle α) and the optimal orientation is $\alpha = 0$ (or, equivalently, $\alpha = 90, 180$, etc.). In another analysis for this material, a triangular strain rosette presented in Fig. 8.3d was considered. This rosette has one optimization parameter, namely the rotation angle α. The results of the optimization analysis indicate that if the triangle is equilateral, then all the configurations are equivalent, i.e., sensitivity of results to misalignments of α is the same (and rather low) at any position of the rosette.

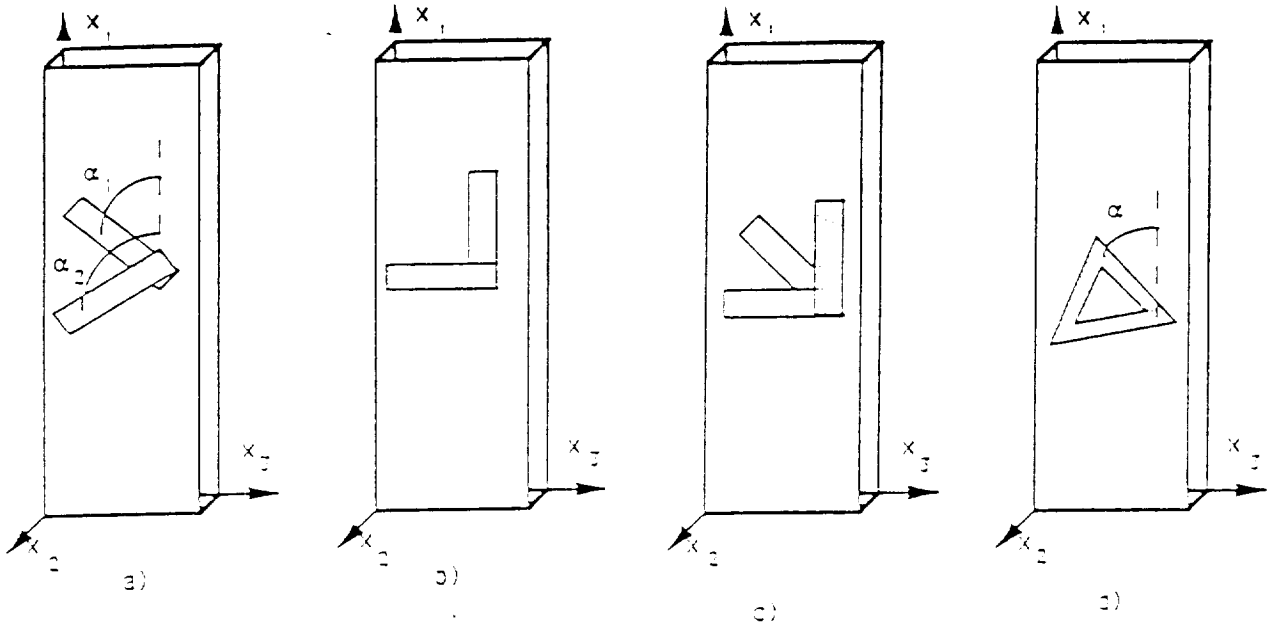

Figure 8.3: Optimization of strain gauges for isotropic material. (a) general configuration, (b) optimal configuration of two gauges, (c) optimal configuration of a rosette, and (d) configuration of a triangular rosette.

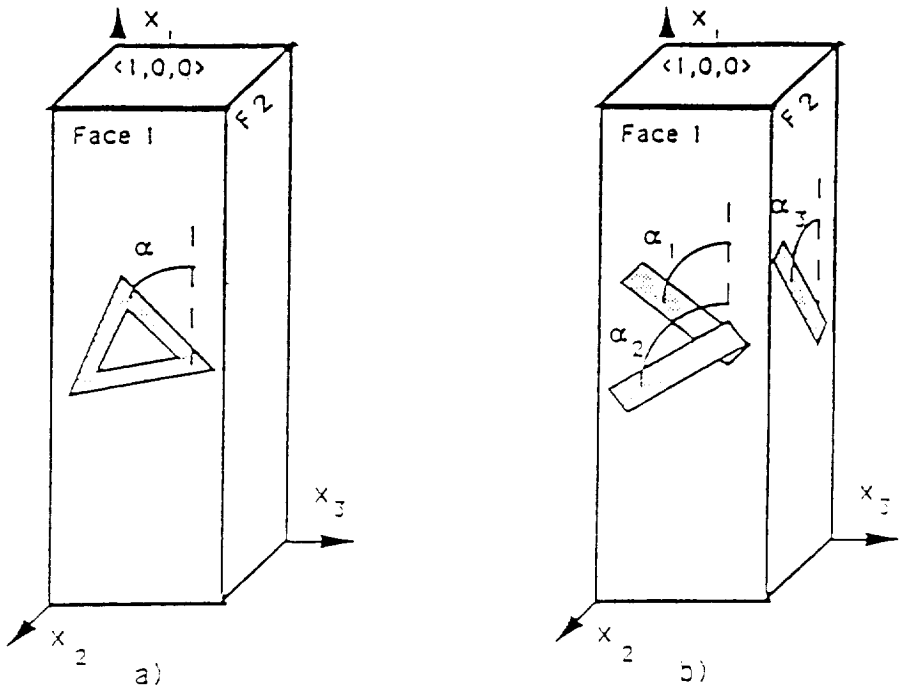

Figure 8.4: optimization of strain gauges for cubic syngony. (a) configuration of a triangular rosette and (b) three independent strain gauges.

The single crystal alloys used in the manufacturing of turbine blades are usually of cubic syngony. For this crystal system, there are three independent material constants, so that a minimum of three measurements (strain gauges) are necessary. Thus, as the first example, we considered one sample with the material axes aligned with the edges of a sample and with the direction of tension (Fig. 8.4) (Miller indices for consecutive sample axes were: $< 100 >$, $< 010 >$, $< 001 >$). The first optimization case considered was a triangular rosette with one optimization parameter, the angle α (Fig. 8.4a). The answer obtained in this case is that there exists no configuration of the rosette that can provide sufficient information (the system of equations is always singular). The same result was obtained even if three or more independent strain gauges were considered (Fig. 8.4b). The explanation of this result is simple: one of the independent material constants for the cubic system is the shear modulus and, for the perfectly aligned crystal configuration presented in Fig. 8.4, a tensile test does not produce any shear mode of deformation. Thus, there exists no information available to calculate the shear modulus.

As the next case we considered two samples of cubic structure: the one analyzed before and a second sample, with Miller indices corresponding to the primary, secondary and tertiary axes $< 1,1,1 >$, $< 1,2,-3 >$, and $< -5,4,1 >$, respectively. In each sample, a two-gauge rosette was used, with both the location (face 1 or 2) and the orientation (angle α) considered as optimization parameters. The solution obtained in this case is presented in Fig. 8.5a (both angles are equal to zero). If three-gauge rosettes are considered, the optimal configuration is slightly different (see Fig. 8.5b). In this case, the optimum angles are $\alpha_1 = 20°$, $\alpha_2 = 0$ with

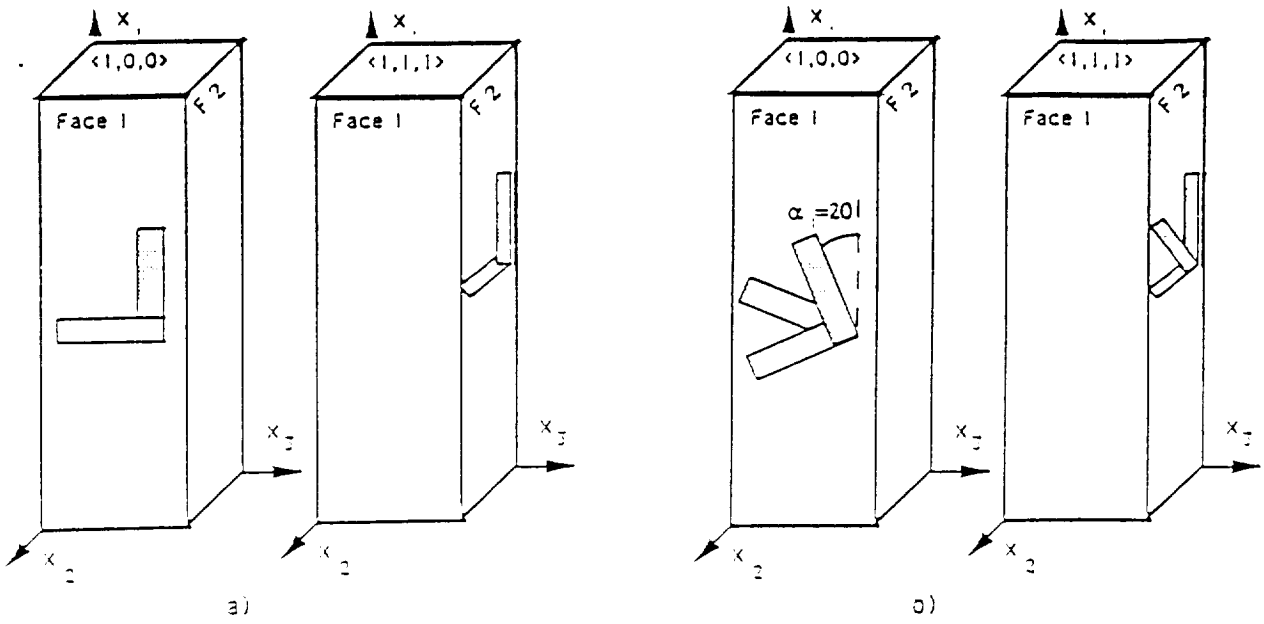

Figure 8.5: Optimization of strain gauges for cubic syngony. (a) optimal configuration of two-gauge rosettes and (b) optimal configuration of three-gauge rosettes.

the location of gauges as presented in Fig. 8.5b. Note that in order to calculate the optimal configuration, all the samples have to be considered simultaneously, because the results are "coupled." For example, if the Miller indices of sample 2 of Fig. 5b were changed, then the optimum orientation of the rosette in sample 1 would be different from the above example.

These simple examples illustrate the basics of the optimization procedure and the type of results obtainable. As previously mentioned, it is possible with this formulation to consider more complex crystal classes than cubic, since the procedure developed here is completely general.

8.6.2 Optimization of Calculation of Stresses from Strain Measurements

As an example of calculation of stresses from strain measurements, let us consider a sample of the material of cubic syngony, presented in Fig. 8.6.

The axes of the material coordinate system $\{\hat{x}_i\}$ are defined by three vectors represented in the reference coordinate system E^3 as:

$$\begin{aligned} \hat{e_1} &= \{0., \ 0.3162, \ -0.9487\} \\ \hat{e_2} &= \{0., \ 0.9487, \ 0.3162\} \\ \hat{e_3} &= \{1, \ 0, \ 0\} \end{aligned}$$

The three independent constants for the cubic material are $a_1 = 1.0 \times 10^{-6}$, $a_2 = -0.3 \times$

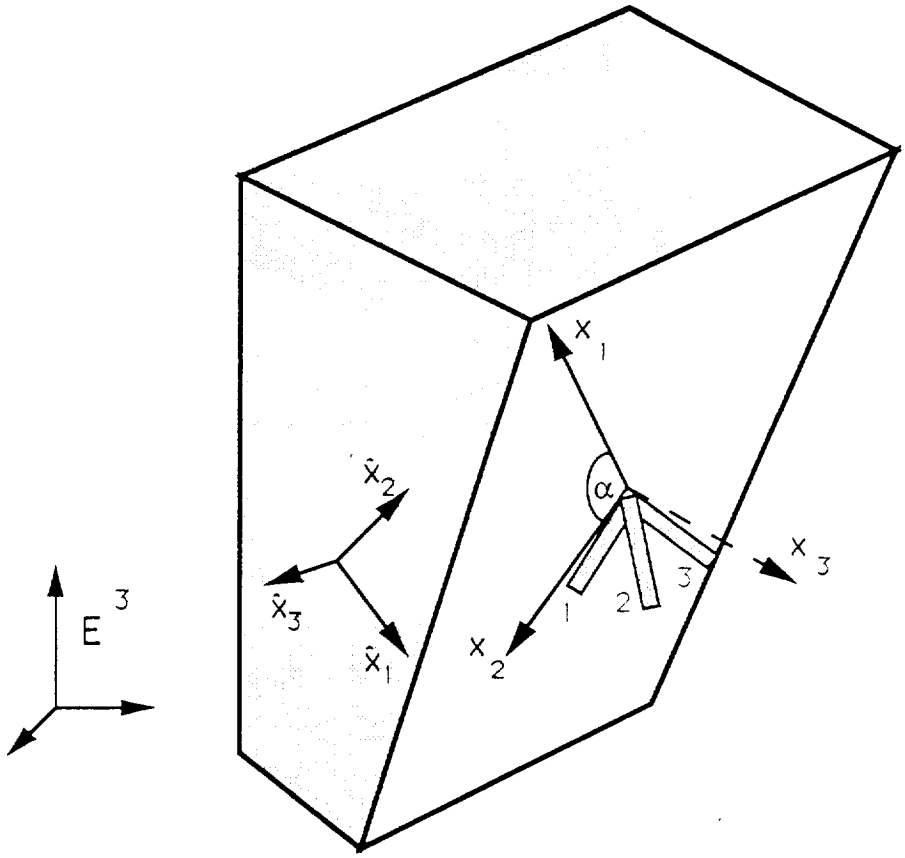

Figure 8.6: Optimization of orientation of strain rosette for the evaluation of stress in anisotropic samples.

10^{-6}, $a_3 = 4.0 \times 10^{-6}$, so that the symmetric compliance matrix defined in the material coordinate system is of the form

$$ {}^{S}\boldsymbol{S} = 10^{-6} \times \begin{bmatrix} 1.0 & -0.3 & -0.3 & 0 & 0 & 0 \\ -0.3 & 1.0 & -0.3 & 0 & 0 & 0 \\ -0.3 & -0.3 & 1.0 & 0 & 0 & 0 \\ 0 & 0 & 0 & 4.0 & 0 & 0 \\ 0 & 0 & 0 & 0 & 4.0 & 0 \\ 0 & 0 & 0 & 0 & 0 & 4.0 \end{bmatrix} $$

The coordinate system $\{x_i\}$, in which stresses will be calculated, is defined by three vectors $\boldsymbol{e}_i$, $i = 1, 2, 3$, specified as:

$$ \begin{aligned} \boldsymbol{e}_1 &= \{0.5774, \ -0.2573, \ \ 0.7715\} \\ \boldsymbol{e}_2 &= \{0.5774, \ -0.5345, \ -0.6172\} \\ \boldsymbol{e}_3 &= \{0.5744, \ \ 0.8018, \ -0.1543\} \end{aligned} $$

The strains are measured by a three gauge strain rosette, presented in Fig. 8.6. The orientation of this rosette is an optimization parameter in this case.

After the execution of the optimization version of the OPTAM–S code, the optimal value of the angle α was calculated to be 95°, which corresponds to the orientation presented in Fig. 8.6.

For the configuration obtained from the optimization run, a stress calculation version of the code was executed, with strain readings corresponding to consecutive gauges of the rosette being: $\varepsilon^{(1)} = 0.01$, $\varepsilon^{(2)} = 0.0035$, $\varepsilon^{(3)} = -0.003$. The calculated non–zero components of the stress tensor are: $\sigma_{11} = 296.7$, $\sigma_{12} = -524.8$, $\sigma_{22} = 6986.3$.

9 References

1. Atluri, S. N., Gallagher, R. H., and Zienkiewicz, O. C., eds., **Hybrid and Mixed Finite Element Methods,** John Wiley & Sons, New York, 1983.

2. Bathe, K. J., **Finite Element Procedures in Engineering Analysis**, Prentice-Hall, New York, 1982.

3. Becker, E. B., Carey, G. F., and Oden, J. T., **Finite Elements: An Introduction,** Prentice–Hall, Eaglewood Cliffs, 1981.

4. Bethoney, W. M., Nunes, J., Kidd, J. A., "Compressive Testing of Metal Matrix Composites," **Testing Technology of Metal Matrix Compositves**, ASTM STP 964, P. R. Di Giovanni and N. R. Adsid, Eds., American Society for Testing of Materials, Philadelphia, pp. 319–328, 1988.

5. Golub, G. H., Van Lohan, Ch. F., **Matrix Computaions**, The John Hopkins University Press, Baltimore, Maryland, 1983.

6. Gurtin, M. E., **An Introduction to Continuum Mechanics**, Academic press, 1981.

7. Irons, B. M., "Quadrature Rules for Brick Based Finite Elements," *Int. J. Num. Meth. Engng.*, **3**, 293–294, 1971.

8. Koerber, G. G., **Properties of Solids**, Prentice-Hall, New Jersey, 1962.

9. Lekhnitskii, S. G., **Theory of Elasticity for Anisotropic Elastic Body**, Holden-Day, San Francisco, 1983.

10. Nagy, P., Seitz, K., Bowen, K., "Evaluation of Taylored Single Crystal Airfoils," Williams International, Final Report for NASA Marshall Space Flight Center, March, 1986.

11. Nye, J. F., **Physical Properties of Crystals**, Oxford University Press, London, 1957.

12. Oden, J. T. and Carey, G. F., **Finite Elements: Mathematical Aspects**, Vol. IV, Prentice Hall, Englewood Cliffs.

13. Oden, J. T., G. W. Fly, and L. Mahadevan, "A Hybrid–Stress Finite Element Approach for Stress and Vibration Analysis in Linear Anisotropic Elasticity," COMCO TR-87-05, October 1987.

14. Okabe, M., "Complete Lagrange Family for the Cube in Finite Element Interpolations," *Int. J. for App. Mech. and Engng.*, Vol. 29, pp. 51–66, 1981.

15. Pian, T. H. H. and Chen, D. P., "Alternative Ways for Formulation of Hybrid Stress Elements," *Int. J. for Num. Meth. in Engng.*, Vol 18, pp. 1679–1684, 1982.

16. Pian, T. H. H. and Chen, D. P., "On the Suppression of Zero Energy Deformation Modes," *Int. J. for Num. Meth. in Engng.*, Vol. 19, pp. 1741–1752, 1983.

17. Pian, T. H. H., Sumihara, K., and Kang, D., "New Variational Formulations of Hybrid Stress Elements," **Nonlinear Structural Analysis**, NASA Conference Publication 2297, pp. 17–29, 1984.

18. Punch, E. F. and Atluri, S. N., "Development and Testing of Stable, Invariant, Isoparametric Curvilinear 2- and 3-D Hybrid–Stress Elements," *Comp. Meth. in Appl. Mech. and Engng.*, Vol. 47, pp. 331–356, 1984.

19. Punch, E. F. and Atluri, S. N., "Applications of Isoparametric Three–Dimensional Hybrid–Stress Finite Element and Least Order Stress Fields," *Computers & Structures*, Vol. 19 (3), pp. 409–430, 1984.

20. Rubenstein, R., Punch, E. F., and Atluri, S. N., "An Anlysis of, and Remedies for, Kinematic Modes in Hybrid–Stress Finite Elements: Selection of Stable, Invariant Stress Fields," *Comp. Meth. in Appl. Mech. and Engng.*, Vol. 28, pp. 63–92, 1983.

21. "Second Order Tensor Finite Elements," NASA Marshall Space Flight Center, Contract Number NAS8-37283, Interim Report, November, 1989.

22. Spilker, R. C., Maskeri, S. M., and Kania, E., "Plane Isoparametric Hybrid–Stress Elements: Invariance and Optimal Sampling," *Int. J. for Num. Meth. in Engng.*, Vol. 17, pp. 1469–1496, 1981.

23. Spilker, R. L., and Singh, S. P., "Three–Dimensional Hybrid–Stress Isoparametric Quadratic Displacement Elements," *Int. J. for Num. Meth. in Engng.*, Vol. 18, pp. 445–465, 1982.

24. Spilker, R. L., "Invariant 8–Node Hybrid–Stress Elements for Thin and Moderately Thick Plates," *Int. J. for Num. Meth. in Engng.*, Vol. 18, pp. 1153–1178, 1982.

25. Whetstone, W. D., "SPAR Structural Analysis System Reference Manual - System Level 13A, Vol. 1 - Program Execution," NASA CR-158970-1, December 1978.

26. Wooster, W. A., **Tensors and Group Theory for Physical Properties of Crystals**, Oxford University Press, London, 1973.

27. Zienkiewicz, O. C., **The Finite Element Method,** 3rd Edition, McGraw–Hill, New York, 1977.

Appendix A
Description of the Spar Reference Manual Updates

A Appendix – Description of Spar Reference Manual Updates

A.1 Tab Processor Updates

A new TAB sub–processor, SMAT, was created to provide an alternative to using AUS/TABLE to generate material flexibility coefficients (compliance matrices) for use with solid elements.

Based on inputs provided by the user, SMAT generates entries in PROP BTAB 2 21 as required by ELD when using solid elements. SMAT may be used with the previously existing solid element types S41, S61, and S81 as well as with the new element types S42 and S82.

The input required by SMAT is listed below. The detailed description of this input is given in Appendix B.

$n, w, nref$

E_1, E_2, E_3

G_{12}, G_{13}, G_{23}

$\upsilon_{12}, \upsilon_{13}, \upsilon_{23}$

(DIRCOS) $(1, J), J = 1, 3)$
(DIRCOS) $(2, J), J = 1, 3)$
(DIRCOS) $(3, J), J = 1, 3)$
} input only if $nref = 0$, or blank

$\alpha_x, \alpha_y, \alpha_z$

$Y_{xx}, Y_{yy}, Y_{zz}, Y_{xy}, Y_{yz}, Y_{zx}$

A.2 ELD Processor Updates

ELD was modified to accept for the new solid element types S42 and S82. These element types represent the COMCO three–dimensional anisotropic hybrid stress elements.

The S42 and S82 element material properties are obtained from the SPAR data set PROP BTAB 2 21 as with the other solid element types. This data set may be constructed with the AUS processor as before or with the new TAB subprocessor, SMAT.

The system diagonal mass matrix, DEM, produced by the processor E includes terms for S42 and S82 element types. No consistent mass matrix is available for any of the solid element types at this time.

The same mesh generation capabilities exist for the S82 element as for the S81 element, i.e., the hexahedral element network generator.

A.3 EKS Processor Updates

Modifications were made to EKS, the element intrinsic stiffness and stress matrix generator, to incorporate the S42 and S82 element types.

Although the changes to EKS are transparent to the user, the bulk of the SPAR updates were associated with EKS. The COMCO code was modified, adapted to the SPAR format, and incorporated into EKS such that the intrinsic stiffness matrices inserted into the element information packets were compatible with K, the system stiffness matrix generator. No modifications to K were required.

The E processor now generates the data sets "S42 EFIL" and "S82 EFIL," which contain the element information packets for the S42 and S82 elements, respectively. E also generates the system diagonal mass matrix, DEM, which contains terms for S42 and S82 elements. However, no modifications were required to E.

A.4 GSF/PSF Processor Updates

GSF was updated to generate stress data sets for the new S42 and S82 elements. Output data sets are named "STRS S42 iset ncon" and "STRS S82 iset ncon," respectively, which is consistent with data sets produced for other element types.

Control cards designating S42 and S82 elements may be included in GSF input as described in the SPAR Reference Manual, Ref. 1. If control cards of this kind are not given, stresses will be computed for all elements, including S42 and S82 elements.

No updates were made to PSF. A problem with the stress display at the corners of S82 which was present in the initial version of the code has now been corrected. Namely, the stress values printed for the element corners are now evaluated at the element corners instead of the integration points as was the case in the earlier code version.

A.5 Plot Processor Updates

GGS and PLTTEX were updated to recognize and plot the new S42 and S82 elements. These elements may be selected by element type, group, and index, or will be included if "ALL" is specified.

A.6 EADS Data Sets

The SPAR modifications have been fully implemented on the NASA/MSFC EADS computer system. The current source codes reside in the following data sets:

TAB	CMLP410.SPAR.FORT(PRGTAB)
EDS	CMLP410.SPAR.FORT(PRGELD)
EKS	CMLP410.SPAR.FORT(PRGEKS)
GSF	CMLP410.SPAR.FORT(PRGGSF)
GGS	CMLP410.SPAR.FPRT(PRGGGS)
PLTTEX	CMLP410.SPAR.FORT(PLTTEX)

Appendix B
SPAR Reference Manual Updates

B Appendix—SPAR Reference Manual Updates

APPENDIX B – SPAR REFERENCE MANUAL – (CONTENTS)

TABLE 1-1: SPAR Element Repertoire.

NAME	DESCRIPTION	See Volume 1 Sections:
E21	General straight beam elements such as channels, wide–flanges, angles, tubes, zees, etc.	3.1.7–9
E22	Beams for which the intrinsic stiffness matrix is given.	3.1.10
E23	Bar – Axial stiffness only.	3.1.11
E24	Plane beam.	3.1.12
E25	Zero–length element used to elastically connect geometrically coincident joints.	3.1.10
	Two–dimensional (area) elements:	3.1.13
E31	Triangular membrane	
E32	Triangular plate.	
E33	Triangular combined membrane and bending element.	
E41	Quadrilateral membrane.	
E42	Quadrilateral plate.	
E43	Quadrilateral combined membrane and bending element.	
E44	Quadrilateral shear panel.	3.1.14
	Three–dimensional solids:	3.2.2.3
S41	Tetrahedron (pyramid).	
S42	4–node tetrahedral hybrid (COMCO)	
S61	Pentahedron (wedge).	
S81	Hexahedron (brick).	
S82	8–node anisotropic hybrid (COMCO)	
	Compressible fluid elements:	12., 3.2.2.3
F41	Tetrahedron (pyramid).	
F61	Pentahedron (wedge).	
F81	Hexahedron (brick).	

Notes:

- See Section 7.2 for examples of stress output.
- See Volume 2 (Theory) for element formulation details.
- Aeolotropic constitutive relations permitted, all area elements.
- Laminated cross sections permitted for *E33, E43*.
- Membrane/bending coupling permitted for *E33, E43*.
- *E41, E42, E43, E44* may be warped.

– Aeolotropic constitutive relations permitted for 3–D solids.
– Non–structural mass permitted for line and area elements.

3.1.18 Solid Element Materials (SMAT)

Based on inputs provided by the user, SMAT generates entries in PROP BTAB 2 21 as required by ELD when using solid elements. A description of the contents of each input record to SMAT follows.

n, *w*, *nref*
E_1, E_2, E_3
G_{12}, G_{13}, G_{23}
ν_{12}, ν_{13}, ν_{23}
(DIRCOS *(1,J)*, *J = 1, 3)*
(DIRCOS *(2,J)*, *J = 1, 3)* input only if *nref = 0*, or blank
(DIRCOS *(3,J)*, *J = 1, 3)*
α_x α_y α_z
Y_{xx}, Y_{yy}, Y_{zz}, Y_{xy}, Y_{yz}, Y_{zx}

where

n = the material constant entry

w = weight density (weight/unit volume)

nref = Alternate Reference Frame (see ALTREF)

If *nref* > *0*, frame *nref* specifies material orientation relative to the element axes.
If *nref = 0*, this orientation is given by DIRCOS values.

E_1 = Modulus of elasticity in material direction – 1
E_2 = Modulus of elasticity in material direction – 2
E_3 = Modulus of elasticity in mateial direction – 3

G_{12} = Shear modulus in 1–2 plane
G_{13} = Shear modulus in 1–3 plane
G_{23} = Shear modulus in 2–3 plane

ν_{12} = Poisson's ratio of comp in dir–2 to tension in dir–1
ν_{13} = Poisonn's ratio of comp in dir–3 to tension in dir–1
ν_{23} = Poisson's ratio of comp in dir–3 to tension in dir–2

DIRCOS (I,J) = Direction cosine matrix relating the material axis–i to the element axis-j.

α_x, α_y, α_z = Linear thermal expansion coefficients

Y_{xx} Y_{yy} Y_{zz} Y_{xy} Y_{yz} Y_{zx} = reference or yield stress for use in stress displays. See PSF.

EXAMPLE:

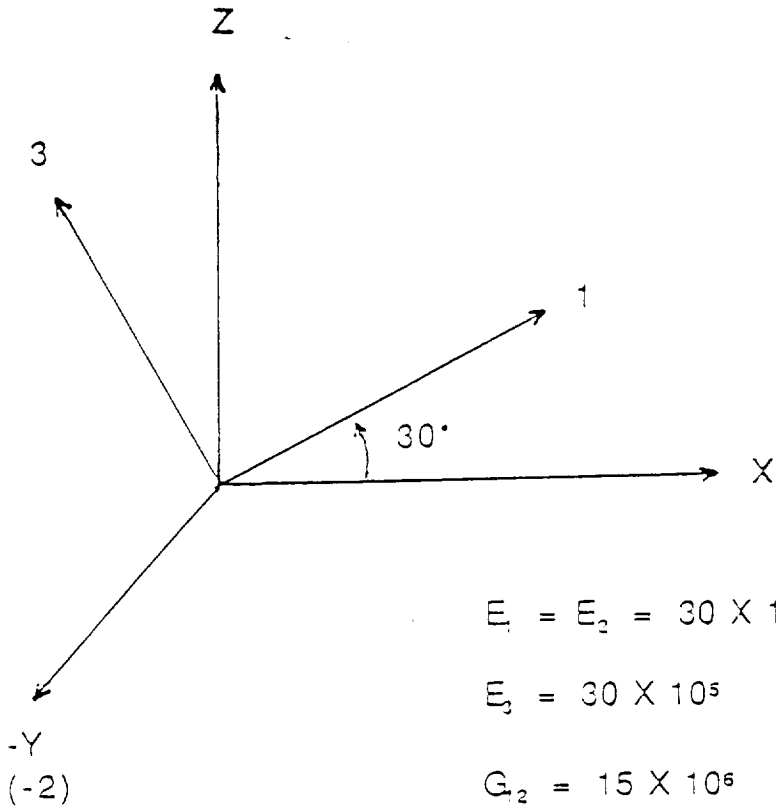

$E_1 = E_2 = 30 \times 10^6$

$E_3 = 30 \times 10^5$

$G_{12} = 15 \times 10^6$

$G_{13} = G_{23} = 15 \times 10^5$

$\nu_{12} = \nu_{13} = \nu_{23} = .3$

or

```
SMAT:   1  .283
        30.+6,30.+6,30.+5
        15.+6,15.+5,15.+5
        0.3,0.3,0.3
        0.866,0.000,0.500
        0.000,1.000,0.000
        -.500,0.000,0.866
        0.,0.,0.
        1.,1.,1.,1.,1.,1.
```

```
ALTREF: 2  2,-30.

SMAT:   1  .283  2
        30.+6,30.+6,30.+5
        15.+6,15.+5,15.+5
        0.3,0.3,0.3
        0.,0.,0.
        1.,1.,1.,1.,1.,1.
```

3.2.2.3 Three–Dimensional Elements

Only one table pointer, NSECT (or the synonym NPROP), applies. The default value of NSECT is 1. For fluid elements, NSECT points to a line in a table named PROP BTAB 2 20. For solids, NSECT points to a line in PROP BTAB 2 21. Before executing ELD, the user must construct these tables via AUS/TABLE, as indicated below. Mesh generation facilities are described at the end of this section.

Fluid elements *F41, F61, F81:*

For additional information see Section 12. It should be noted that FSM is the only processor which produces system matrices containing fluid element terms. Fluid element terms are not included in the system diagonal mass matrix, DEM, produced by processor *E*, nor in the system matrices produced by *K*, *M*, or *KG*. No form of static temperature, dislocational, or pressure loading is defined for fluid elements. GSF produces no stress data for fluid elements.

Section properties are defined as follows:

@XQT AUS

TABLE *(NI = 2, NJ =* the number of different fluids): PROP BTAB 2 20

J = 1 : ρ, β $ Mass density, bulk modulus for fluid 1.

J = 2 : ρ, β $ Mass density, bulk modulus for fluid 2.

Solid elements *S41, S42, S61, S81, S82 :*

Solid element terms are included in the system diagonal mass matrix, DEM, produced by *E*, and in the system matrices produced by *K* and *M*, but not those produced by *KG*. Properties are defined as follows:

@XQT AUS

TABLE *(NI = 31, NJ =* number of different solids): PROP BTAB 2 21

J = 1$ Properties of material 1 follow.

w>

a_{11}>

a_{21} a_{22}>

a_{31} a_{32} a_{33}>

a_{41} a_{42} a_{43} a_{44}>

a_{51} a_{52} a_{53} a_{54} a_{55}>

a_{61} a_{62} a_{63} a_{64} a_{65} a_{66}>

$\alpha_x \quad \alpha_y \quad \alpha_z >$

$Y_{xx} \; Y_{yy} \; Y_{zz} \; Y_{xy} \; Y_{yz} \; Y_{zx} \$$

$J = 2\$$ Properties of material 2 follow. (Same sequence as above).

Appendix C
Compliance Matrices for Various Crystal Classes

C Appendix—Compliance Matrices for Various Crystal Classes

In this appendix, the specific forms of compliance matrices and independent material constants are presented. The compliance matrices presented here are of the symmetric form ${}^{S}\boldsymbol{S}$ is obtained when the engineering strain measures $\lambda_{ij} = 2\varepsilon_{ij}, i \neq j$ are used in the strain vector. Note that the nonsymmetric compliance matrices $\boldsymbol{S}$, corresponding to the use of strain measures ε_{ij}, can be easily calculated according to the formula:

$$S_{ij} = {}^{S}S_{ij} \quad i = 1,2,3 \quad j = 1,\ldots,6$$

$$S_{ij} = \tfrac{1}{2}\ {}^{S}S_{ij} \quad i = 4,5,6 \quad j = 1,\ldots,6$$

The independent material constants and compliance matrices for various types of crystal classes are listed below:

TRICLINIC - classes 1,2

For the material of triclinic structure in classes 1,2, there exists 21 independent compliance constants $a_1,\ldots,a_{21}$. The location of these constants in the symmetric compliance matrix is defined by:

$${}^{S}\boldsymbol{S} = \begin{bmatrix} a_1 & a_2 & a_3 & a_4 & a_5 & a_6 \\ & a_7 & a_8 & a_9 & a_{10} & a_{11} \\ & & a_{12} & a_{13} & a_{14} & a_{15} \\ & & & a_{16} & a_{17} & a_{18} \\ & & & & a_{19} & a_{20} \\ & & & & & \\ & & & & & a_{21} \end{bmatrix}$$

MONOCLINIC - classes 3–5

For the material of monoclinic structure in classes 3–5, there exists 13 independent compliance constants $a_1,\ldots,a_{13}$. The location of these constants in the symmetric compliance

matrix is defined by:

$$ {}^{S}\boldsymbol{S} = \begin{bmatrix} a_1 & a_7 & a_8 & 0 & 0 & a_9 \\ & a_2 & a_{10} & 0 & 0 & a_{11} \\ & & a_3 & 0 & 0 & a_{12} \\ & & & a_4 & a_{13} & 0 \\ & & & & a_5 & 0 \\ & & & & & a_6 \end{bmatrix} $$

ORTHORHOMBIC - classes 6–8

For the material of orthorhombic structure in classes 6–8, there exists eight independent compliance constants $a_1, \ldots, a_8$. The location of these constants in the symmetric compliance matrix is defined by:

$$ {}^{S}\boldsymbol{S} = \begin{bmatrix} a_1 & a_7 & a_7 & 0 & 0 & 0 \\ & a_2 & a_8 & 0 & 0 & 0 \\ & & a_3 & 0 & 0 & 0 \\ & & & a_4 & 0 & 0 \\ & & & & a_5 & 0 \\ & & & & & a_6 \end{bmatrix} $$

TETRAGONAL - classes 9–11

For the material of tetragonal structure in classes 9–11, there exists seven independent compliance constants $a_1, \ldots, a_7$. The location of these constants in the symmetric compliance matrix is defined by:

$$ {}^{S}\boldsymbol{S} = \begin{bmatrix} a_1 & a_5 & a_6 & 0 & 0 & a_7 \\ & a_1 & a_6 & 0 & 0 & -a_7 \\ & & a_2 & 0 & 0 & 0 \\ & & & a_3 & 0 & 0 \\ & & & & a_3 & 0 \\ & & & & & a_4 \end{bmatrix} $$

TETRAGONAL - classes 12–15

For the material of tetragonal structure in classes 12–15, there exists six independent compliance constants $a_1, \ldots, a_6$. The location of these constants in the symmetric compliance

matrix is defined by:

$$ {}^{S}\boldsymbol{S} = \begin{bmatrix} a_1 & a_5 & a_6 & 0 & 0 & 0 \\ & a_1 & a_6 & 0 & 0 & 0 \\ & & a_2 & 0 & 0 & 0 \\ & & & a_3 & 0 & 0 \\ & & & & a_3 & 0 \\ & & & & & a_4 \end{bmatrix} $$

TRIGONAL–HEXAGONAL - classes 16–17

For the material of trigonal–hexagonal structure in classes 16–17, there exists eight independent compliance constants $a_1, \ldots, a_8$. The location of these constants in the symmetric compliance matrix is defined by:

$$ {}^{S}\boldsymbol{S} = \begin{bmatrix} a_1 & a_4 & a_5 & a_6 & -a_7 & 0 \\ & a_1 & a_5 & -a_6 & a_8 & 0 \\ & & a_2 & 0 & 0 & 0 \\ & & & a_3 & 0 & 2a_8 \\ & & & & a_3 & 2a_6 \\ & & & & & 2(a_1 - a_4) \end{bmatrix} $$

TRIGONAL–HEXAGONAL - classes 18–20

For the material of trigonal–hexagonal structure in classes 18–20, there exist six independent compliance constants $a_1, \ldots, a_6$. The location of these constants in the symmetric compliance matrix is defined by:

$$ {}^{S}\boldsymbol{S} = \begin{bmatrix} a_1 & a_4 & a_5 & a_6 & 0 & 0 \\ & a_1 & a_5 & -a_6 & 0 & 0 \\ & & a_2 & 0 & 0 & 0 \\ & & & a_3 & 0 & 0 \\ & & & & a_3 & 2a_6 \\ & & & & & 2(a_1 - a_4) \end{bmatrix} $$

TRIGONAL–HEXAGONAL - classes 21–27

For the material of trigonal–hexagonal structure in classes 21–27, there exist five independent compliance constants $a_1, \ldots, 1_5$. The location of these constants in the symmetric compliance

matrix is defined by:

$$ {}^{S}\boldsymbol{S} = \begin{bmatrix} a_1 & a_4 & a_5 & 0 & 0 & 0 \\ & a_1 & a_5 & 0 & 0 & 0 \\ & & a_2 & 0 & 0 & 0 \\ & & & a_3 & 0 & 0 \\ & & & & a_3 & 0 \\ & & & & & 2(a_1 - a_4) \end{bmatrix} $$

CUBIC - classes 28–32

For the material of cubic structure there exist three independent compliance constants a_1, a_2 and a_3. Their inderpretation in terms of Young modulus E, Poisson's ratio ν and shear modulus G is given by:

$$ a_1 = \frac{1}{E} $$

$$ a_2 = -\frac{1}{\nu E} $$

$$ a_3 = \frac{1}{G} $$

The location of material constants in the symmetric compliance matrix is defined by:

$$ {}^{S}\boldsymbol{S} = \begin{bmatrix} a_1 & a_2 & a_2 & 0 & 0 & 0 \\ & a_1 & a_2 & 0 & 0 & 0 \\ & & a_1 & 0 & 0 & 0 \\ & & & a_3 & 0 & 0 \\ & & & & a_3 & 0 \\ & & & & & a_3 \end{bmatrix} $$

ISOTROPIC

For the isotropic material there exist two independent compliance constants a_1 and a_2. Their interpretation in terms of Young modulus E and Poisson's ratio ν is:

$$ a_1 = \frac{1}{E} $$

$$ a_2 = -\frac{1}{\nu E} $$

The location of material constants in the symmetric compliance matrix is defined by:

$$ {}^{S}\boldsymbol{S} = \begin{bmatrix} a_1 & a_2 & a_2 & 0 & 0 & 0 \\ & a_1 & a_2 & 0 & 0 & 0 \\ & & a_1 & 0 & 0 & 0 \\ & & & 2(a_1 - a_2) & 0 & 0 \\ & & & & 2(a_1 - a_2) & 0 \\ & & & & & 2(a_1 - a_2) \end{bmatrix} $$

A more detailed discussion of crystal structure and compliance matrices for various crystal classes can be found in reference [8].

LOCATOR MATRICES

The non-zero elements of the locator matrices $\boldsymbol{L}$ for each of the compliance matrices can be easily reconstructed by considering consecurive independent material constants a_k and observing that ${}^{S}L_{ijk}$ is the coefficient in matrix ${}^{S}S_{ij}$ corresponding to the constant a_k. For example, for isotropic material, the "layer" of the compliance matrix corresponding to a_1 is

$$ [\ {}^{S}L_{ij1}] = \begin{bmatrix} 1 & 0 & 0 & 0 & 0 & 0 \\ 0 & 1 & 0 & 0 & 0 & 0 \\ 0 & 0 & 1 & 0 & 0 & 0 \\ 0 & 0 & 0 & 2 & 0 & 0 \\ 0 & 0 & 0 & 0 & 2 & 0 \\ 0 & 0 & 0 & 0 & 0 & 2 \end{bmatrix} $$

and the "layer" corresponding to a_2 is

$$ [\ {}^{S}L_{ij2}] = \begin{bmatrix} 0 & 1 & 1 & 0 & 0 & 0 \\ 1 & 0 & 0 & 0 & 0 & 0 \\ 1 & 1 & 0 & 0 & 0 & 0 \\ 0 & 0 & 0 & -2 & 0 & 0 \\ 0 & 0 & 0 & 0 & -2 & 0 \\ 0 & 0 & 0 & 0 & 0 & -2 \end{bmatrix} $$